NACA

RESEARCH MEMORANDUM

WIND-TUNNEL INVESTIGATION OF THE EFFECTS OF LIP GEOMETRY ON DRAG AND PRESSURE RECOVERY OF A NORMAL-SHOCK NOSE INLET ON A BODY OF REVOLUTION AT MACH NUMBERS OF 1.41 AND 1.81

By A. Warner Robins

Langley Aeronautical Laboratory
Langley Field, Va.

NATIONAL ADVISORY COMMITTEE
FOR AERONAUTICS

WASHINGTON
February 3, 1958

Classification cancelled (or changed to Unclassified)

By Authority of Nasa Tech Ltr Announcement #17
(OFFICER AUTHORIZED TO CHANGE)

By 14 Apr 60
NAME AND

NK
GRADE OF OFFICER MAKING CHANGE)

27 Apr 61
DATE

1G

NACA RM L57K08

[redacted]

NATIONAL ADVISORY COMMITTEE FOR AERONAUTICS

RESEARCH MEMORANDUM

WIND-TUNNEL INVESTIGATION OF THE EFFECTS OF LIP GEOMETRY ON DRAG AND PRESSURE RECOVERY OF A NORMAL-SHOCK NOSE INLET ON A BODY OF REVOLUTION AT MACH NUMBERS OF 1.41 AND 1.81

By A. Warner Robins

SUMMARY

A wind-tunnel investigation has been made to determine some of the effects of lip geometry on drag and pressure recovery of a normal-shock nose inlet. Total-pressure recoveries, external drags, duct total-pressure distributions, lip and forebody pressure distributions, and schlieren photographs are presented. The models were tested at Mach numbers of 1.41 and 1.81 with the Reynolds number varying from 1.2×10^6 to 1.8×10^6 based on model maximum diameter. Angle of attack was varied from -5° to 15°.

The results indicate that the effects of lip blunting on external drag at supersonic speeds are large. Outward lip camber increases the uniformity of duct total-pressure distributions over those for the inward-cambered lip but showed higher spillage drags. The forebody half-angle has a large effect on external drag, the 10° half-angle forebody configuration with sharp lip showing approximately twice the drag of the comparable 5° configuration.

INTRODUCTION

Previous research (refs. 1 and 2) shows that, for normal-shock nose-inlets, an advantage in external drag is obtained with the use of sharp inlet lips. References 3 to 7, however, show substantial performance losses due to the poor internal-flow characteristics of sharp-lipped configurations at low speeds and at high-angle-of-attack operation up to transonic speeds. Therefore, considerable knowledge of the effects of lip geometry on drag, pressure recovery, and engine-face total-pressure profiles is required in order to make a rational choice in design.

[redacted]

[redacted]

Since previous investigations have been insufficiently systematic to satisfy this requirement, a joint program was undertaken at the Langley 8-foot transonic and the Langley 4- by 4-foot supersonic pressure tunnels to determine some of the effects of inlet-lip geometry on drag and pressure recovery at transonic and supersonic speeds. Reference 8 presents the results for the transonic range, and the present paper presents those for Mach numbers of 1.41 and 1.81.

This paper presents drag, duct total pressures, and lip and forebody pressures on models having a systematic variation in lip bluntness and lip camber for angles of attack from -5° to 15° and for Reynolds numbers, based on model diameter, from 1.2×10^6 to 1.8×10^6.

SYMBOLS

A	cross-sectional area
A_f	fuselage maximum cross-sectional area
a	lip-profile axial dimension (fig. 4)
b	lip-profile radial dimension (fig. 4)
C	lip-profile station (fig. 4)
$2b/R$	lip-bluntness parameter
C_{D_x}	external-drag coefficient (based on A_f and defined in reference 8)
C_p	pressure coefficient, $\frac{p - p_o}{q_o}$
D	body maximum diameter
d	distance from lip leading edge to model axis (fig. 4)
F	strain-gage axial force
H	total pressure
$\overline{H}$	average total pressure
M	Mach number

[redacted]

m	internal mass-flow rate
m/m_o	mass-flow ratio, $\frac{m}{\rho_o V_o A_1}$
N	lip leading-edge station
p	static pressure
q	dynamic pressure
R	inlet minimum radius
V	velocity
x	distance measured parallel to axis of body, positive downstream ($x = 0$ at leading edge of lip 1A)
y	distance from inlet axis to inlet lip
α	angle of attack of model center line
ρ	mass air density

Subscripts:

o	free stream
1	inlet minimum area station
2	venturi rake station
b	afterbody base annulus
c	strain-gage chamber
d	venturi dump
i	inner
l	lip
O	outer
max	maximum
adj	adjusted

[redacted]

[redacted]

All total-pressure data are shown without subscript and are measured at the pressure-recovery rake station. (See fig. 1.)

MODELS AND TESTS

Models

The layout of the models is shown in figure 1. The duct area distribution is shown in figure 2. In order to accommodate the instrumentation required, two interchangeable central bodies were employed; one was rigidly connected to the sting and contained the pressure instrumentation, and the other was connected through a strain-gage balance and provided for drag measurements. Both central bodies could be fitted with the same afterbody and with either of the two forebodies. An exit plug shown in figure 1 was provided for mass-flow control.

The two forebody assemblies, noses 1 and 2, had 5° and 10° half-angles, respectively. Photographs of these forebodies and their interchangeable nose pieces are shown in figure 3.

Figure 4 shows the inlet-lip variations tested. The ordinates for these lips may be found in table I. The lips of configurations 1A to 1E were generated by 2.5:1 ellipses and make up a series in which bluntness is progressively varied. The bluntness parameter used in this paper as well as that used in reference 8 $2b/R$ is the ratio of the length of the minor diameter of the lip-generating ellipse to the inlet minimum radius. It should be noted that a change in forebody fineness ratio is necessarily produced by a change in lip bluntness.

Lips 1C, 1G, and 1H comprise a lip-camber series in which lip bluntness remains approximately the same. Lip 1F has a circular generatrix and has its leading edge at the same axial station as lips 1C, 1G, and 1H.

Lips 2A and 2B have the same degree of lip bluntness as lips 1A and 1C, respectively, but are mounted on 10° half-angle forebodies.

Instrumentation

The pressure model was fitted with two sets of internal survey rakes as shown in figure 1. The forward rake system provided for the measurement of the duct total-pressure data presented, whereas the rear rakes, located in the venturi, were used for mass-flow measurement. Each model was provided with a row of orifices extending from within the inlet at the beginning of the curve of the inlet lip, around the lip profile

(except 1A and 2A), and along the surface of the model forebody. These orifices were located in the angle-of-attack plane on the upper surfaces. Base-pressure measurements were made on the annulus at the model exit and in the venturi dump section.

The force-model instrumentation did not provide for pressure measurement at the forward rake station although the forward rake assembly remained within the model throughout the force tests. The rear rake assembly and the venturi-dump orifices, which were sting-mounted, were used as in the pressure model. A strain-gage balance, located as shown in figure 1, provided for drag measurements. Additional base-pressure measurements were made in the balance chamber.

Test Conditions

The test conditions for the pressure models were as follows:

Mach numbers	1.41 and 1.81
Reynolds numbers based on model maximum diameter:	
At M_o = 1.41	1.8×10^6
At M_o = 1.81	1.6×10^6
Stagnation pressure, atm	0.95
Stagnation temperature, ^oF	100

The test conditions for the force models are as follows:

Mach numbers	1.41 and 1.81
Reynolds numbers based on model maximum diameter:	
At M_o = 1.41	1.4×10^6
At M_o = 1.81	1.2×10^6
Stagnation pressure, atm	0.75
Stagnation temperature, ^oF	100

Boundary-layer transition was fixed for each configuration by a strip of carborundum grains in shellac encircling the model 1 inch back of the lip leading edge.

RESULTS AND DISCUSSION

Presentation of Results

For the purpose of more clearly visualizing the inlet operating conditions, a key figure with a system of symbols as shown near the top of figure 5 is used as a guide for figures 6 to 12 and 16 to 18. Three

operating conditions and their symbols are shown in figure 5 as follows: supersonic flow just back of the throat corresponding to the range indicated by the circular symbols in the key; sonic-throat flow without supersonic flow back of the throat corresponding to the square symbols; and subsonic-throat flow corresponding to the range indicated by the diamond and triangle symbols. The several symbols (diamond, triangle, and inverted triangle) are used to more explicitly identify the portion of the subsonic-throat range considered. Identification by actual value of mass-flow ratio is not made on the keyed figures since identical values of mass-flow ratio for different configurations do not necessarily correspond to the same inlet operating conditions. This condition is a result of the use of inlet minimum area (same for all configurations) in mass-flow ratio calculations instead of actual capture area which varies from model to model depending upon the degree of lip bluntness or camber. For example, at supersonic speeds a mass-flow ratio of 1.0 for configuration 1E (blunt lip) would correspond to subsonic flow in the inlet throat, and it would correspond to a choked-throat condition in configuration 1A (sharp lip). In addition to the figure keys which serve only as a qualitative guide, numerical values of mass flow and average total-pressure recovery are presented in table II.

Drag data are available for all configurations at both Mach numbers 1.41 and 1.81. Not all configurations were tested as pressure models, however, so that a complete set of data is available only for configurations 1A, 1C, 1E, 1G, 1H, and 2B. The figures are divided into several groups according to the type of data presented.

Figure 6 shows the pressure distribution along the forebodies for all the configurations tested as pressure models. In figure 7, pressure distributions around the lip sections in the angle-of-attack plane for configurations varying in lip bluntness (configurations 1A, 1C, and 1E) are presented. Except for 5° angle-of-attack conditions, data for upper lip sections only are shown. The pressure distributions on the lower lip in the figures for 5° angle of attack were actually obtained from measurements on the upper lips at -5° angle of attack. The corresponding forebody pressure distributions, however, are presented in figure 6 as -5° angle-of-attack data and are so listed in table II. The same type of presentation is made in figures 8 and 9 in which data for configurations varying in lip camber (configurations 1G, 1C, and 1H), and configurations varying in forebody half-angle (configurations 1C and 2B), respectively, are presented. Lip pressure coefficients at angles of attack of 0°, 5°, 10°, and 15° and Mach numbers of 1.41 and 1.81 are presented.

Figures 10, 11, and 12 show schlieren photographs of the flow at the inlet at 0° angle of attack and at Mach numbers of 1.41 and 1.81. The photographs of figure 10 are of configurations 1A, 1C, and 1E which

vary in lip bluntness. The configurations vary in lip camber (configurations 1G, 1C, and 1H) in figure 11. Figure 12 shows schlieren photographs of two sets of configurations which vary in forebody half-angle, one set with sharp inlet-lips (configurations 1A and 2A), and another with moderately blunted lips (configurations 1C and 2B).

Figures 13, 14, and 15 show average total-pressure-recovery results and external drag coefficients for various angles of attack and Mach numbers of 1.41 and 1.81. In figures 16, 17, and 18 are presented the total-pressure contours at the pressure-recovery rake (see fig. 1) as seen looking downstream. Data for various angles of attack and Mach numbers of 1.41 and 1.81 are shown. Figures 19 and 20 summarize the drags at an angle of attack of 0° for several configurations at transonic (ref. 8) and supersonic speeds.

Discussion of Results

Surface-pressure distributions.- For the models tested, lip bluntness, lip camber, mass-flow rate, and Mach number appear to have little or no effect on the pressure distributions (fig. 6) back of a point approximately $1\frac{1}{2}$ inlet diameters from the inlet lip.

Average total-pressure recoveries and drags.- Figure 13 presents average total-pressure recoveries for configurations 1A, 1C, and 1E and external drag coefficients for configurations 1A, 1B, 1C, 1D, and 1E. At both Mach numbers 1.41 and 1.81, the average total-pressure recoveries of these configurations (1A, 1C, and 1E) were not appreciably different although maximum mass flows for the blunt lips were greater than those for the sharp-lip configuration, especially at a Mach number of 1.81. External drag coefficients are seen to vary with lip bluntness, although the variation of external drag with mass flow was generally very similar for all these configurations.

Figure 14 presents average total-pressure recoveries and external drag coefficients for the configurations varying in lip camber (configurations 1G, 1C, and 1H). In addition, drag data for configuration 1F, the lip of which had a circular generatrix, is presented. Average total-pressure recoveries were approximately the same for the configurations of the lip-camber series (1G, 1C, and 1H) except at the higher angles of attack where a reduction was found for the configuration with the inward-cambered lip (1G). External drags for these configurations were approximately the same at maximum mass flows, configuration 1G generally exhibiting the lowest spillage drag.

The average total-pressure recoveries for configurations 1A, 1C, and 2B, and the external drag coefficients of configurations 1A, 1C, 2A,

and 2B are presented in figure 15. These configurations vary in forebody half-angle as well as in lip bluntness, configurations 1A and 2A being sharp-lip inlets and configurations 1C and 2B having the same degree of moderate bluntness. Average total-pressure recoveries for configurations 1C and 2B are approximately the same for all test conditions. The drag penalty due to lip blunting for both the 5° and 10° configurations was appreciable.

It will be noted that, for all configurations tested, average total-pressure recoveries were within 1 percent of free-stream Pitot pressures at the lowest mass flows and, except for the sharp-lip and inward-cambered-lip configurations, these values of recovery were approximated at angles of attack of 0° and 5° up to mass flows near choking. In addition, it should be noted that values of mass-flow ratio throughout the paper are erroneously high. Note especially the values for configuration 1A where the maximum mass-flow ratio should not exceed unity. These errors are associated with the use of an area-weighting method of calculating internal-flow properties as reported in reference 9.

Duct total-pressure contours.- Total-pressure contours for some of the configurations in the lip-bluntness series (configurations 1A, 1C, and 1E) are presented in figure 16 in the form of contour plots. The sharp-lip configuration (configuration 1A) showed less uniform distributions than either the configuration with the moderately blunted lip (configuration 1C) or the configuration with the greatest lip bluntness (configuration 1E) at high mass-flow rates and at the higher angles of attack. The total-pressure distributions for the configuration with maximum lip bluntness did not appear to be more uniform than those for the configuration with moderate lip bluntness.

Figure 17 presents duct total-pressure distributions for the lip-camber series (configurations 1G, 1C, and 1H). For mass flows at which the flow at the inlet throat is near sonic and for angles of attack of 10° and 15°, the configuration with inward lip camber (configuration 1G) showed much poorer distributions than either the uncambered-lip configuration or the configuration with outward camber. The total-pressure distributions for the configuration with outward-cambered lips (configuration 1H) did not, however, appear to be more uniform than those for the configuration without lip camber (configuration 1C) at $M = 1.41$ but did exhibit more uniformity at $M = 1.81$.

Total-pressure distributions for configurations 1C and 2B which had the same lip bluntness but forebody half-angles of 5° and 10°, respectively, are presented in figure 18. The differences in total-pressure distribution are small between the two configurations, configuration 1C showing slightly more uniform distribution at $M = 1.41$.

It will be noted that for all configurations tested, with the exception of configurations 1A and 1G, duct total-pressure distributions were generally good when compared with those of scoop inlets or external compression inlets.

Summary of drag results.- Figure 19 presents a compilation of zero angle-of-attack external-drag coefficients from reference 8 and present data for the configurations in the lip-bluntness series for mass flows producing near-sonic flow in the inlet throats. From Mach number 1.0 upward, drag penalties associated with lip blunting generally become increasingly large until at a Mach number of 1.81, for example, the drag of the most blunt configuration is over 250 percent of the drag of the sharp-lip configuration. This drag comparison, however, is unfair to the configurations with lip bluntness, since, as is seen in figure 13, the flow capacities of the nose inlets with blunt lips were greater than those for the sharp-lip configurations at supersonic speeds. This effect was most pronounced at a Mach number of 1.81. (See fig. 13(b).) If the inlet openings were sized so as to produce a lip-bluntness series having equal flow capacity, the minimum areas of the inlets would decrease with increasing lip bluntness and the drag increments due to lip bluntness would be partially compensated for by the lower drag of the smaller inlet. This system of sizing would result in a fair comparison at a particular Mach number and at the maximum flow capacities of each of the inlets in the bluntness series but would require data for a series of inlets having the same ratio of true capture area to maximum frontal area. The external drag coefficients of figure 19 have therefore been adjusted accordingly. These adjustments involved neglecting the difference in skin-friction drag between the hypothetical body and that tested and assuming that the pressures on the rear halves of the configuration forebodies of those in the lip-bluntness series could be extrapolated linearly rearward. The adjusted drag coefficient was then written:

$$C_{D_{x,adj}} = C_{D_x} \frac{m_{max,1A}}{m_{max}} + C_p\left(\frac{m_{max}}{m_{max,1A}} - 1\right)$$

where C_p is the average pressure coefficient over the rearward portion of the configuration forebody in question. The term $\frac{m_{max}}{m_{max,1A}} - 1$ is, in effect, the percent increase in configuration frontal area required to produce the same ratio of capture area to maximum frontal area for the inlets tested or

[redacted]

$$\frac{m_{max}}{m_{max,1A}} - 1 = \frac{A_{f,adj} - A_f}{A_f}$$

Values for m_{max} for all blunt-lip configurations were not determined for all test conditions and were therefore estimated. The resulting estimated capture areas did not exceed values for limiting contraction for the Mach number considered.

The adjusted and unadjusted values of external drag coefficient are plotted against the lip-bluntness parameter in figure 20. This figure shows that for such normal-shock nose inlets the overall variation of external drag with lip bluntness would be essentially constant between Mach numbers of 1.4 and 1.8 when the inlets are designed for the same flow capacity and are compared at a design Mach number.

CONCLUSIONS

An investigation of some of the effects of lip bluntness, lip camber, and forebody angle on pressure recoveries and external drags of a normal-shock nose inlet at various angles of attack and at Mach numbers of 1.41 and 1.81 indicates the following conclusions:

1. The effects of lip blunting on external drag at supersonic speeds were large.

2. A moderate degree of lip bluntness gave a more uniform total-pressure distribution than was measured for the sharp-lip configuration at high mass flows and high angles of attack. Use of a high degree of lip bluntness gave no further improvement.

3. The configuration with outward camber showed more uniform duct total-pressure distributions than the inward cambered configuration but had higher spillage drags.

4. Forebody angle had a large effect on external drag with the 10° half-angle configuration having approximately twice the external drag of the comparable 5° configuration.

Langley Aeronautical Laboratory,
National Advisory Committee for Aeronautics,
Langley Field, Va., October 15, 1957.

[redacted]

REFERENCES

1. Sears, R. I., Merlet, C. F., and Putland, L. W.: Flight Determination of Drag of Normal-Shock Nose Inlets With Various Cowling Profiles at Mach Numbers From 0.9 to 1.5. NACA Rep. 1281, 1956. (Supersedes NACA RM L53I25a.)

2. Mossman, Emmet A., and Anderson, Warren E.: The Effect of Lip Shape on a Nose-Inlet Installation at Mach Numbers From 0 to 1.5 and a Method for Optimizing Engine-Inlet Combinations. NACA RM A54B08, 1954.

3. Pendley, Robert E., Milillo, Joseph R., and Fleming, Frank F.: An Investigation of Three NACA 1-Series Nose Inlets at Subsonic and Transonic Speeds. NACA RM L52J23, 1953.

4. Bryan, Carroll R., and Fleming, Frank F.: Some Internal-Flow Characteristics of Several Axisymmetrical NACA 1-Series Nose Air Inlets at Zero Flight Speed. NACA RM L54E19A, 1954.

5. Milillo, Joseph R.: Some Internal-Flow Characteristics at Zero Flight Speed of An Annular Supersonic Inlet and an Open-Nose Inlet With Sharp and Rounded Lips. NACA RM L54E19, 1954.

6. Blackaby, James R., and Watson, Earl C.: An Experimental Investigation at Low Speeds of the Effects of Lip Shape on the Drag and Pressure Recovery of a Nose Inlet in a Body of Revolution. NACA TN 3170, 1954.

7. Fradenburgh, Evan A., and Wyatt, DeMarquis D.: Theoretical Performance Characteristics of Sharp-Lip Inlets at Subsonic Speeds. NACA Rep. 1193, 1954. (Supersedes NACA TN 3004.)

8. Olstad, Walter B.: Transonic-Wind-Tunnel Investigation of the Effects of Lip Bluntness and Shape on the Drag and Pressure Recovery of a Normal-Shock Nose Inlet in a Body of Revolution. NACA RM L56C28, 1956.

9. Wyatt, DeMarquis D.: Analysis of Errors Introduced by Several Methods of Weighting Nonuniform Duct Flows. NACA TN 3400, 1955.

[redacted]

TABLE I.- COORDINATES OF INLET LIPS

[All coordinates are in inches]

Lip 1B		
x	y_o	y_i
1.143	1.305	1.305
1.145	1.314	1.296
1.151	1.323	1.287
1.161	1.332	1.278
1.177	1.341	1.269
1.202	1.350	1.260
1.281	1.362	1.250

Dimensions	
Station N	1.143
Station C	1.281
a	.138
b	.055
d	1.305

Lip 1C		
x	y_o	y_i
2.286	1.361	1.361
2.292	1.384	1.338
2.316	1.411	1.311
2.371	1.441	1.281
2.489	1.468	1.254
2.500	1.469	1.253
2.563	1.474	1.250

Dimensions	
Station N	2.286
Station C	2.563
a	.277
b	.111
d	1.361

Lip 1D		
x	y_o	y_i
3.429	1.416	1.416
3.435	1.437	1.395
3.446	1.459	1.373
3.464	1.480	1.352
3.490	1.501	1.331
3.537	1.522	1.310
3.578	1.542	1.290
3.711	1.573	1.259
3.844	1.586	1.250

Dimensions	
Station N	3.429
Station C	3.844
a	.415
b	.166
d	1.416

Lip 1E		
x	y_o	y_i
4.572	1.471	1.471
4.578	1.502	1.440
4.595	1.533	1.409
4.630	1.567	1.375
4.661	1.591	1.351
4.710	1.617	1.325
4.782	1.644	1.298
4.954	1.681	1.261
5.125	1.698	1.250

Dimensions	
Station N	4.572
Station C	5.125
a	.553
b	.221
d	1.417

TABLE I.- COORDINATES OF INLET LIPS - Concluded

Lip 1F		
x	y_o	y_i
2.286	1.354	1.354
2.288	1.376	1.332
2.297	1.401	1.307
2.317	1.428	1.280
2.381	1.457	1.251
2.390	1.458	1.250

Dimensions	
Station N	2.286
Station C	2.390
a	.104
b	.104
d	1.354

Lip 1G		
x	y_o	y_i
2.286	1.290	1.290
2.292	1.320	1.276
2.312	1.353	1.263
2.336	1.377	1.255
2.354	1.390	1.252
2.386	1.409	1.250
2.436	1.432	
2.652	1.481	
2.781	1.493	

Dimensions	
Station N	2.286
d	1.290

Lip 1H		
x	y_o	y_i
2.286	1.410	1.410
2.288	1.419	1.395
2.296	1.430	1.375
2.315	1.442	1.350
2.349	1.453	1.324
2.353	1.454	1.321
2.411	1.461	1.294
2.427		1.288
2.500		1.268
2.600		1.254
2.686		1.250

Dimensions	
Station N	2.286
d	1.410

Lip 2B		
x	y_o	y_i
1.134	1.370	1.370
1.142	1.397	1.343
1.168	1.426	1.314
1.227	1.457	1.283
1.314	1.479	1.261
1.434		1.250

Dimensions	
Station N	1.134
Station C	1.434
a	.300
b	.120
d	1.370

[redacted]

TABLE II.- MASS-FLOW RATIOS AND PRESSURE RECOVERIES CORRESPONDING TO DATA POINTS IN FIGURES 6 TO 12 AND 16 TO 18

Symbol	$\alpha = -5^\circ$		$\alpha = 0^\circ$		$\alpha = 5^\circ$		$\alpha = 10^\circ$		$\alpha = 15^\circ$	
	m/m_o	$\overline{H}/H_o$	m/m_o	$\overline{H}/H_o$	m/m_o	$\overline{H}/H_o$	m/m_o	$\overline{H}/H_o$	m/m_o	$\overline{H}/H_o$
$M_o = 1.41$; configuration 1A										
○	1.04	0.90	1.04	0.91	1.04	0.89	1.01	0.89	0.98	0.82
□	.98	.93	----	----	.98	.93	.95	.93	.88	.92
◇	.95	.94	.98	.94	.95	.94	.89	.94	.84	.93
△	.87	.95	.88	.94	.87	.94	.73	.95	.73	.95
▽	.60	.95	.59	.95	.60	.95	.60	.95	.60	.95
$M_o = 1.41$; configuration 1C										
○	----	----	----	----	1.06	0.93	1.01	0.93	1.02	0.90
□	1.07	0.92	1.07	0.93	----	----	.95	.94	.94	.92
◇	1.01	.94	1.01	.94	1.01	.94	.89	.94	.88	.93
△	.85	.95	.89	.95	.85	.95	.73	.95	----	----
▽	.60	.95	.59	.95	.60	.95	.60	.95	.60	.95
$M_o = 1.41$; configuration 1E										
○	----	----	----	----	1.08	0.93	1.07	0.91	----	----
□	1.07	0.94	1.09	0.94	1.07	.94	1.04	.93	1.04	0.89
◇	1.02	.94	1.07	.94	1.02	.94	1.01	.94	1.02	.91
△	.85	.95	.89	.95	.85	.95	.73	.95	.73	.95
▽	.60	.95	.60	.95	.60	.95	.60	.95	.60	.95
$M_o = 1.41$; configuration 1G										
○	1.07	0.91	----	----	1.07	0.91	1.04	0.90	1.00	0.86
□	----	----	1.07	0.92	----	----	----	----	----	----
◇	1.01	.93	1.01	.93	1.01	.93	.90	.93	.87	.91
△	.77	.95	.76	.95	.76	.95	.77	.95	.75	.93
▽	.52	.95	.52	.95	.52	.95	.52	.95	.52	.95

TABLE II.- MASS-FLOW RATIOS AND PRESSURE RECOVERIES

CORRESPONDING TO DATA POINTS IN FIGURES 6 TO 12

AND 16 TO 18 - Continued

Symbol	$\alpha = -5°$		$\alpha = 0°$		$\alpha = 5°$		$\alpha = 10°$		$\alpha = 15°$	
	m/m_o	$\bar{H}/H_o$	m/m_o	$\bar{H}/H_o$	m/m_o	$\bar{H}/H_o$	m/m_o	$\bar{H}/H_o$	m/m_o	$\bar{H}/H_o$
$M_o = 1.41$; configuration 1H										
○	1.08	0.92	----	----	1.08	0.93	1.06	0.92	1.04	0.90
□	1.05	.93	1.08	0.93	1.05	.93	----	----	.96	.93
◇	.97	.94	1.05	.93	.97	.94	.97	.94	----	----
△	.84	.95	.84	.95	.84	.95	.84	.95	.84	.94
▽	.58	.95	.57	.95	.58	.95	.57	.95	.57	.95
$M_o = 1.41$; configuration 2B										
○	----	----	----	----	----	----	----	----	----	----
□	1.07	0.92	1.07	0.91	1.07	0.92	1.05	0.91	1.03	0.89
◇	1.04	.92	1.04	.92	1.04	.92	1.03	.92	1.01	.90
△	.84	.94	.84	.95	.84	.94	.84	.94	.83	.94
▽	.52	.95	.52	.95	.51	.95	.52	.95	.52	.95
$M_o = 1.81$; configuration 1A										
○	1.02	0.67	1.03	0.67	1.03	0.67	1.01	0.65	----	----
□	1.01	.78	1.02	.78	1.01	.78	.99	.76	0.94	0.74
◇	----	----	----	----	----	----	----	----	----	----
△	.76	.80	.76	.80	.75	.80	.75	.80	.75	.79
▽	.46	.80	.46	.80	.46	.80	.45	.80	.46	.80
$M_o = 1.81$; configuration 1C										
○	1.16	0.75	----	----	----	----	1.12	0.71	----	----
□	----	----	1.17	0.77	1.16	0.77	1.08	.77	0.98	0.75
◇	1.10	.79	1.10	.79	1.10	.78	1.02	.78	----	----
△	.92	.80	.91	.80	.91	.79	.76	.80	.74	.79
▽	.46	.80	.46	.80	.46	.80	.46	.80	.46	.80

[redacted]

TABLE II.- MASS-FLOW RATIOS AND PRESSURE RECOVERIES CORRESPONDING TO DATA POINTS IN FIGURES 6 TO 12 AND 16 TO 18 - Concluded

Symbol	$\alpha = -5°$		$\alpha = 0°$		$\alpha = 5°$		$\alpha = 10°$		$\alpha = 15°$	
	m/m_o	$\overline{H}/H_o$	m/m_o	$\overline{H}/H_o$	m/m_o	$\overline{H}/H_o$	m/m_o	$\overline{H}/H_o$	m/m_o	$\overline{H}/H_o$
$M_o = 1.81$; configuration 1E										
○	----	----	----	----	----	----	----	----	----	----
□	----	----	----	----	----	----	1.13	0.75	1.09	0.72
◇	1.17	0.79	1.17	0.79	1.17	0.78	----	----	1.05	.74
△	.91	.80	.91	.79	.91	.80	.76	.80	.74	.78
▽	.46	.80	.46	.80	.46	.80	.46	.80	.46	.79
$M_o = 1.81$; configuration 1G										
○	----	----	1.13	0.73	----	----	----	----	----	----
□	1.12	0.76	1.09	.78	1.12	0.75	1.07	0.73	1.01	0.71
◇	1.09	.78	1.02	.79	1.09	.77	1.03	.75	.99	.72
△	.91	.80	.91	.80	.91	.79	.89	.79	.87	.75
▽	.46	.80	.46	.80	.46	.80	.46	.80	.46	.80
$M_o = 1.81$; configuration 1H										
○	----	----	----	----	----	----	----	----	----	----
□	1.17	0.77	1.16	0.78	1.16	0.77	1.15	0.76	1.10	0.73
◇	1.10	.79	1.10	.79	1.10	.79	1.09	.78	1.06	.76
△	.91	.80	.91	.80	.91	.80	.91	.80	.90	.79
▽	.46	.80	.45	.80	.45	.80	.45	.80	.46	.80
$M_o = 1.81$; configuration 2B										
○	----	----	----	----	----	----	----	----	1.06	0.67
□	1.13	0.77	1.15	0.77	1.13	0.76	1.11	0.75	----	----
◇	1.09	.78	1.11	.78	1.09	.78	1.09	.77	1.04	.71
△	.85	.80	.87	.80	.85	.80	.85	.80	.85	.78
▽	.45	.80	.47	.80	.45	.80	.45	.80	.46	.80

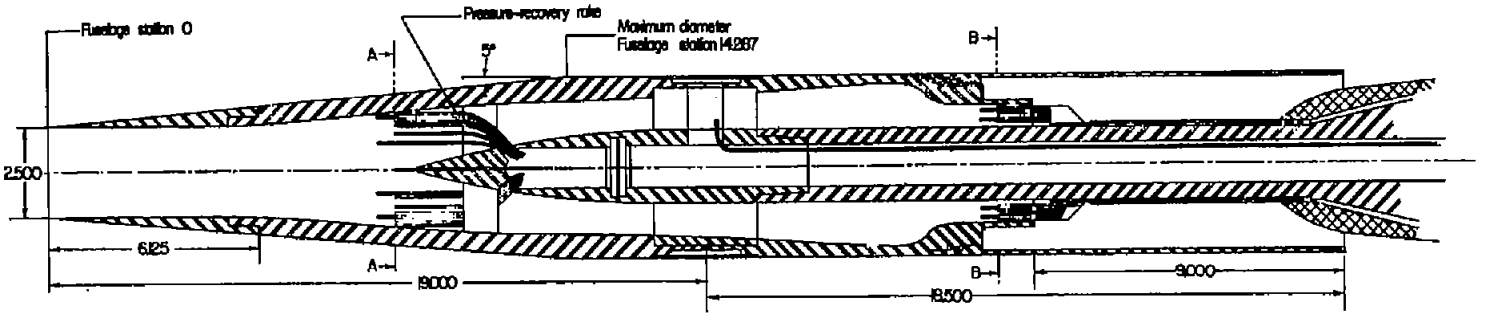

Pressure model shown with nose 1 and lip 1A

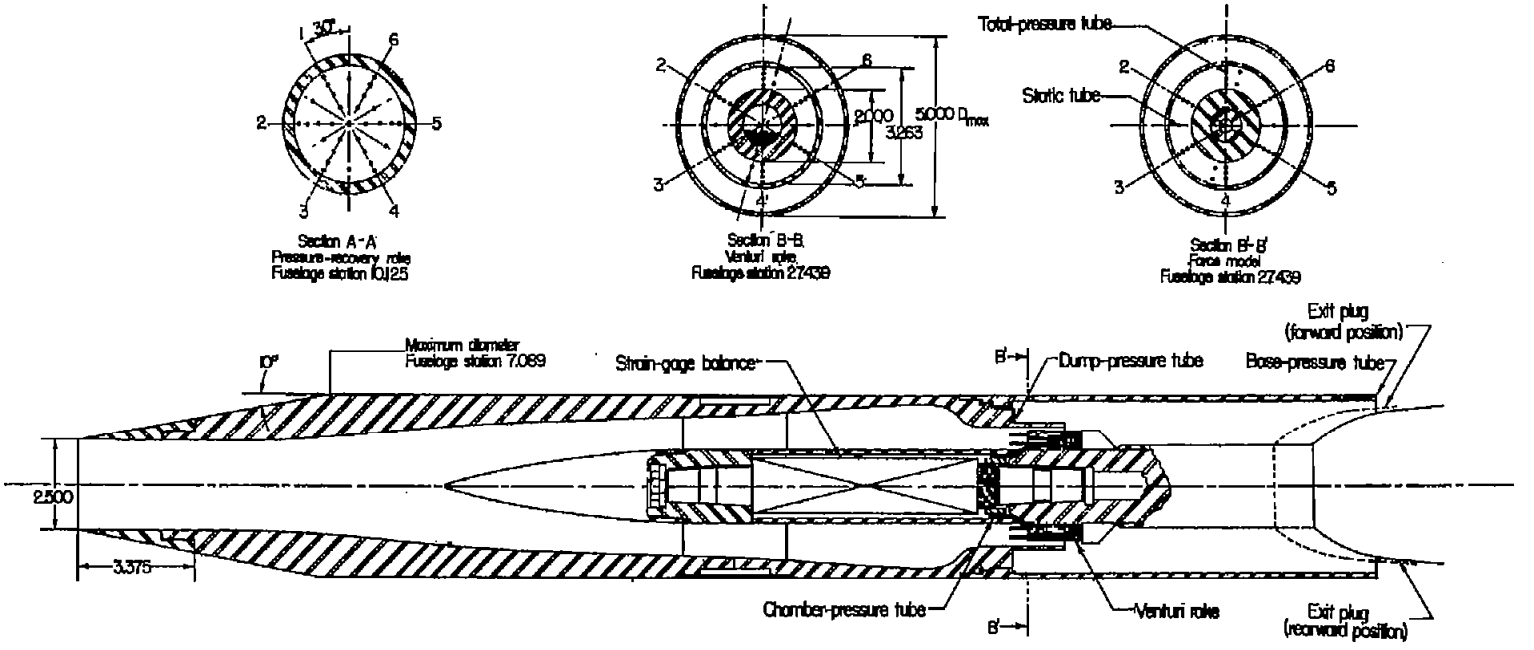

Force model shown with nose 2 and lip 2A

Figure 1.- Schematic drawing of nose-inlet fuselage assemblies. All linear dimensions are in inches.

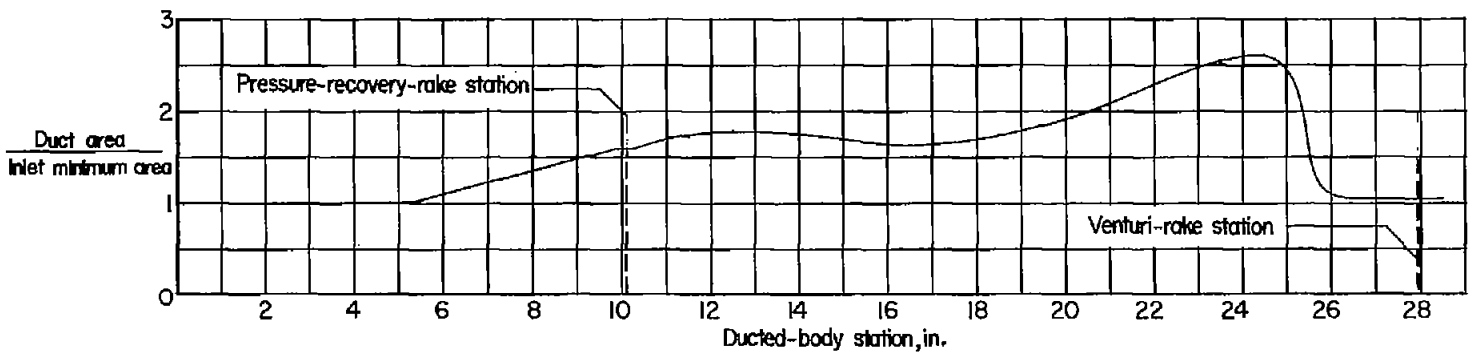

Figure 2.- Variation of inlet duct area with longitudinal station.

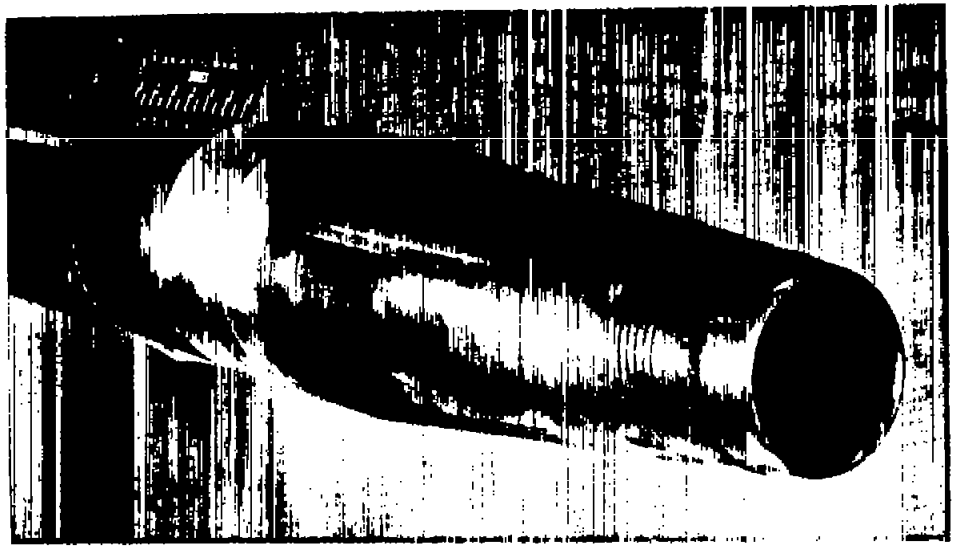

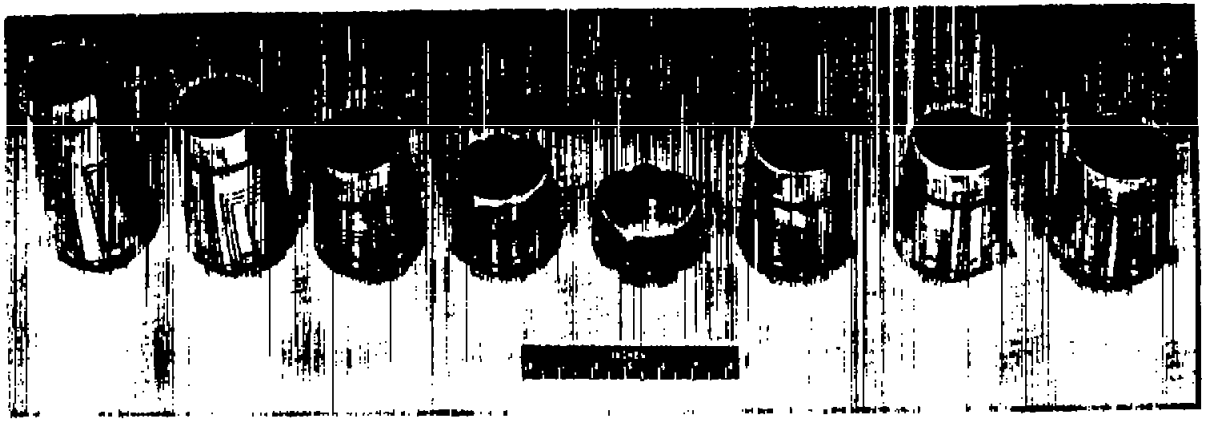

L-57-1622

(a) 5° model and interchangeable nose sections.

Figure 3.- Photographs of models.

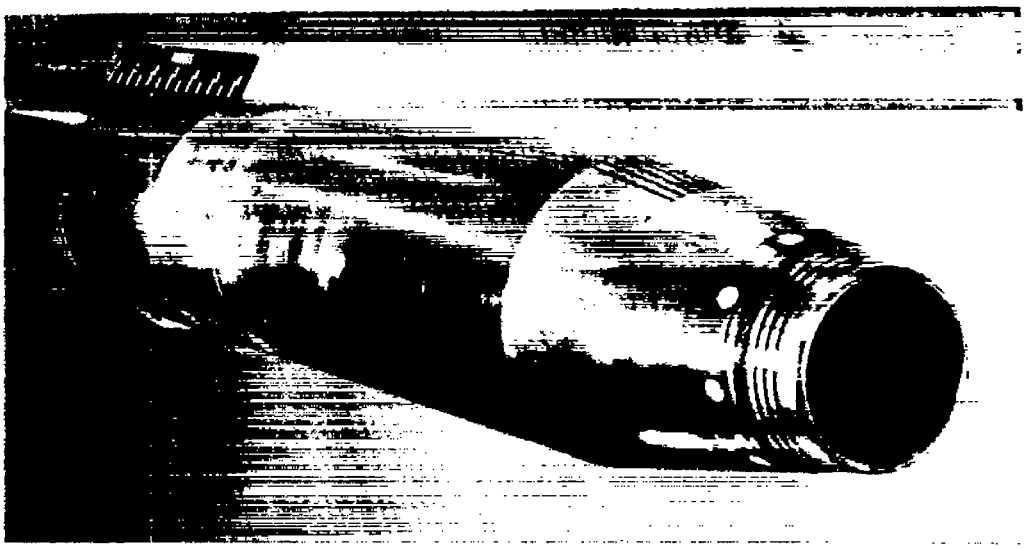

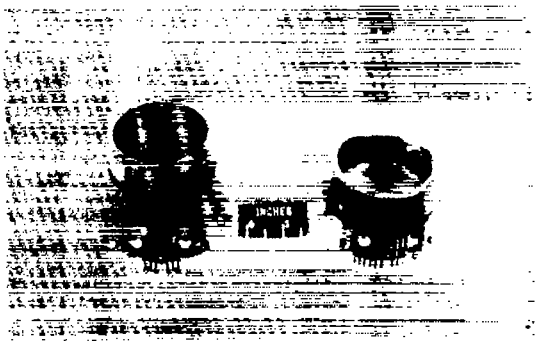

L-57-1623

(b) 10° model and interchangeable nose sections.

Figure 3.- Concluded.

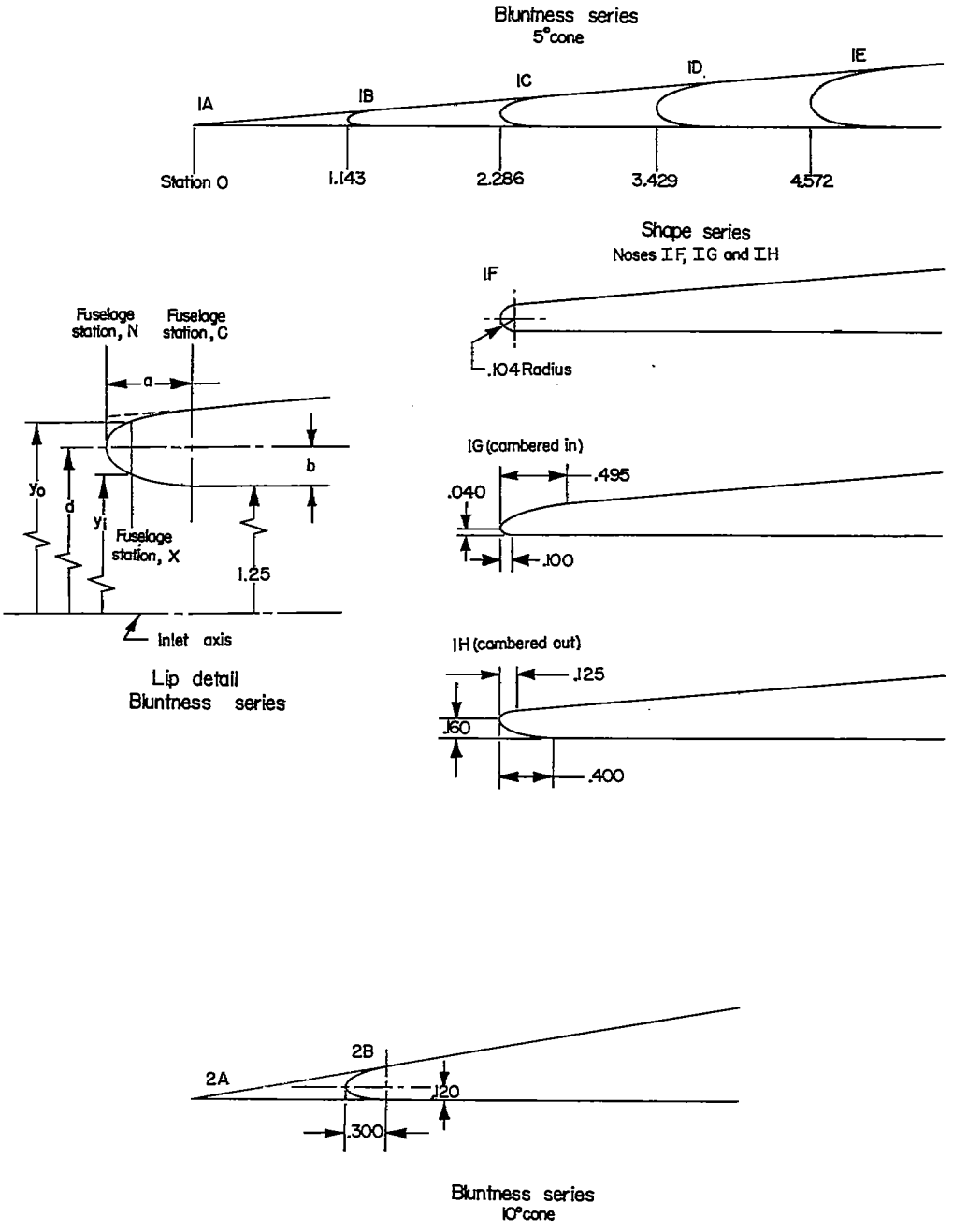

Figure 4.- Nose-inlet configurations. All dimensions are in inches.

[redacted]

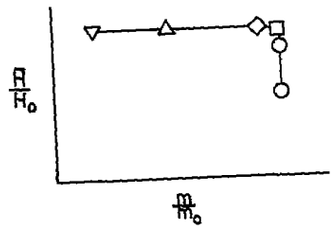

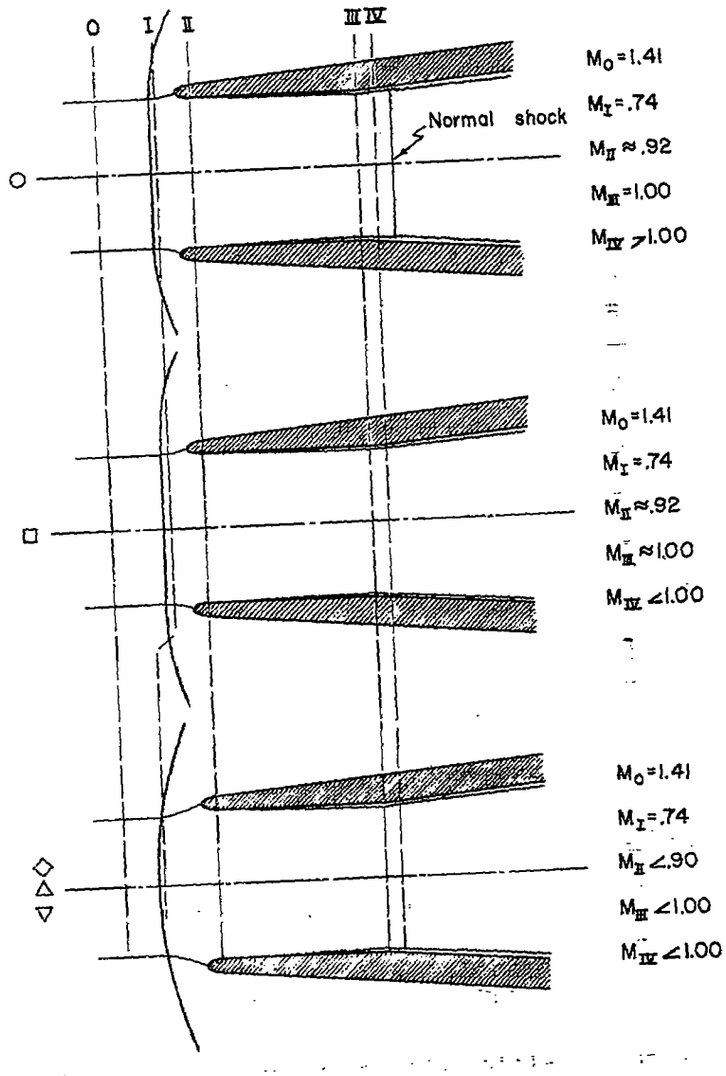

Figure 5.- Scheme of designation of type of inlet operation.

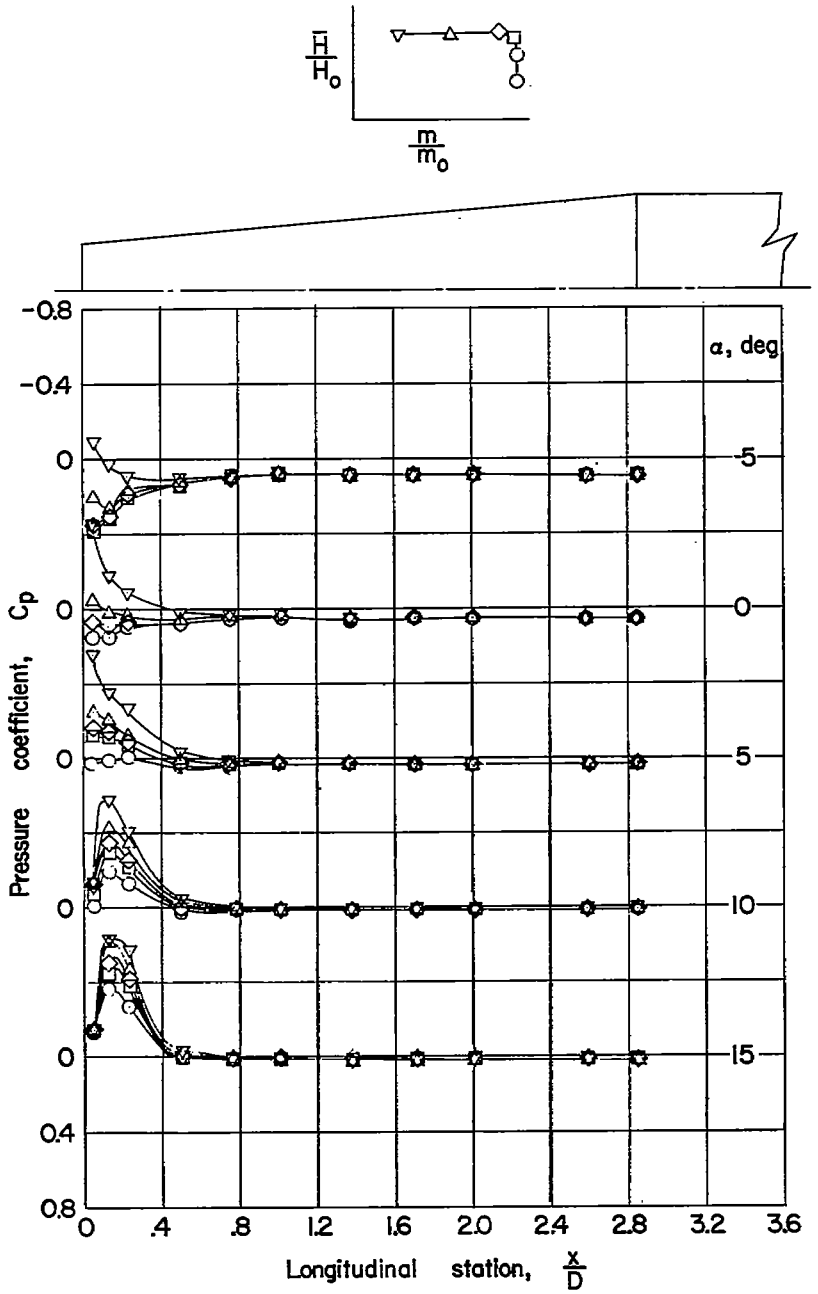

(a) Configuration 1A; $M_o = 1.41$.

Figure 6.- Pressure coefficients in the angle-of-attack plane along the tops of the forebodies.

[redacted]

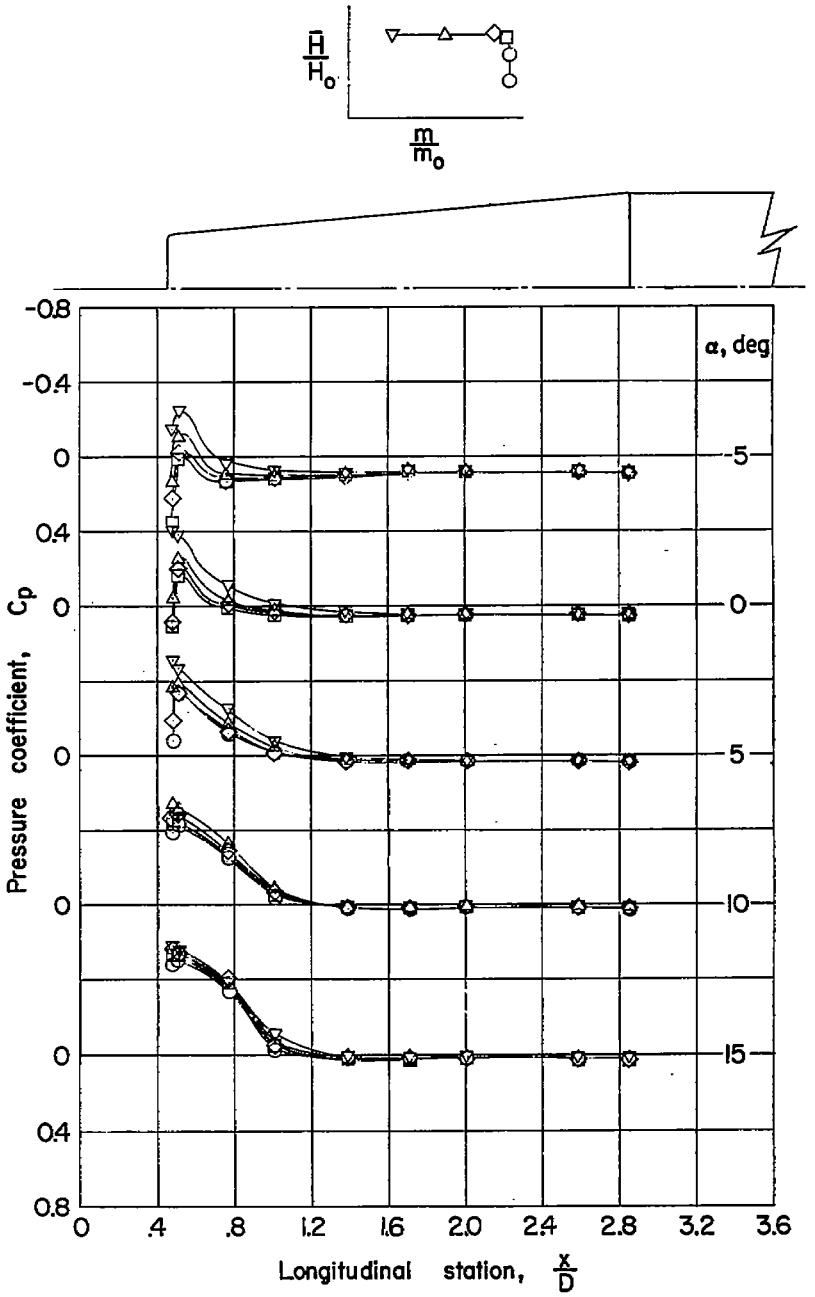

(b) Configuration 1C; M_o = 1.41.

Figure 6.- Continued.

[redacted]

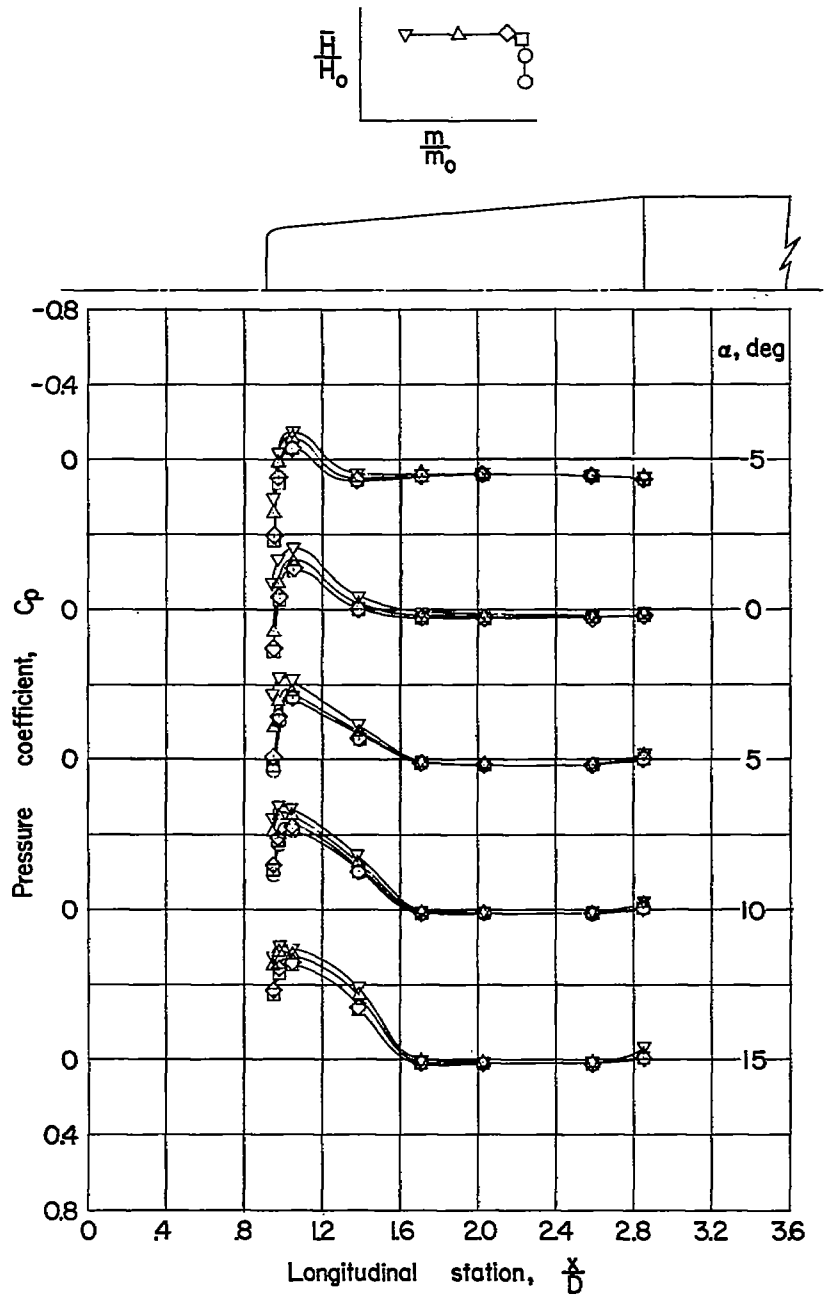

(c) Configuration 1E; M_o = 1.41.

Figure 6.- Continued.

[redacted]

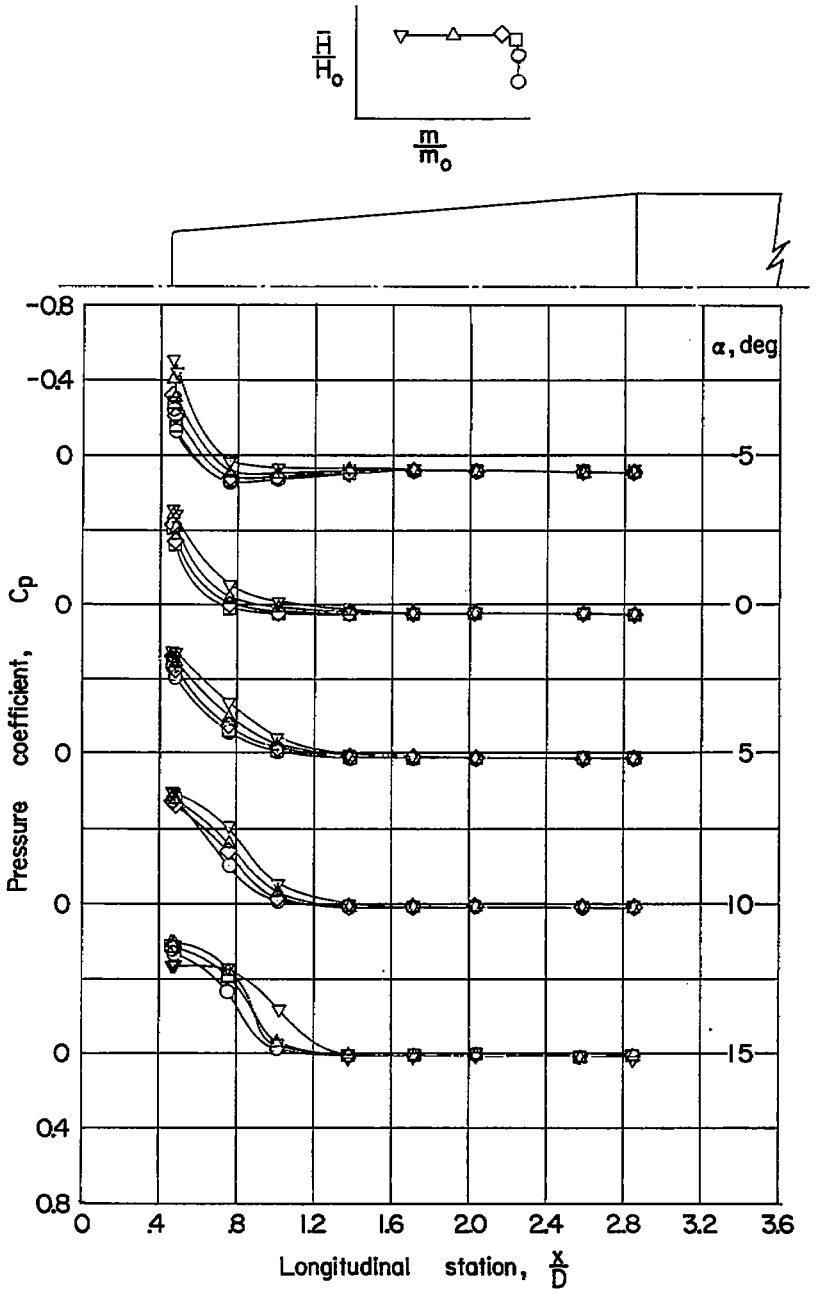

(d) Configuration 1G; M_o = 1.41.

Figure 6.- Continued.

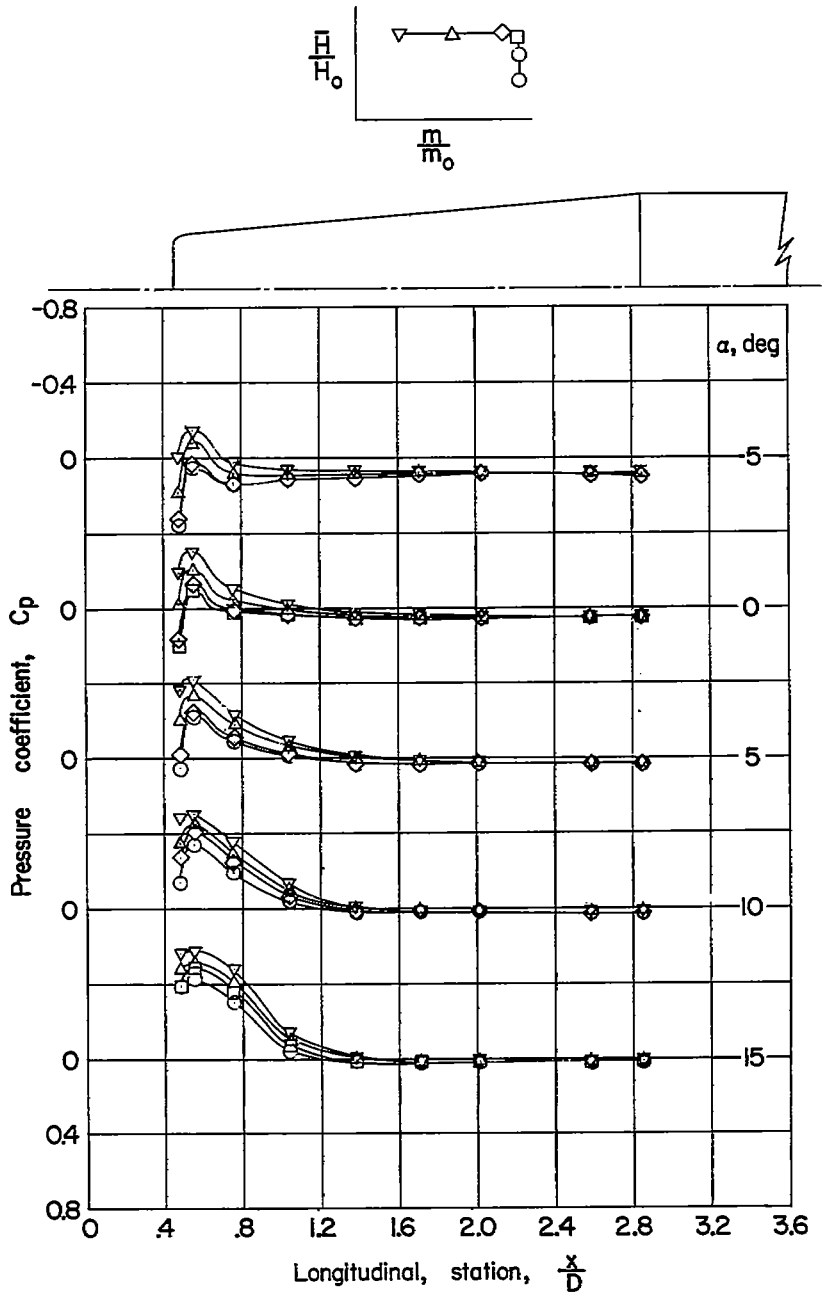

(e) Configuration 1H; M_o = 1.41.

Figure 6.- Continued.

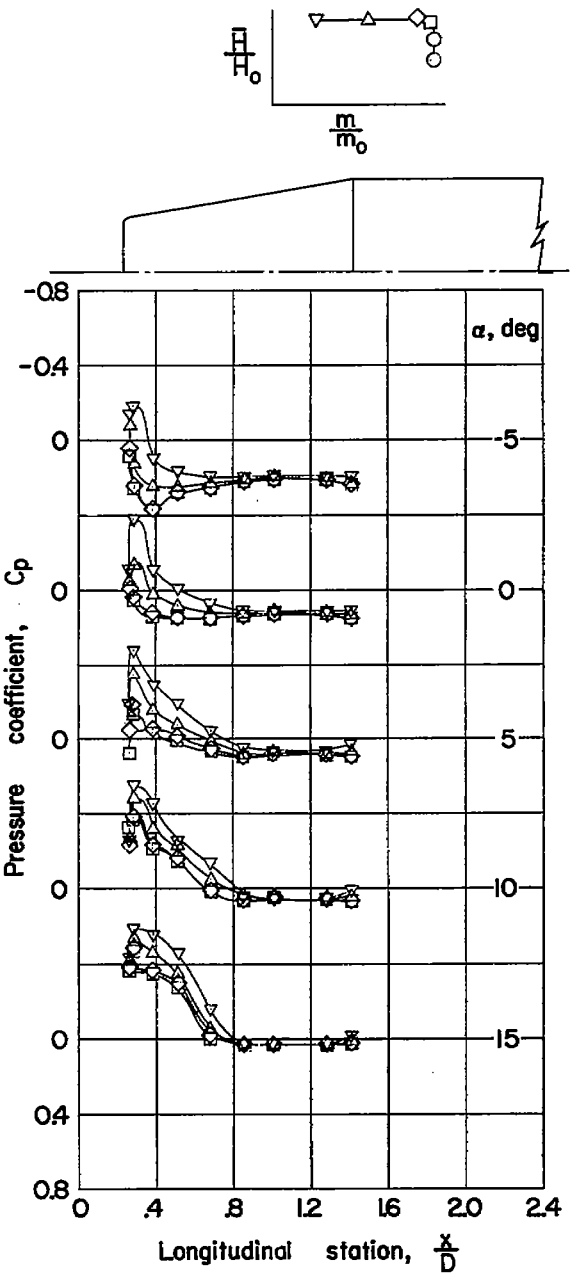

(f) Configuration 2B; M_o = 1.41.

Figure 6.- Continued.

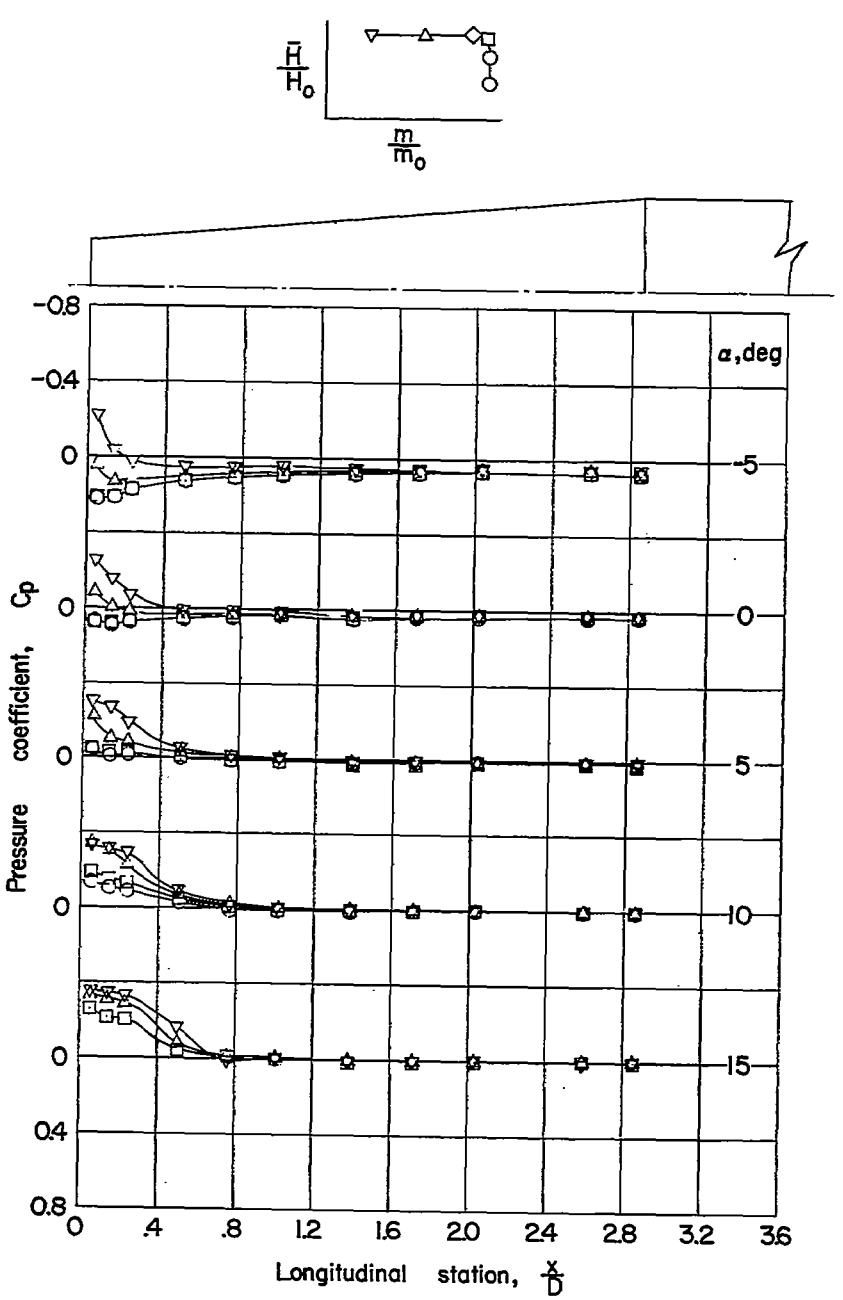

(g) Configuration 1A; M_o = 1.81.

Figure 6.- Continued.

[redacted]

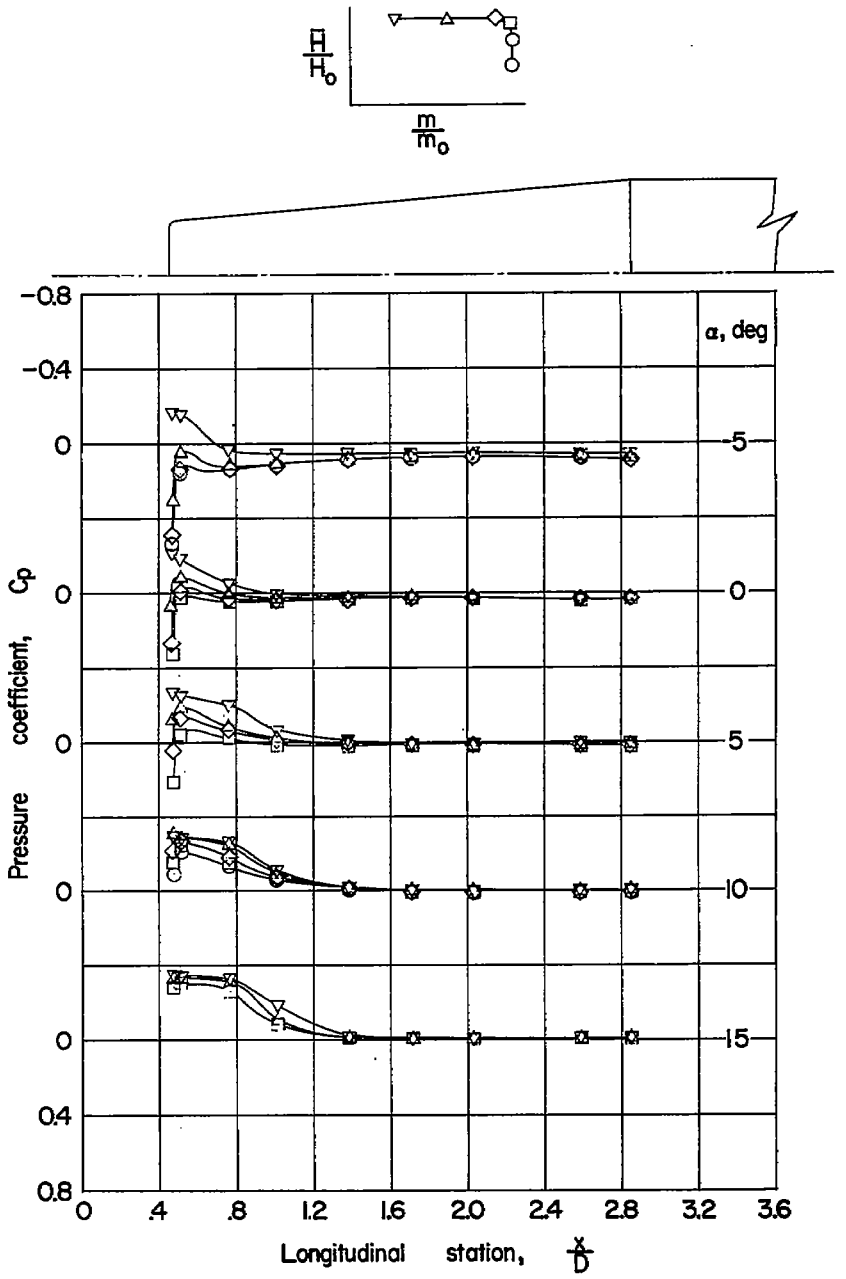

(h) Configuration 1C; M_o = 1.81.

Figure 6.- Continued.

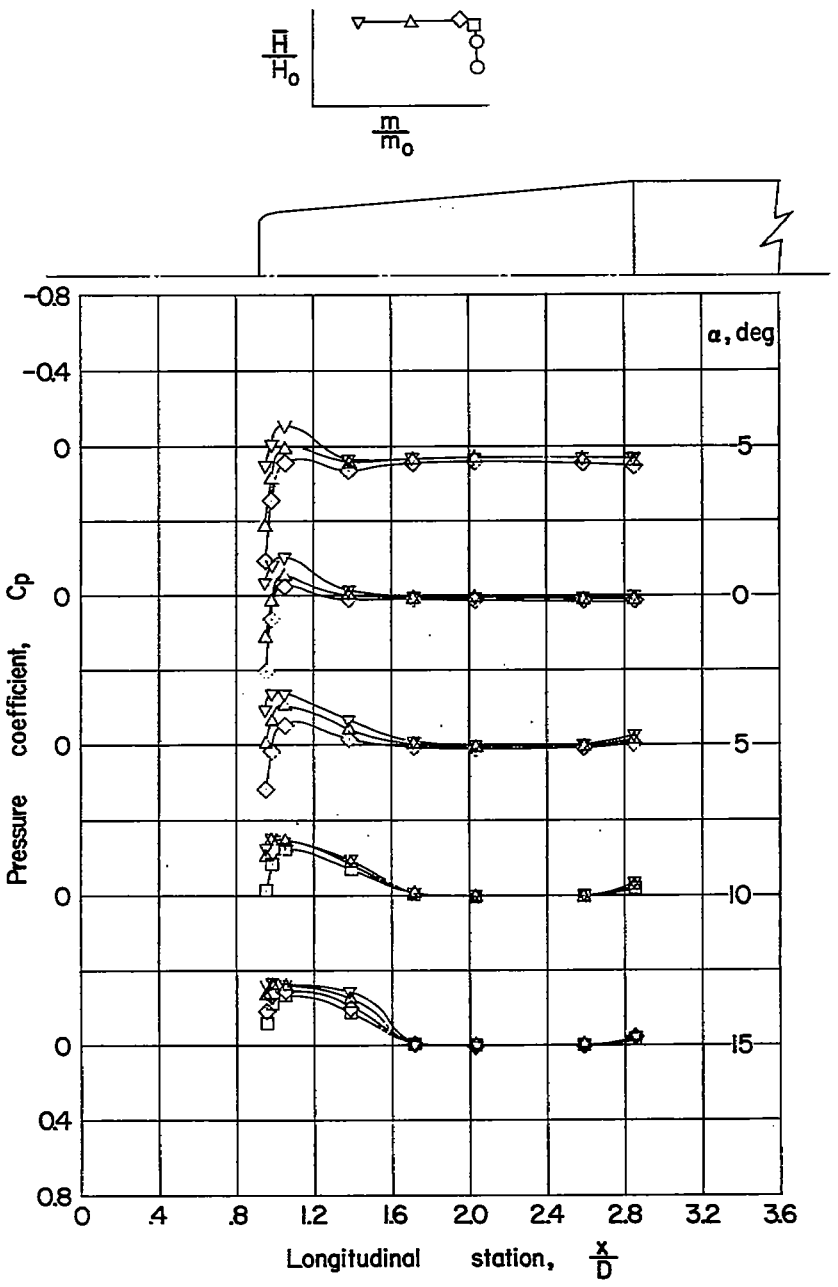

(i) Configuration 1E; M_0 = 1.81.

Figure 6.- Continued.

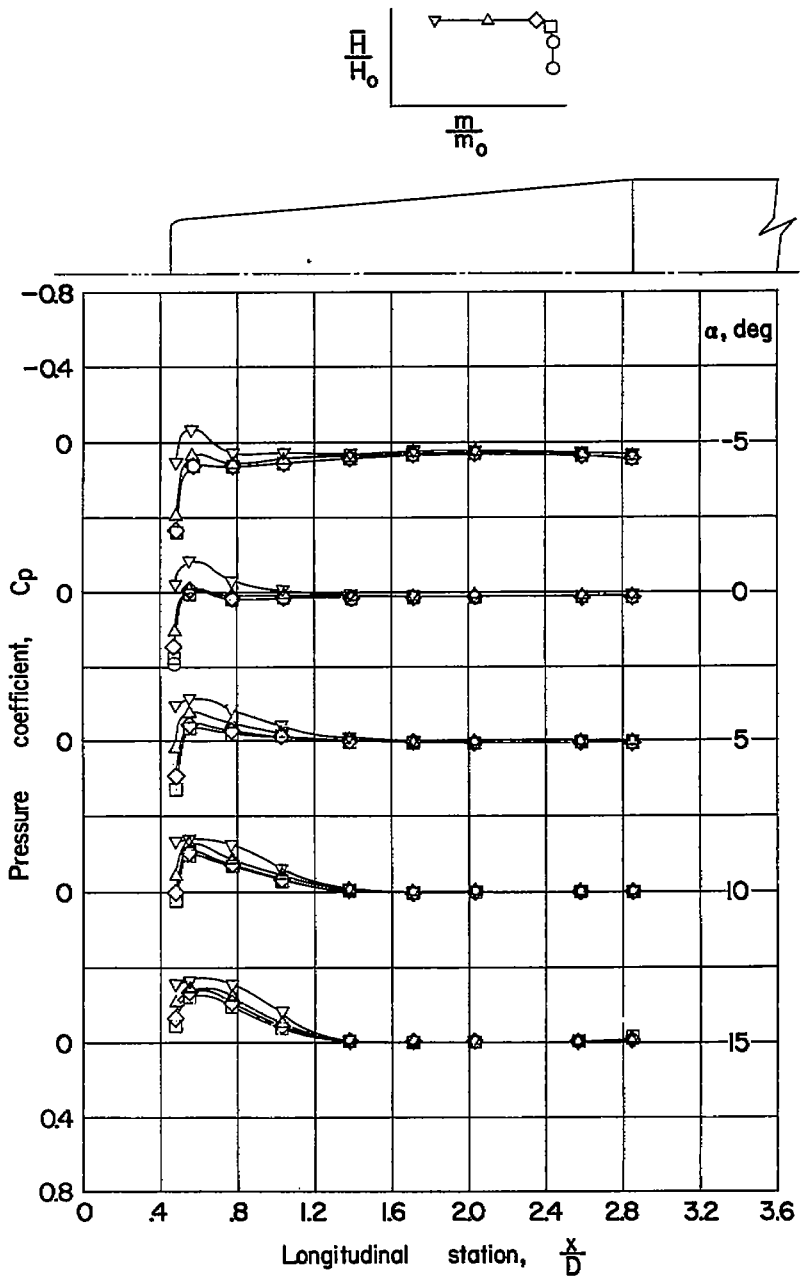

(j) Configuration 1G; M_o = 1.81.

Figure 6.- Continued.

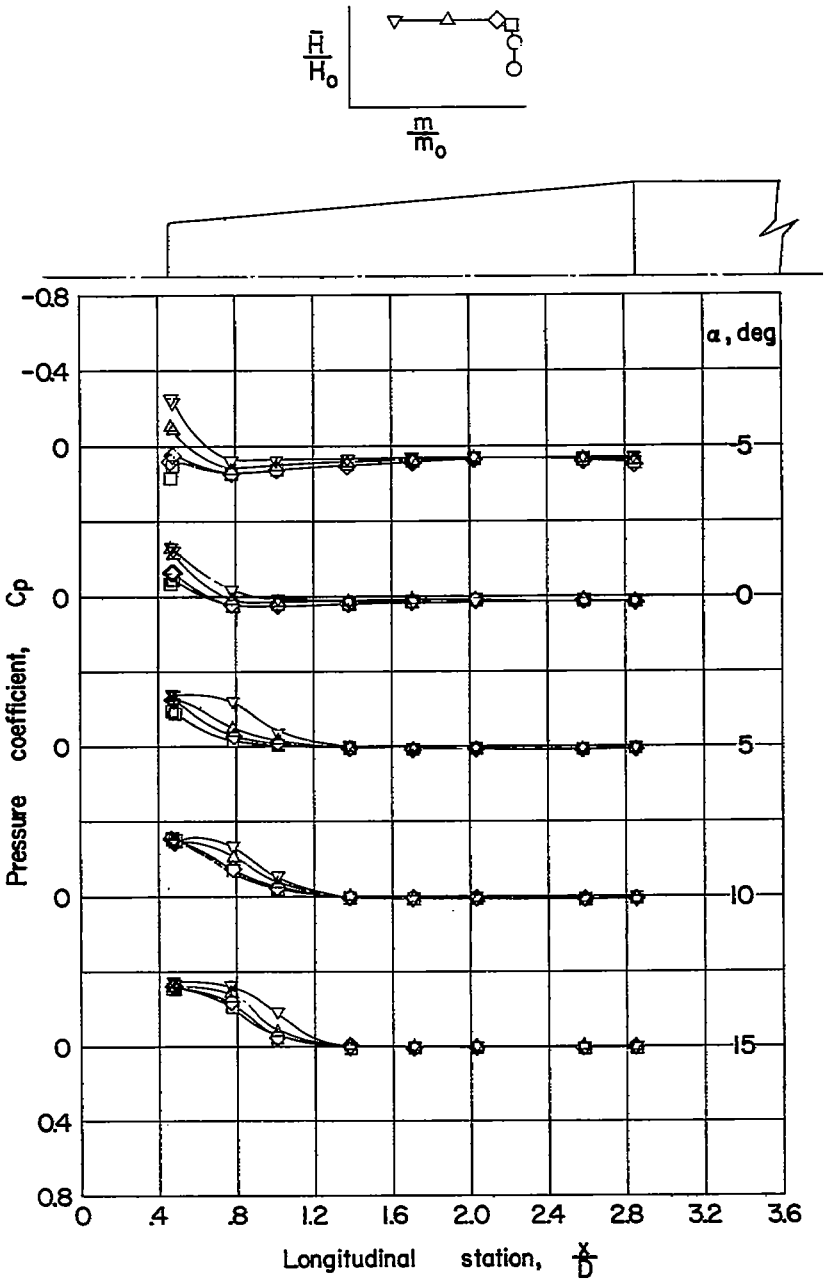

(k) Configuration 1H; M_o = 1.81.

Figure 6.- Continued.

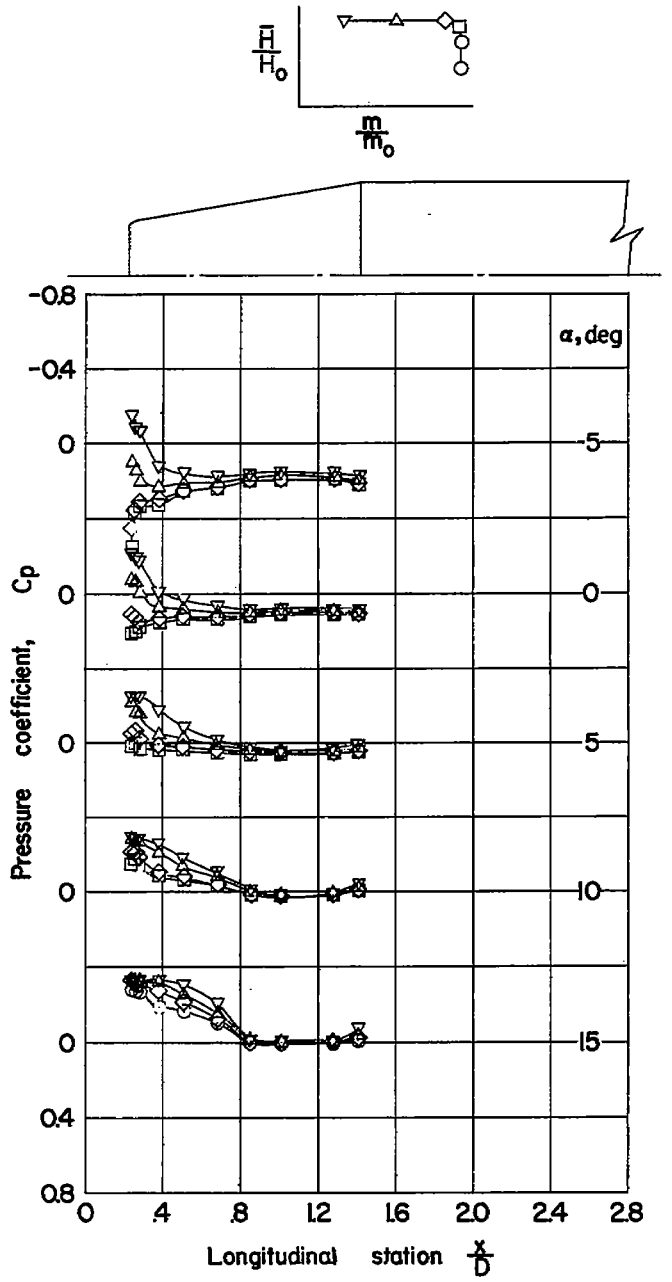

(l) Configuration 2B; M_o = 1.81.

Figure 6.- Concluded.

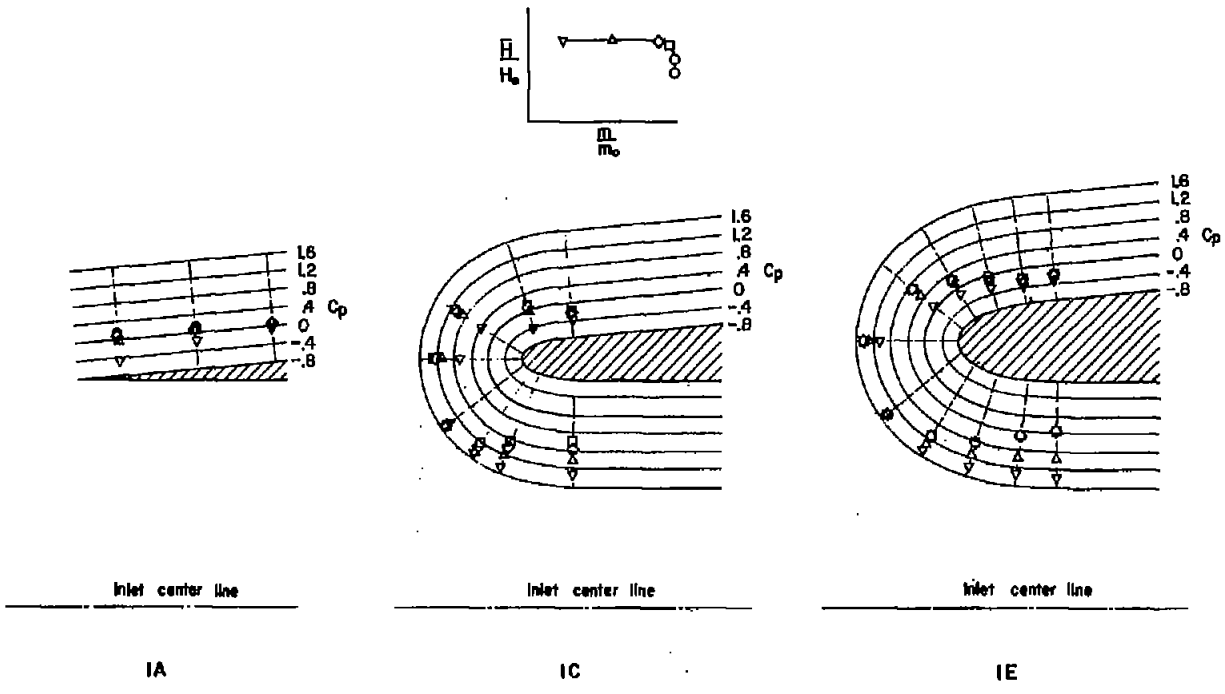

(a) $\alpha = 0^{\circ}$; $M_0 = 1.41$.

Figure 7.- Pressure coefficients around the inlet lips in the angle-of-attack plane for configurations in the lip-bluntness series.

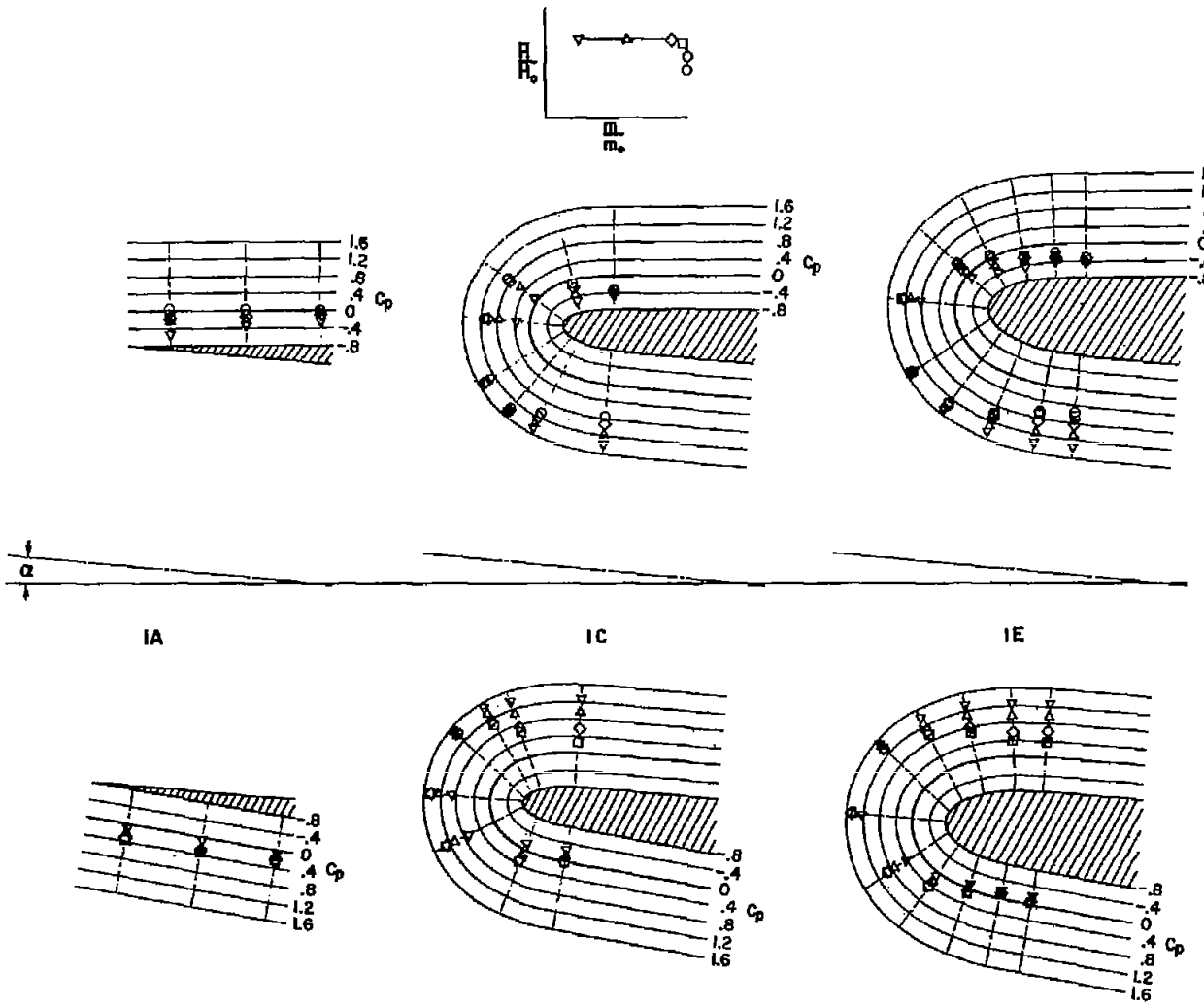

(b) $\alpha = 5^{\circ}$; $M_o = 1.41$.

Figure 7.- Continued.

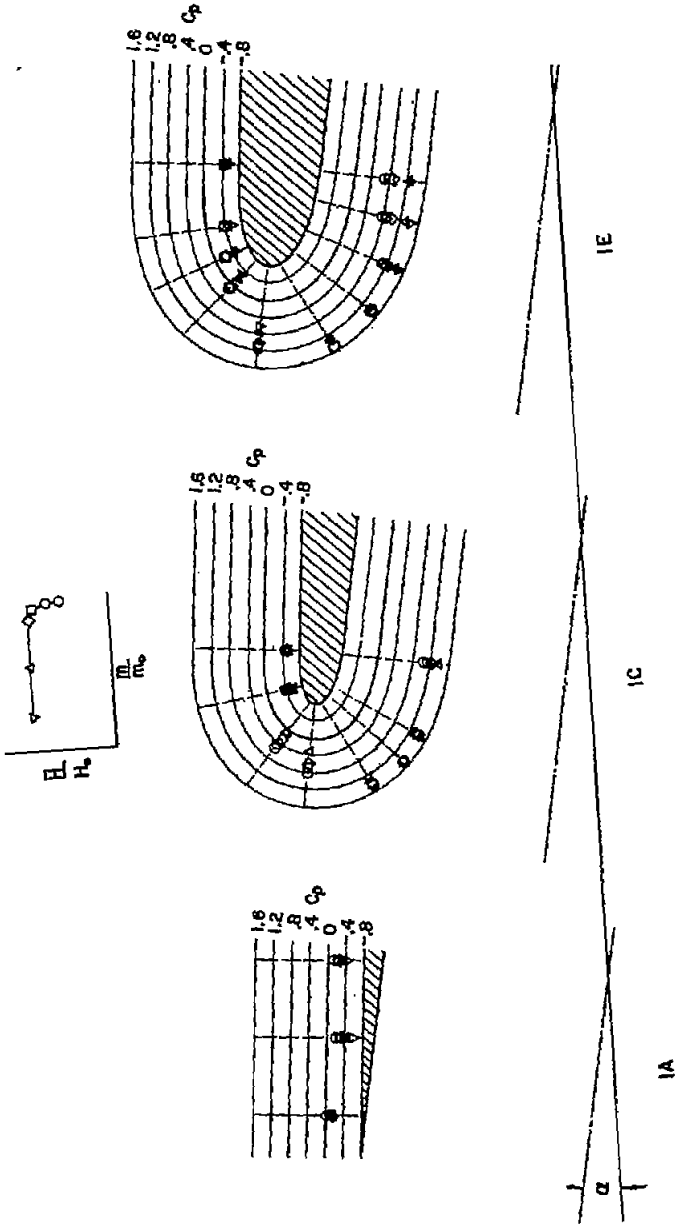

(c) $\alpha = 10°$; $M_o = 1.41$.

Figure 7.- Continued.

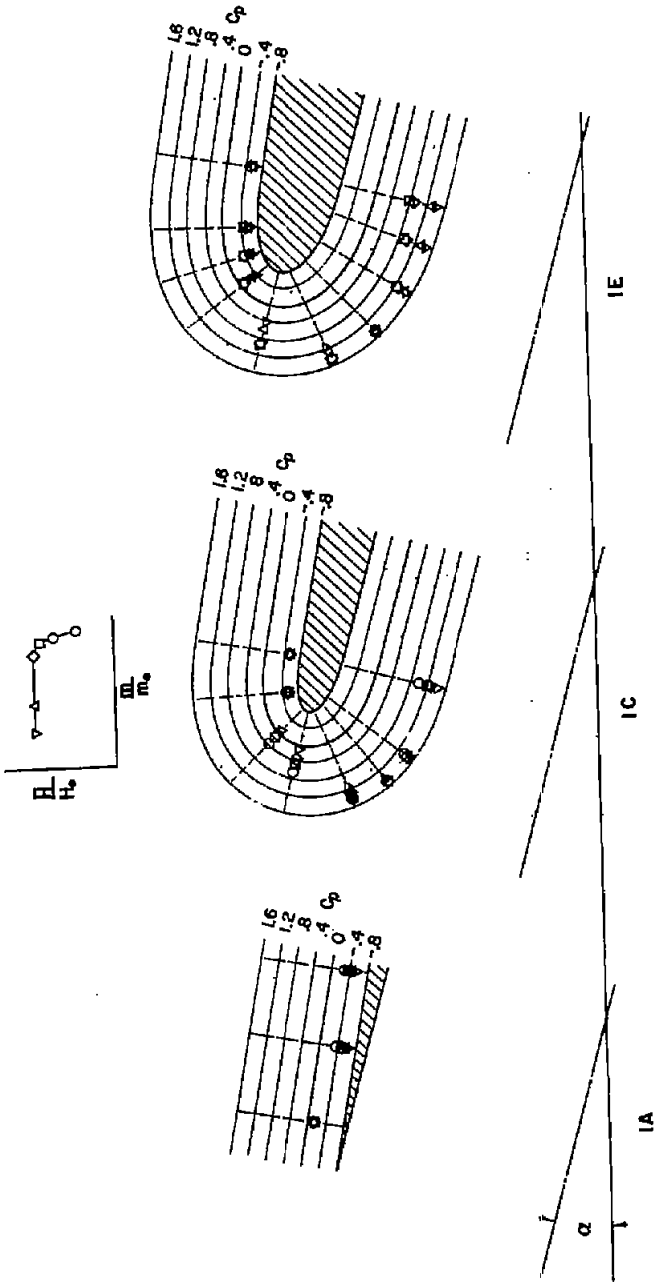

(a) $\alpha = 15^{\circ}$; $M_o = 1.41$.

Figure 7.- Continued.

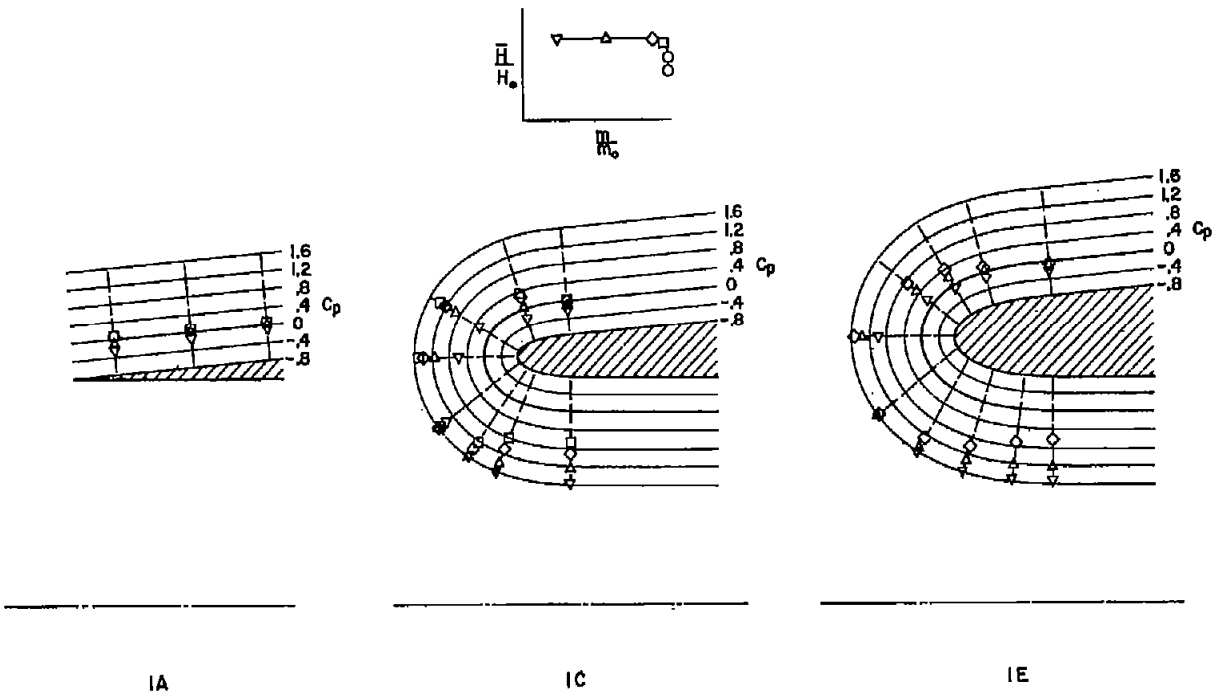

(e) $\alpha = 0^{\circ}$; $M_{O} = 1.81$.

Figure 7.- Continued.

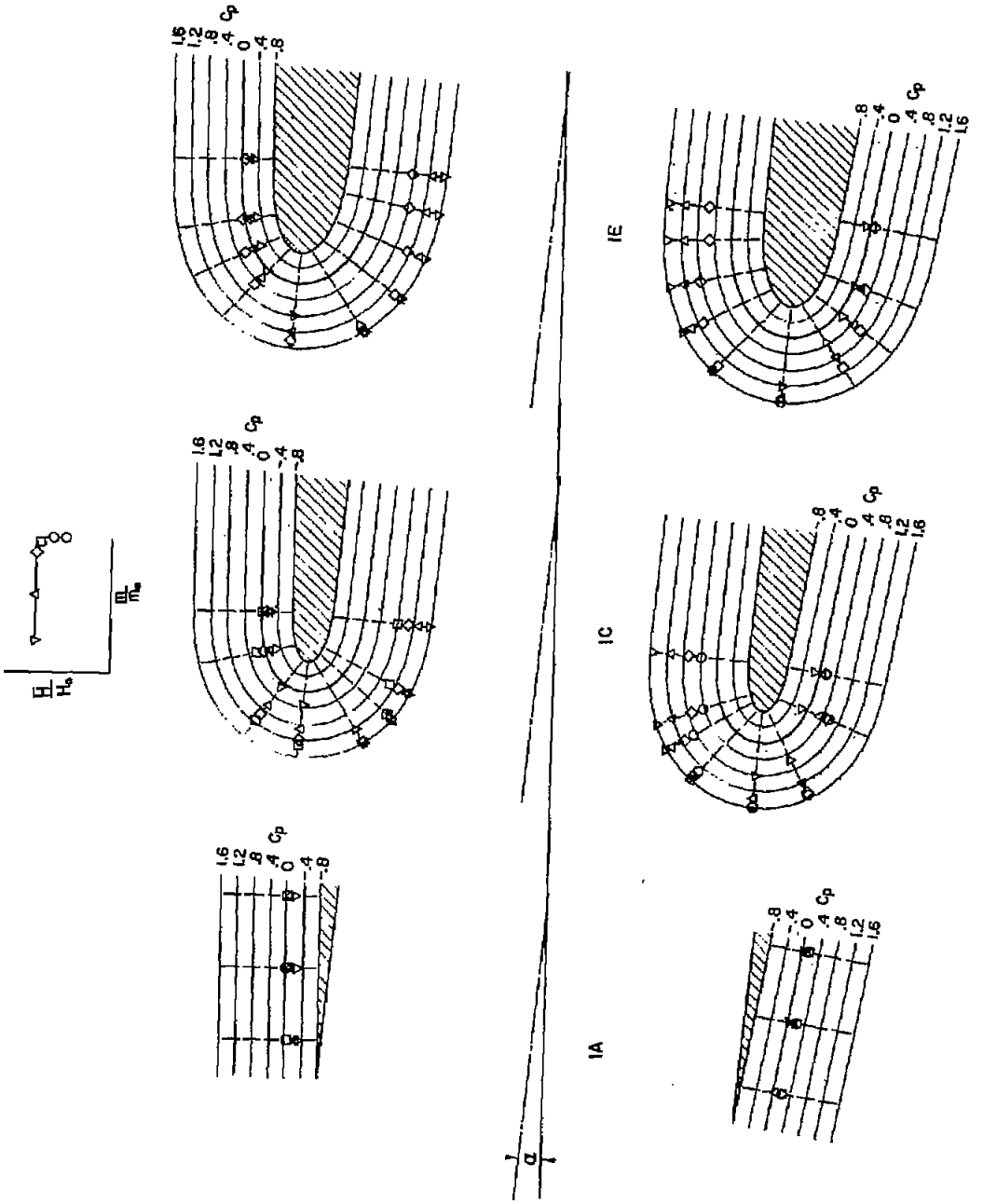

(f) $\alpha = 5^{\circ}$; $M_{\infty} = 5^{\circ}$.

Figure 7.- Continued.

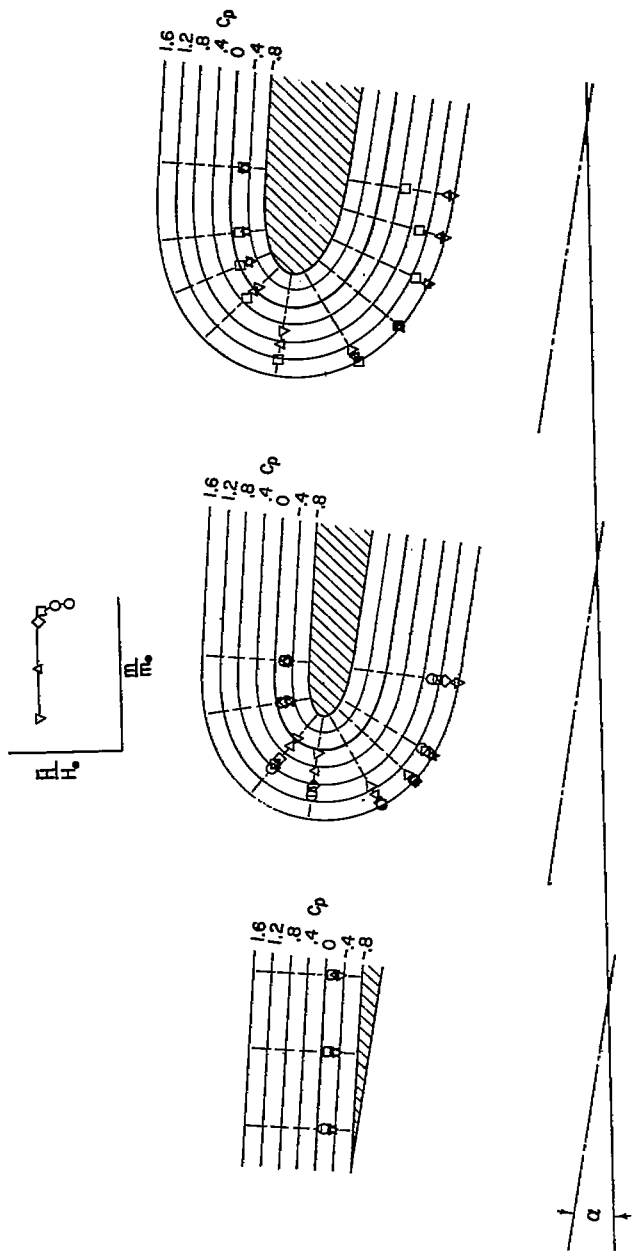

(g) $\alpha = 10^{\circ}$; $M_0 = 1.81$.

Figure 7.- Continued.

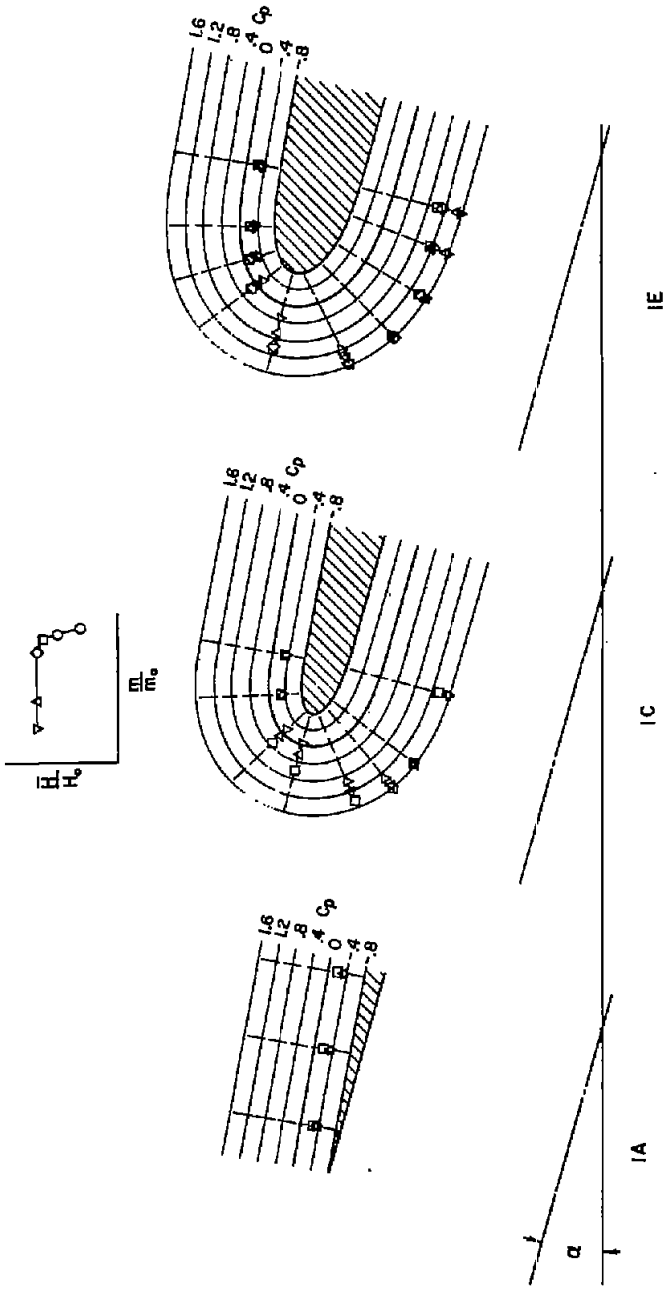

(h) $\alpha = 15^{\circ}$; $M_o = 1.81$.

Figure 7.- Concluded.

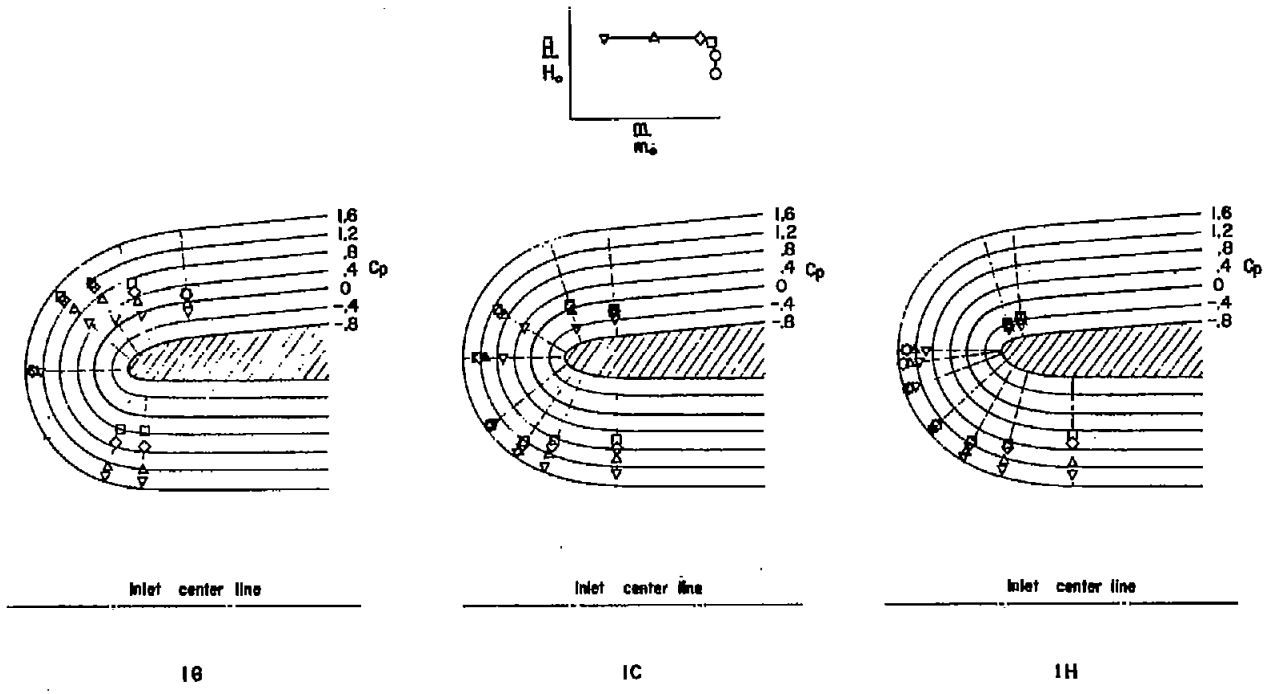

(a) $\alpha = 0^{\circ}$; $M_O = 1.41$.

Figure 8.- Pressure coefficients around the inlet lips in the angle-of-attack plane for configurations in the lip-camber series.

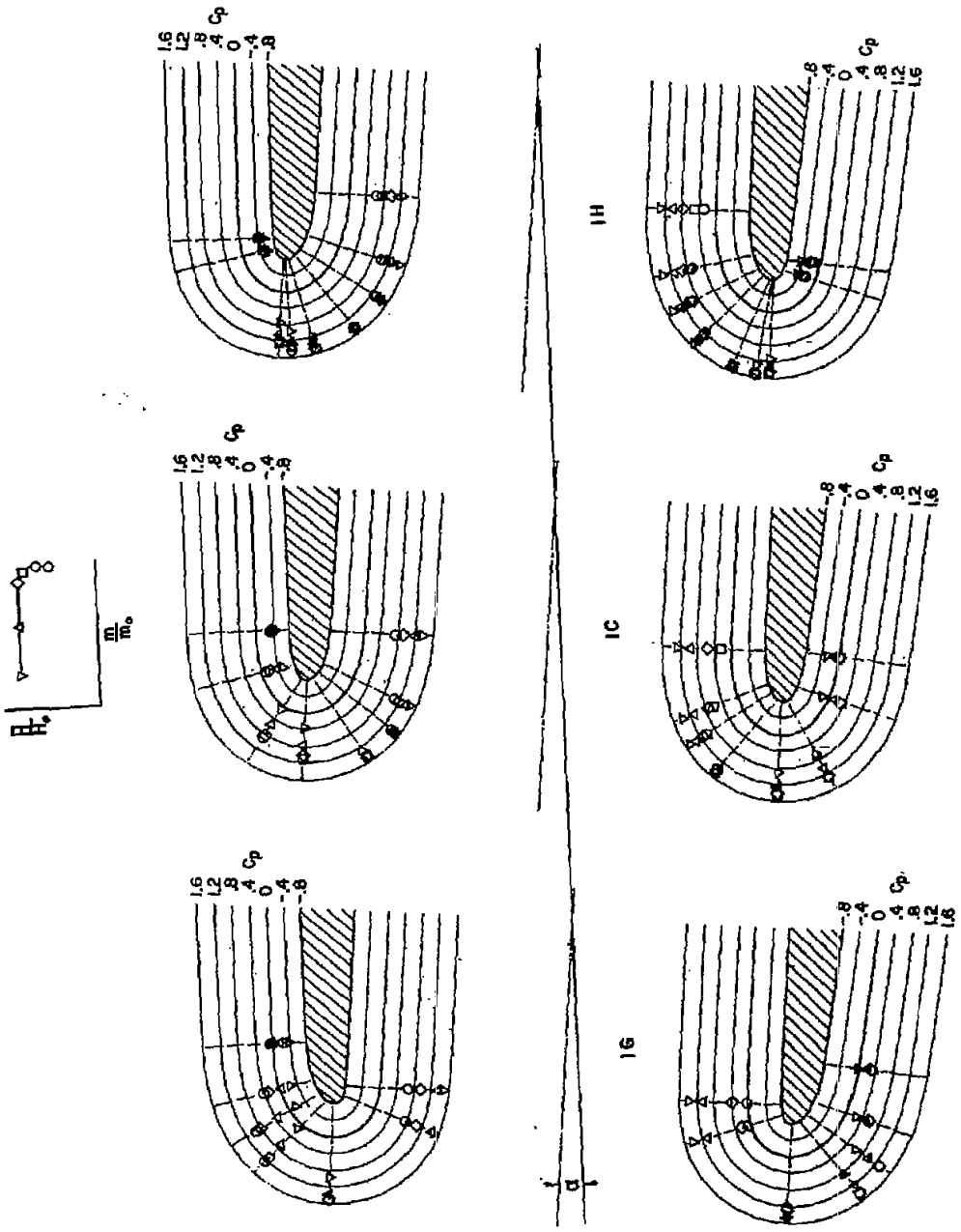

(b) $\alpha = 5^{\circ}$; $M_{\infty} = 1.41$.

Figure 8.- Continued.

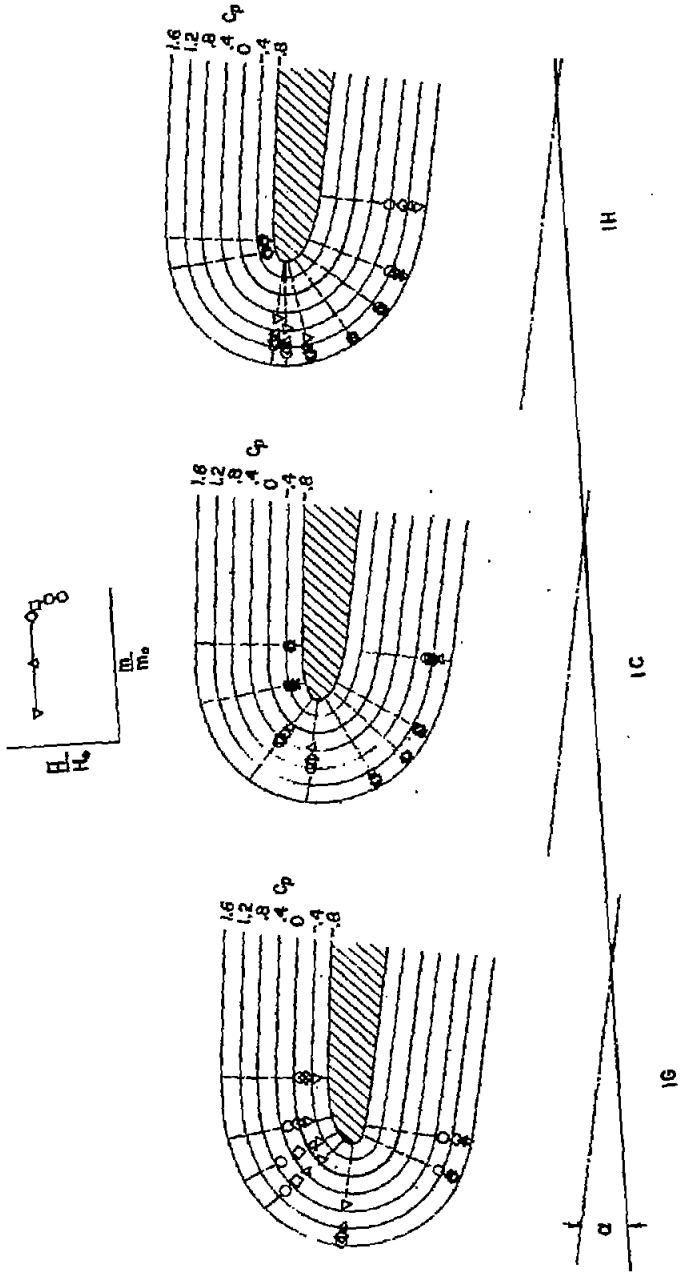

(c) $\alpha = 10^\circ$; $M_o = 1.41$.

Figure 8.- Continued.

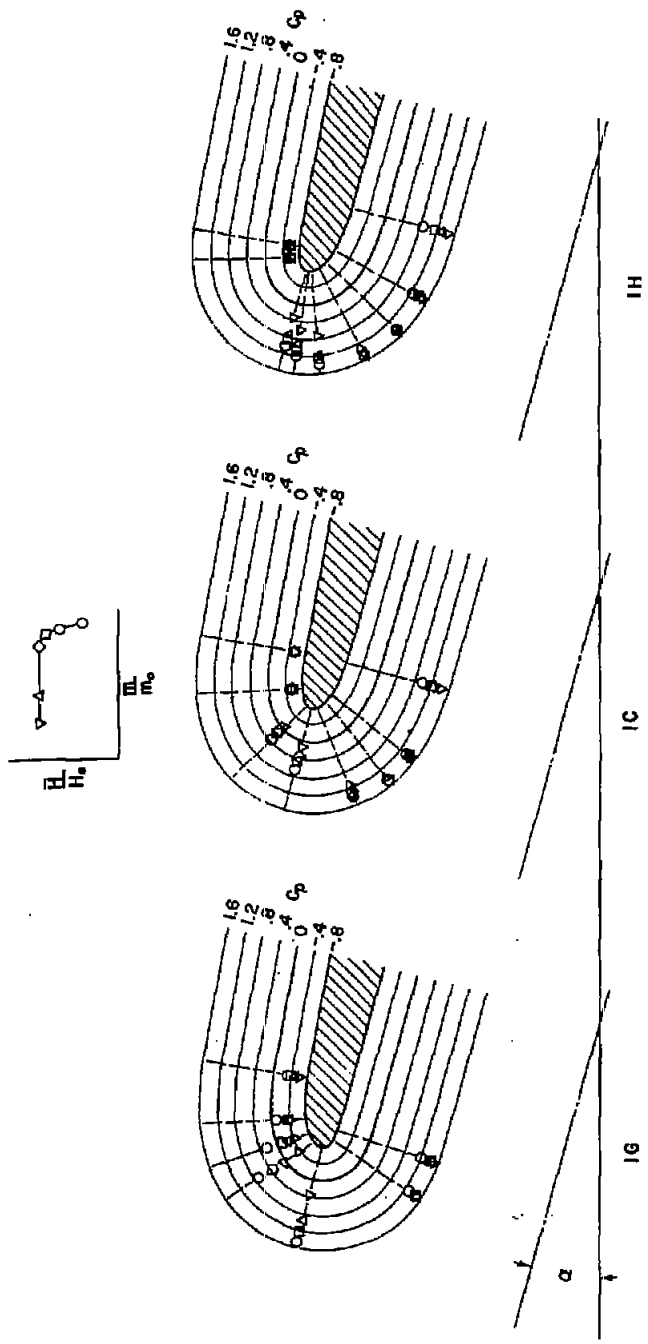

(d) $\alpha = 15°$; $M_o = 1.41$.

Figure 8.- Continued.

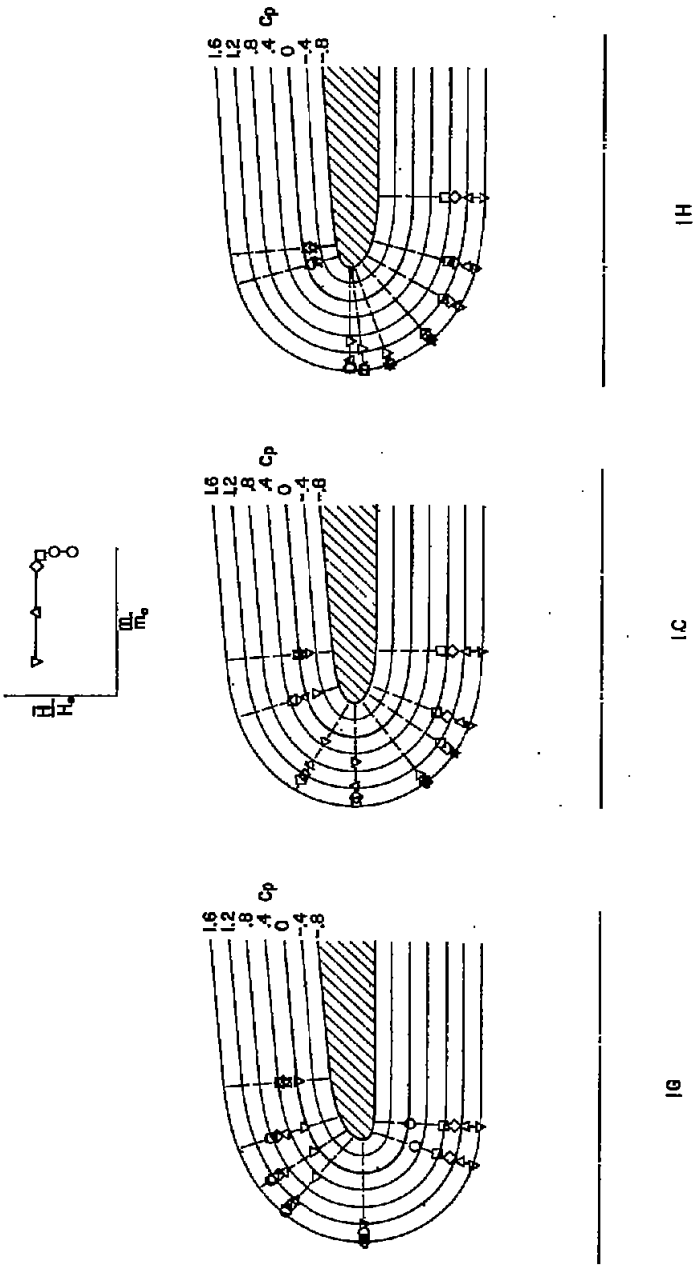

(e) $\alpha = 0°$; $M_o = 1.81$.

Figure 8.- Continued.

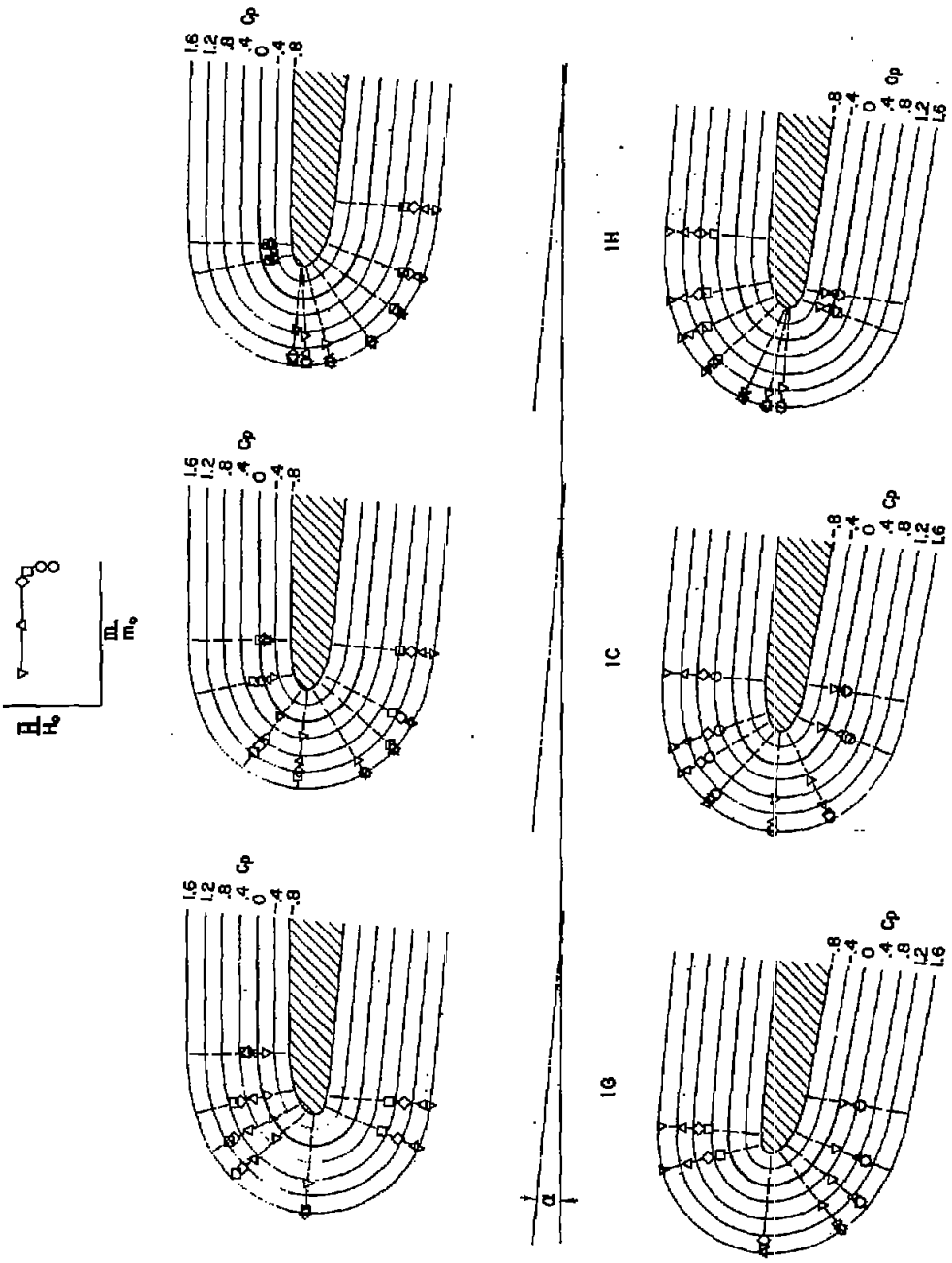

(f) $\alpha = 5^{\circ}$; $M_0 = 1.81$.

Figure 8.- Continued.

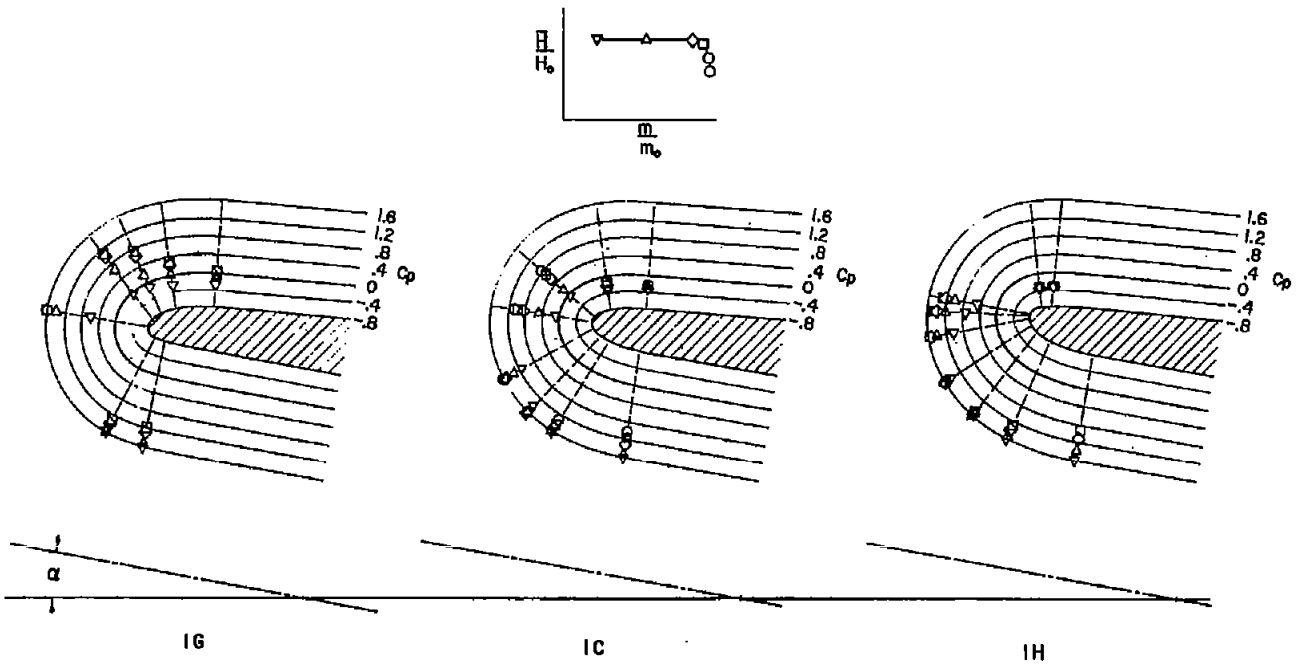

(g) $\alpha = 10^{\circ}$; $M_{\infty} = 1.81$.

Figure 8.- Continued.

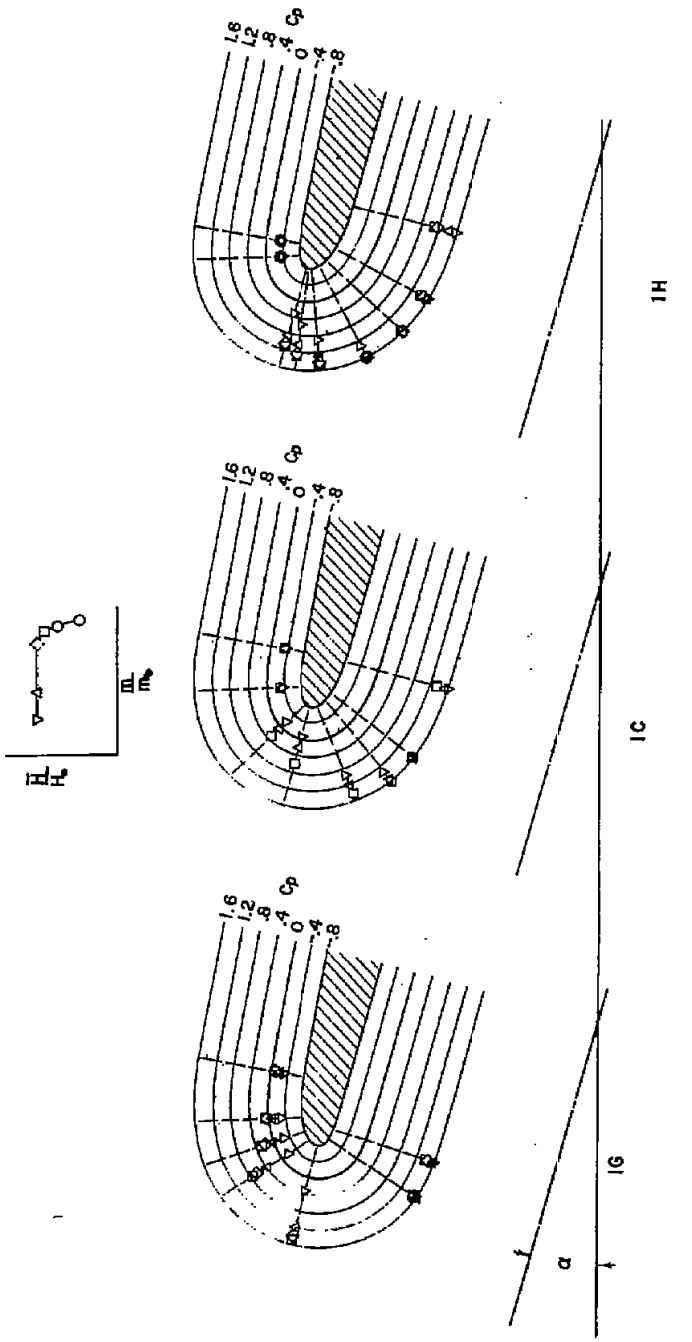

(h) $\alpha = 15^{\circ}$; $M_o = 1.81$.

Figure 8.- Concluded.

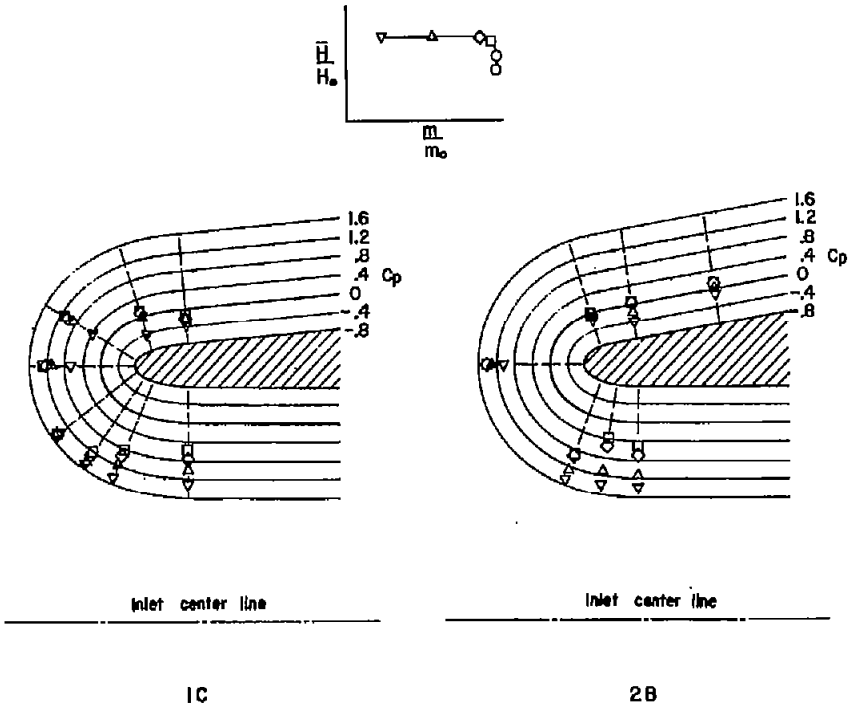

(a) $\alpha = 0^{\circ}$; $M_{O} = 1.41$.

Figure 9.- Pressure coefficients around the inlet lips in the angle-of-attack plane of configurations having the same degree of lip bluntness but having 5° and 10° forebody half-angles.

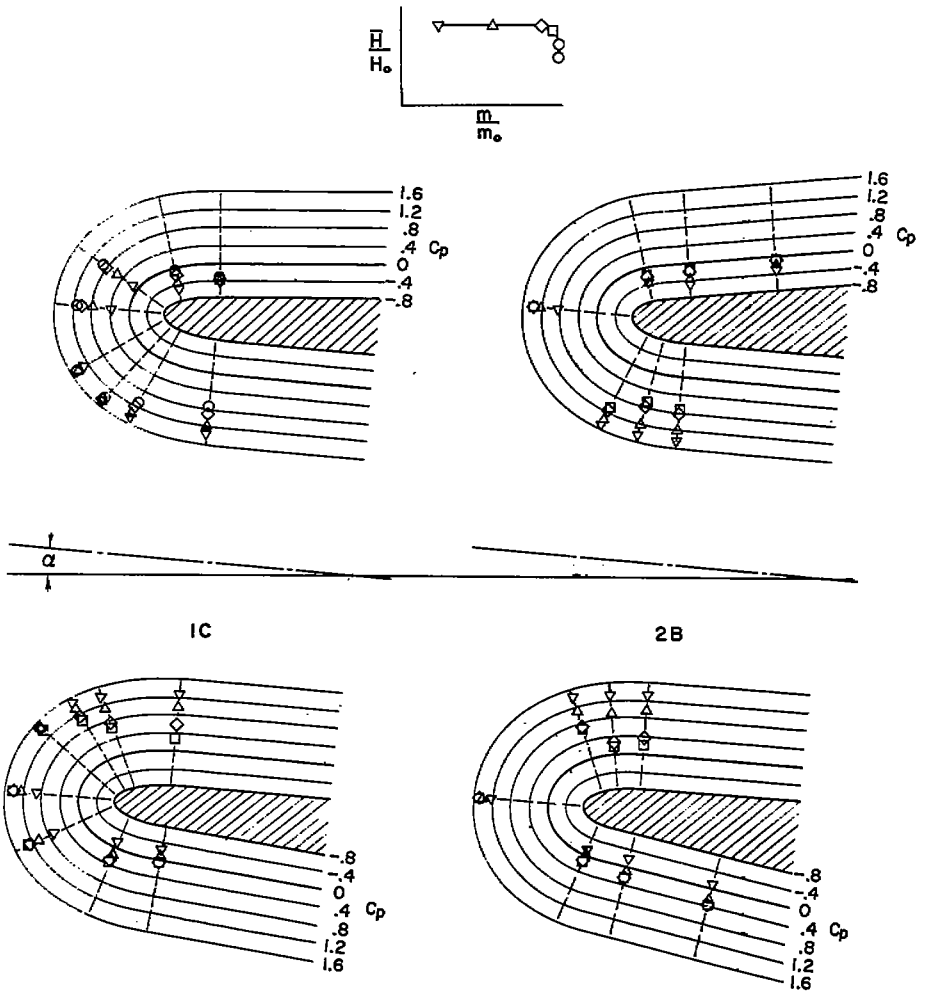

(b) $\alpha = 5^{\circ}$; $M_0 = 1.41$.

Figure 9.- Continued.

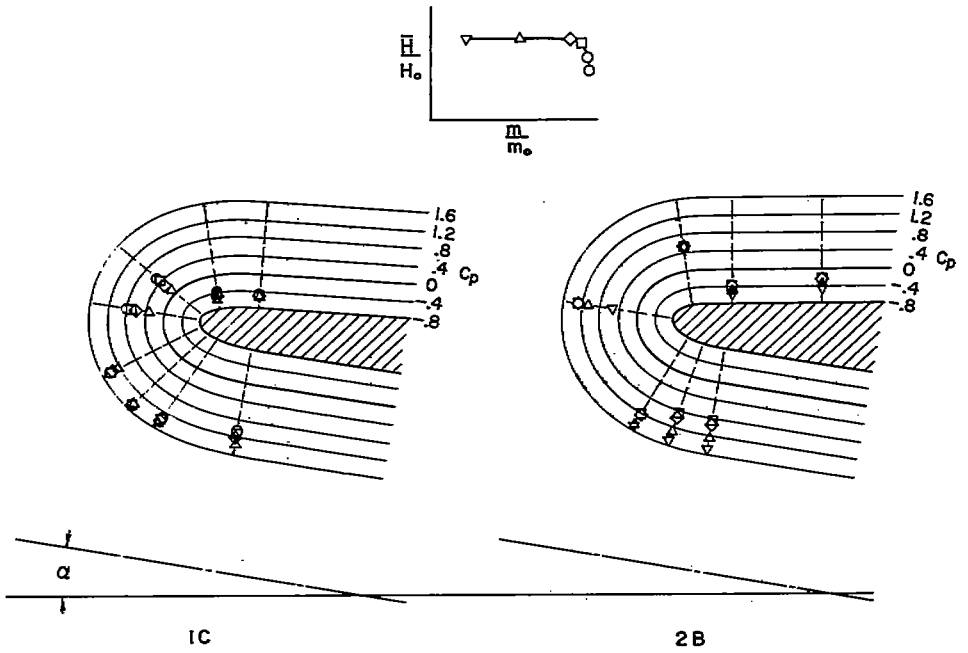

(c) $\alpha = 10^{\circ}$; $M_o = 1.41$.

Figure 9.- Continued.

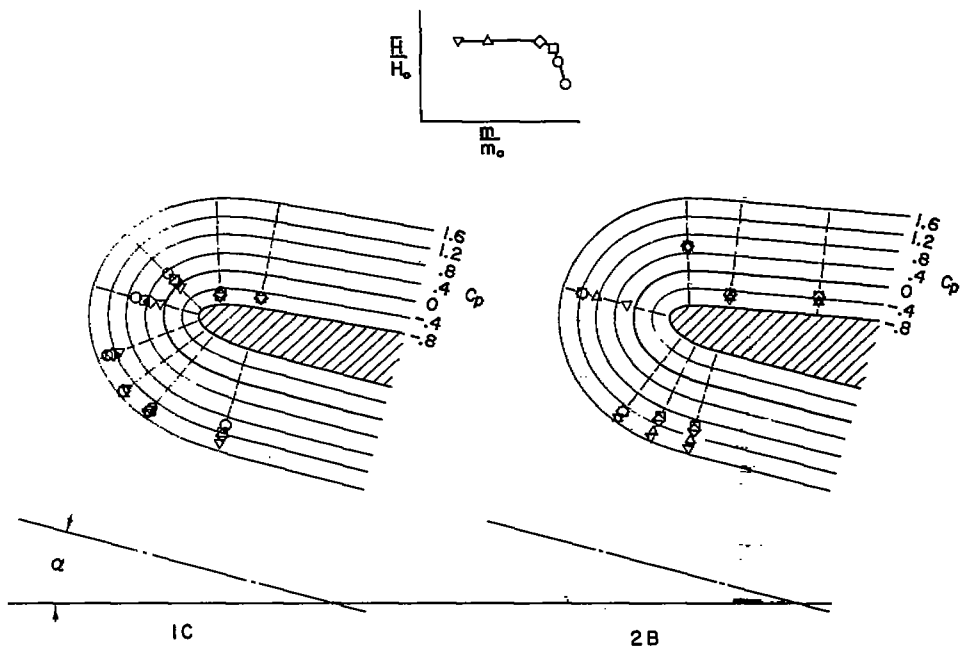

(d) $\alpha = 15^{\circ}$; $M_O = 1.41$.

Figure 9.- Continued.

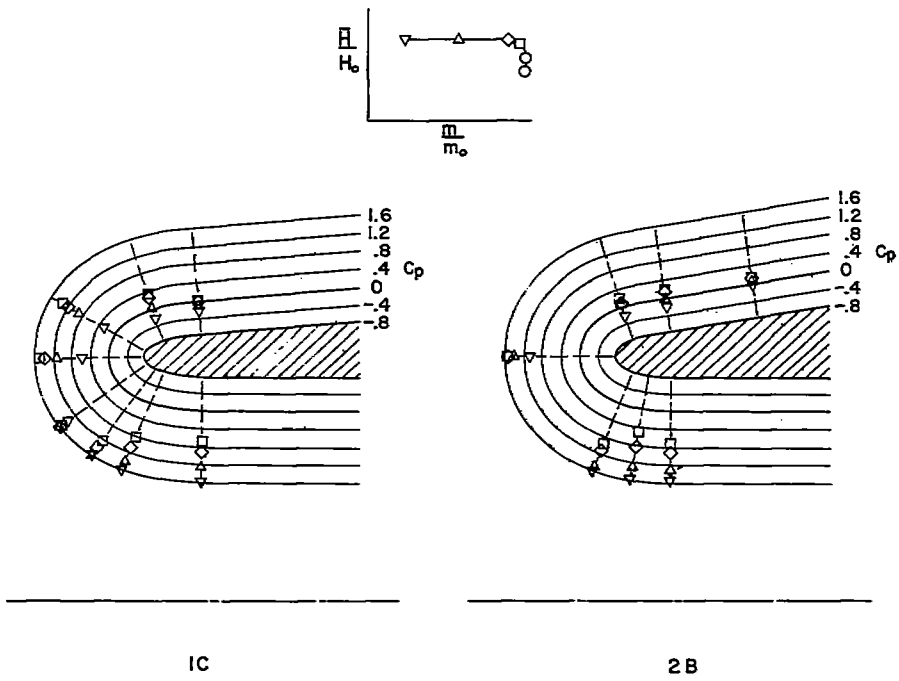

(e) $\alpha = 0^{\circ}$; $M_{o} = 1.81$.

Figure 9.- Continued.

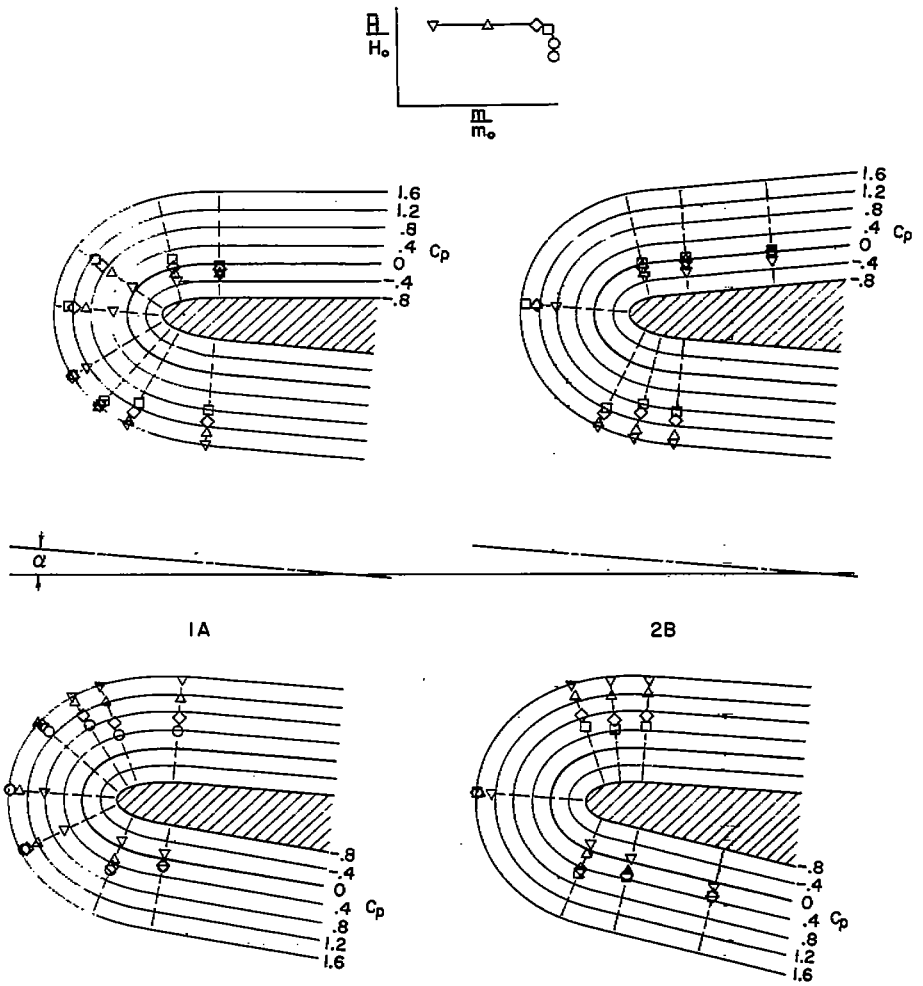

(f) $\alpha = 5^{\circ}$; $M_o = 1.81$.

Figure 9.- Continued.

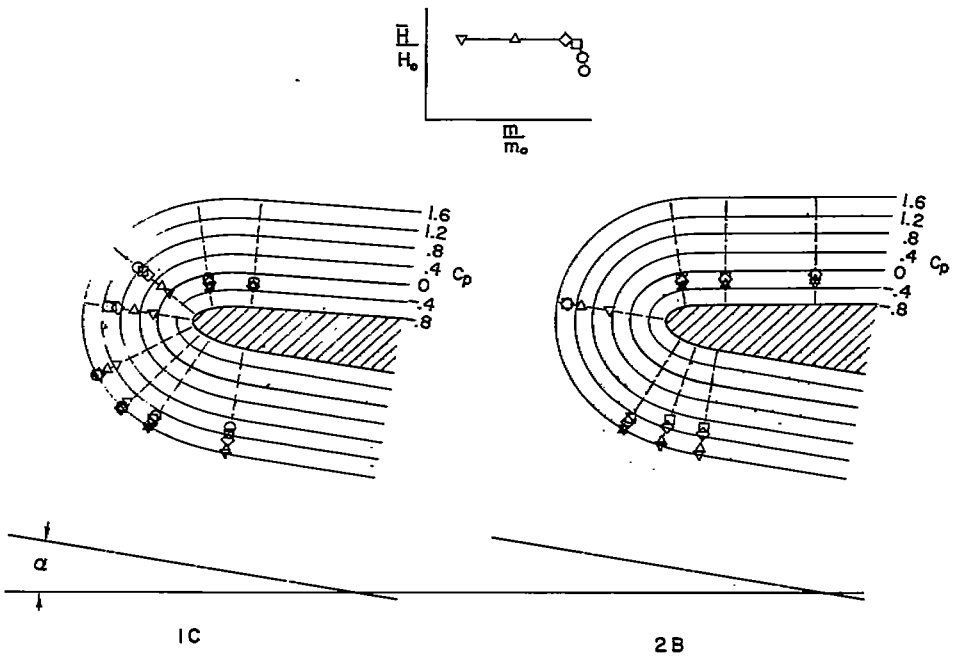

(g) $\alpha = 10^{\circ}$; $M_0 = 1.81$.

Figure 9.- Continued.

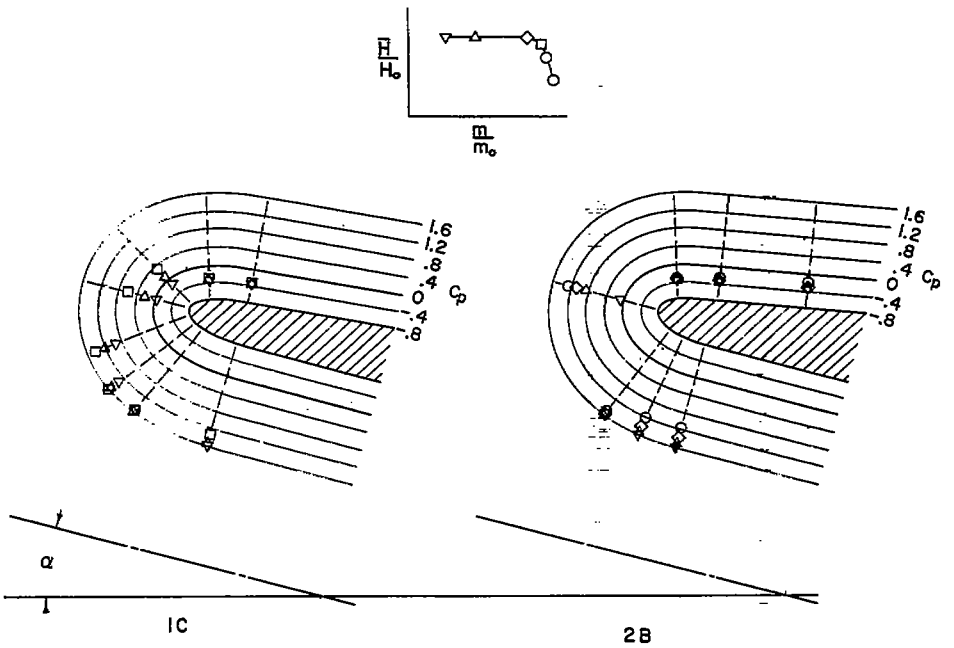

(h) $\alpha = 15^{\circ}$; $M_0 = 1.81$.

Figure 9.- Concluded.

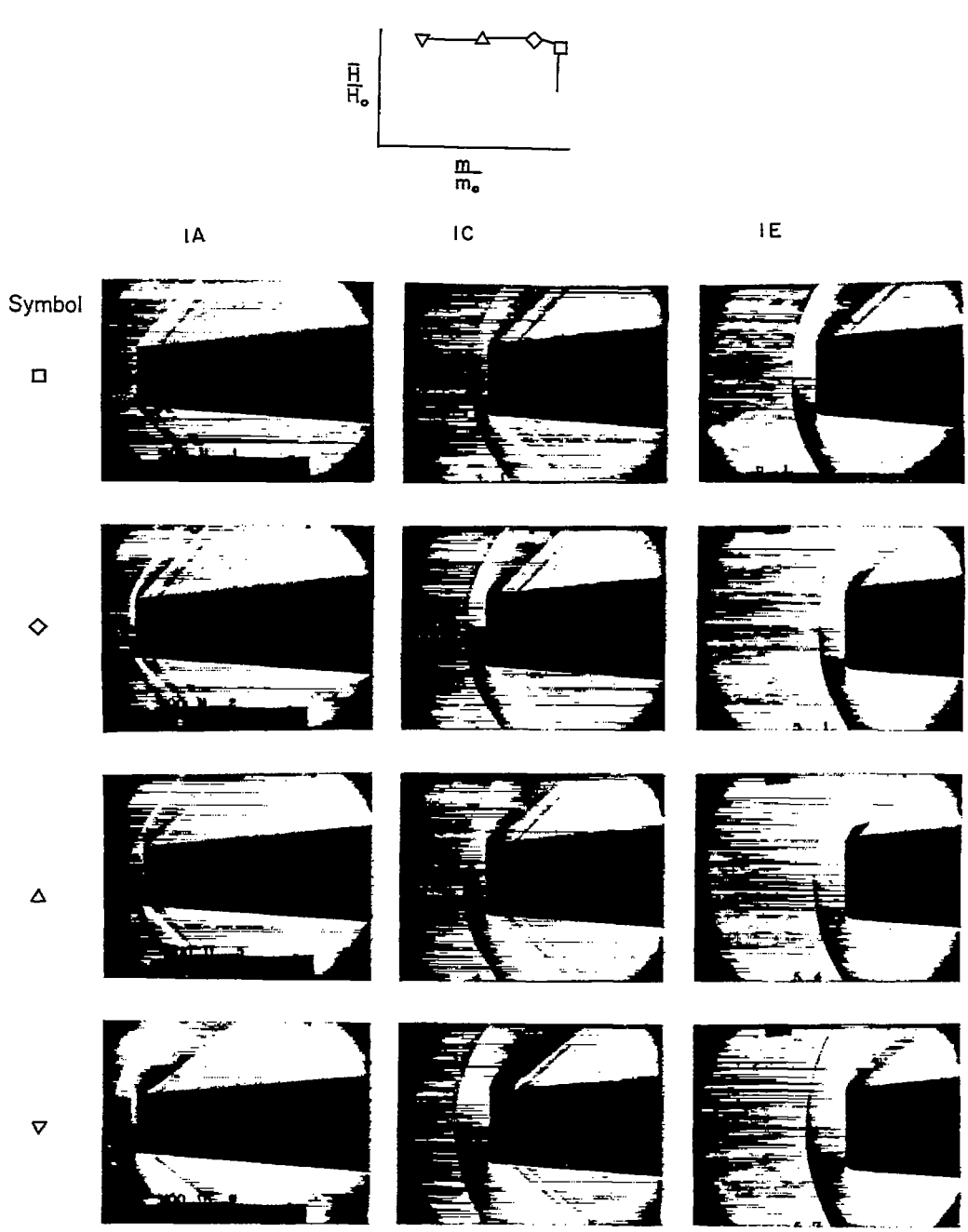

(a) $M_o = 1.41$.

L-57-1624

Figure 10.- Schlieren photographs of flow at the inlets for configurations in the lip-bluntness series at $\alpha = 0^\circ$.

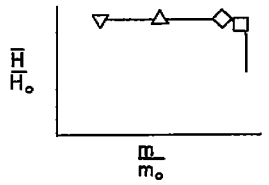

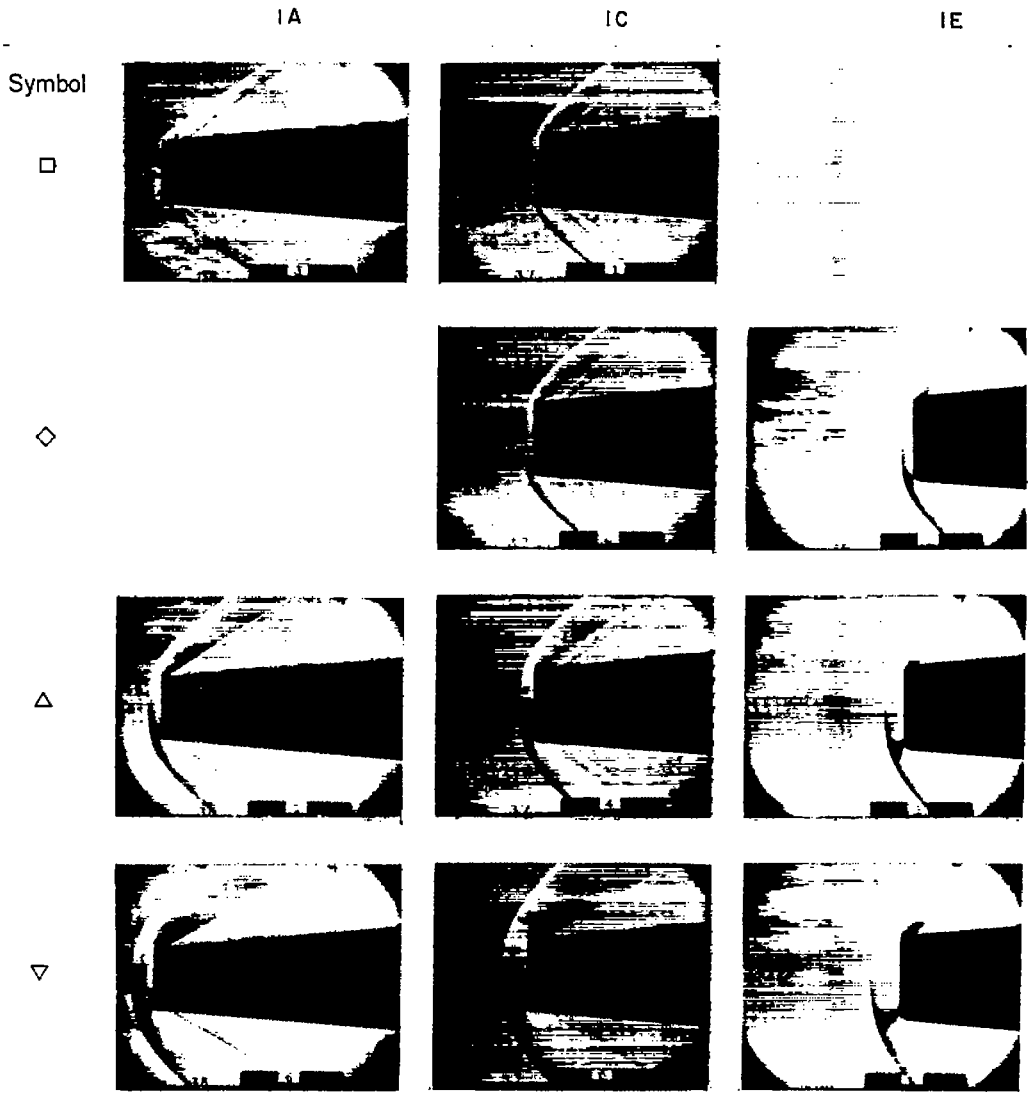

(b) $M_o = 1.81$.

L-57-1625

Figure 10.- Concluded.

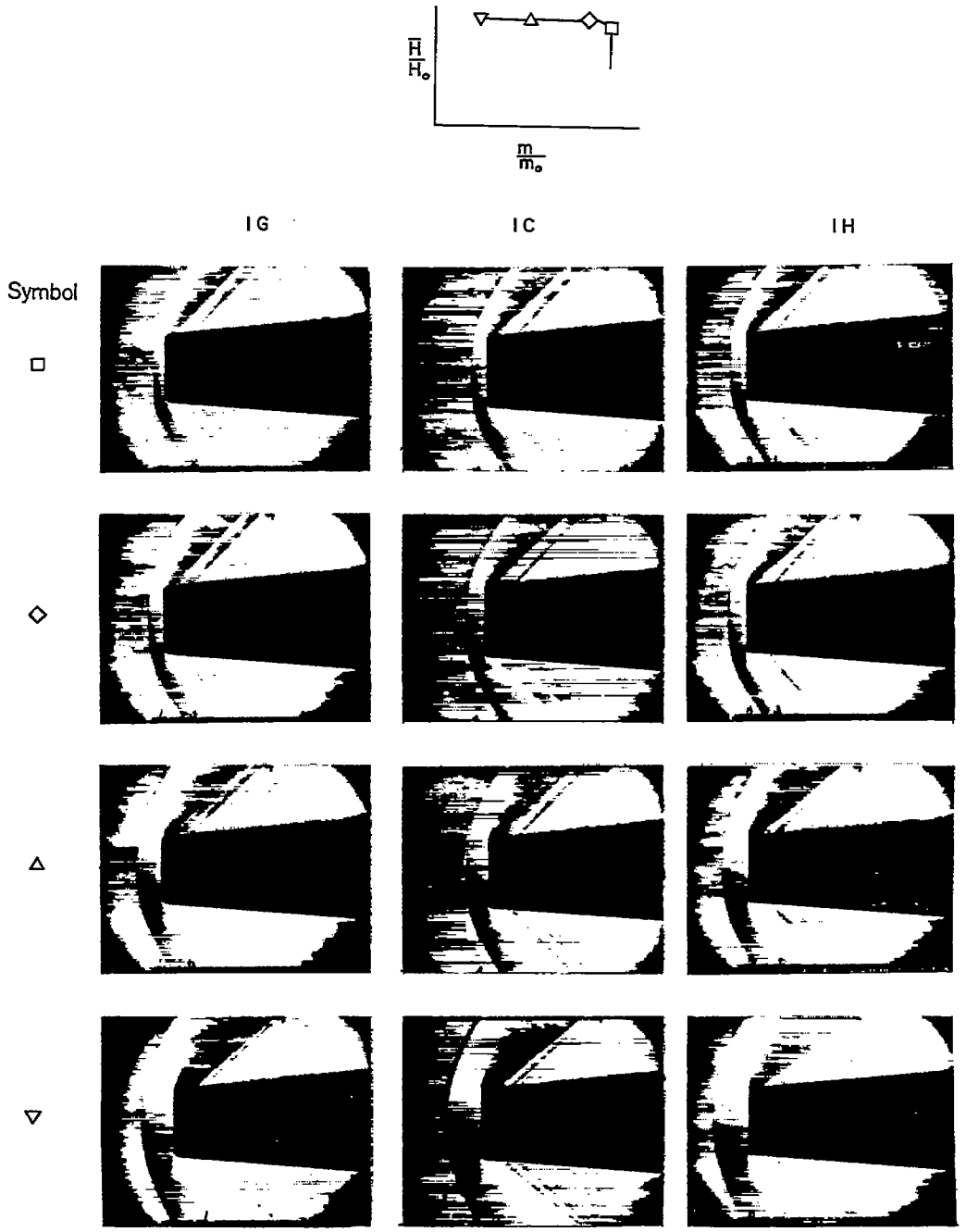

(a) M_o = 1.41. L-57-1626

Figure 11.- Schlieren photographs of flow at the inlets for configurations in the lip-camber series at $\alpha = 0^\circ$.

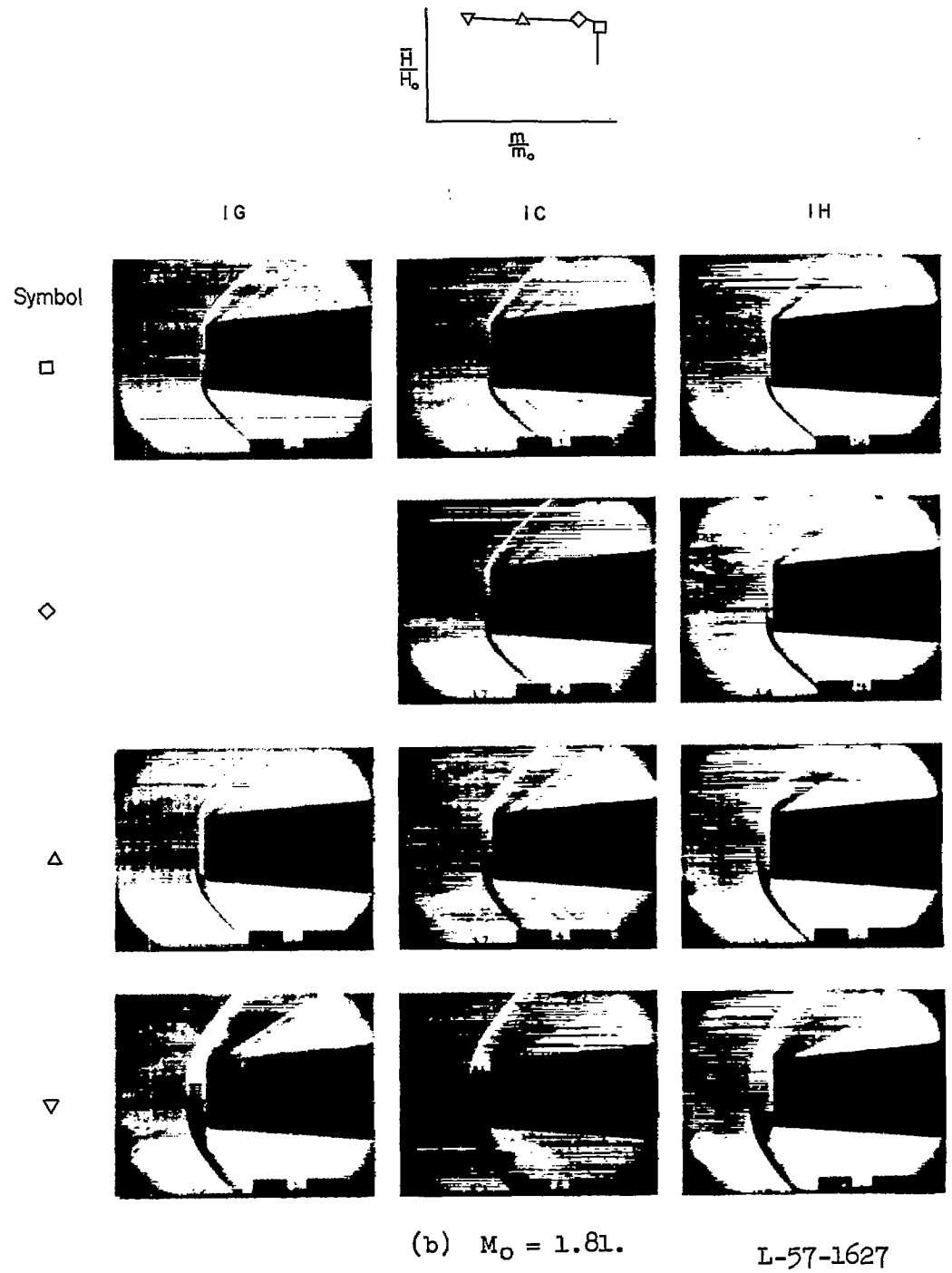

(b) $M_o = 1.81$. L-57-1627

Figure 11.- Concluded.

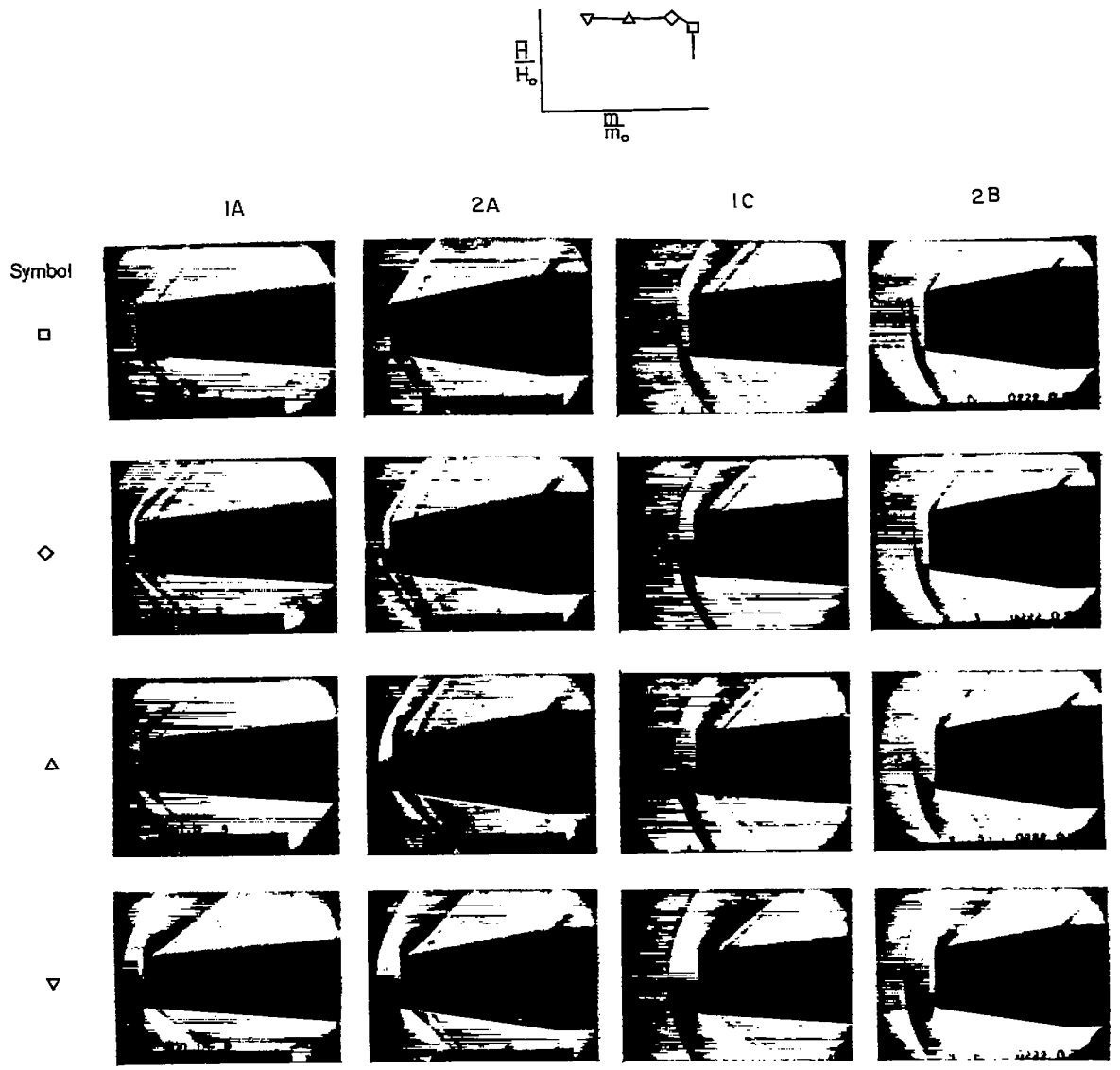

(a) $M_o = 1.41$. L-57-1628

Figure 12.- Schlieren photographs of flow at the inlets for configurations having 5° and 10° forebody half-angles with sharp lips and moderately blunt lips. $\alpha = 0°$.

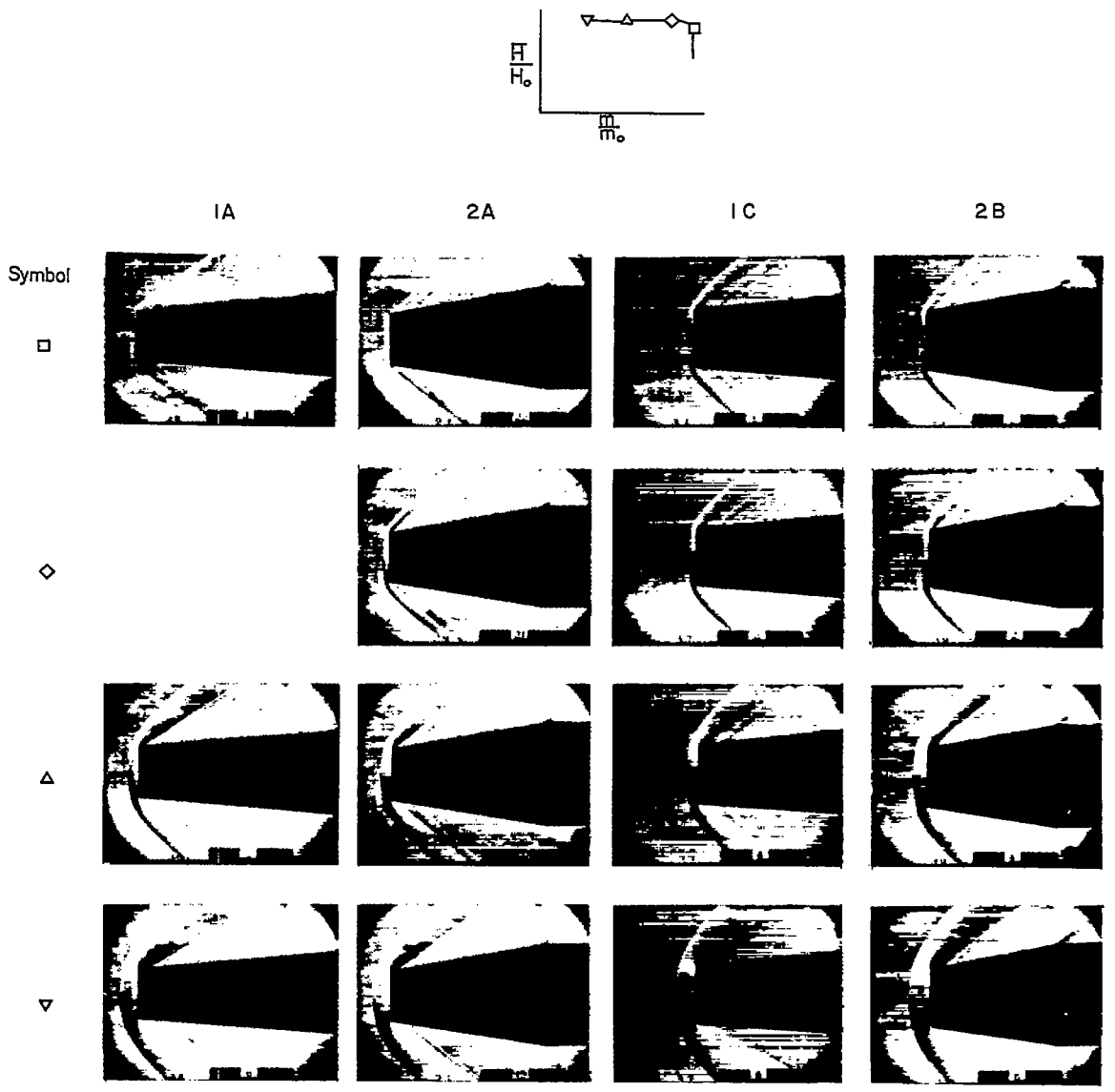

(b) $M_0 = 1.81$.

L-57-1629

Figure 12.- Concluded.

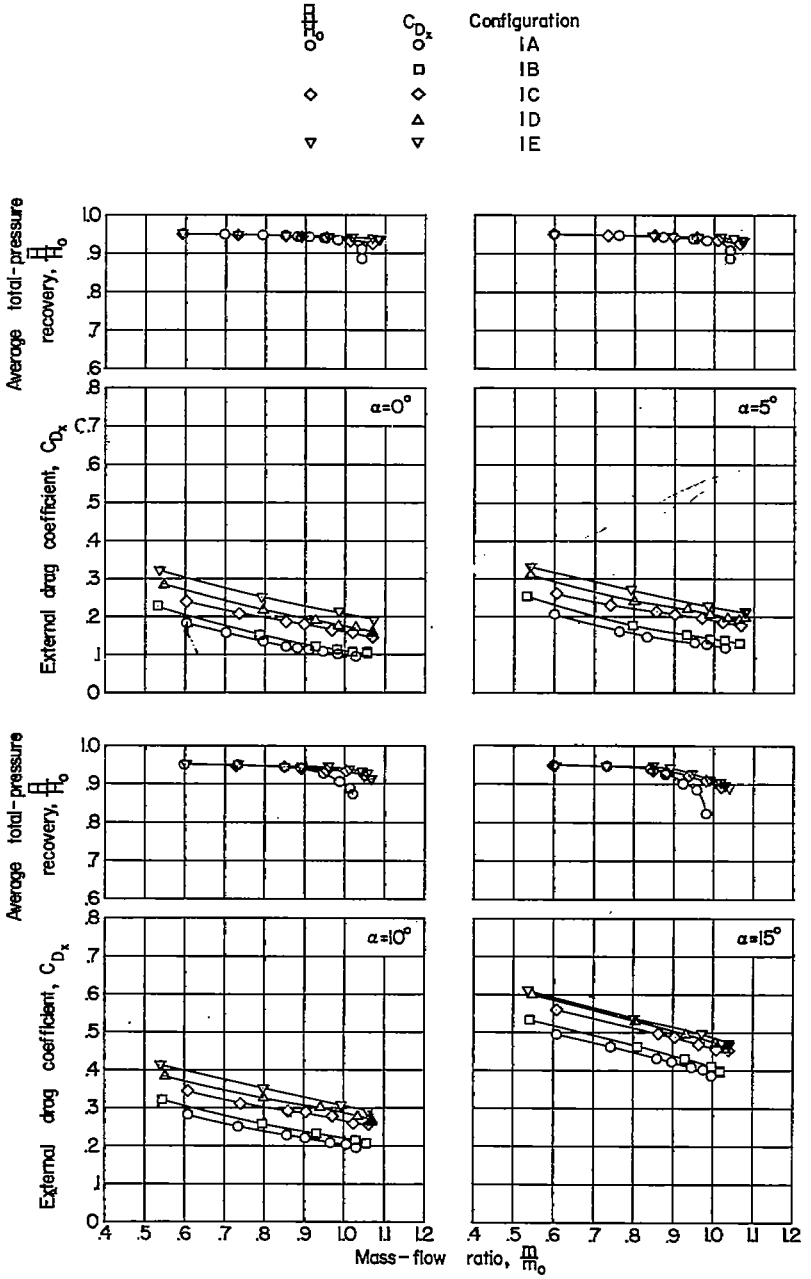

(a) $M_o = 1.41$.

Figure 13.- Average total-pressure recoveries and external drags of the inlet models in the lip-bluntness series.

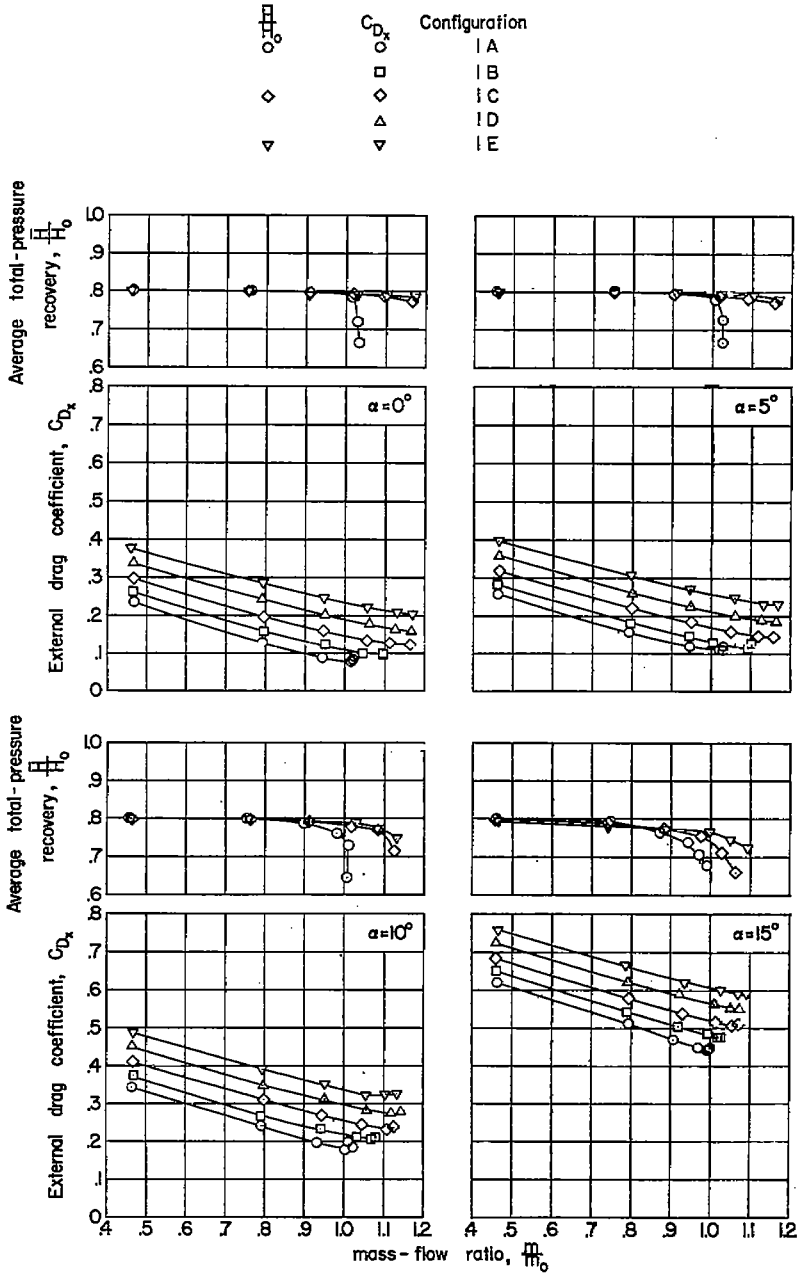

(b) $M_o = 1.81$.

Figure 13.- Concluded.

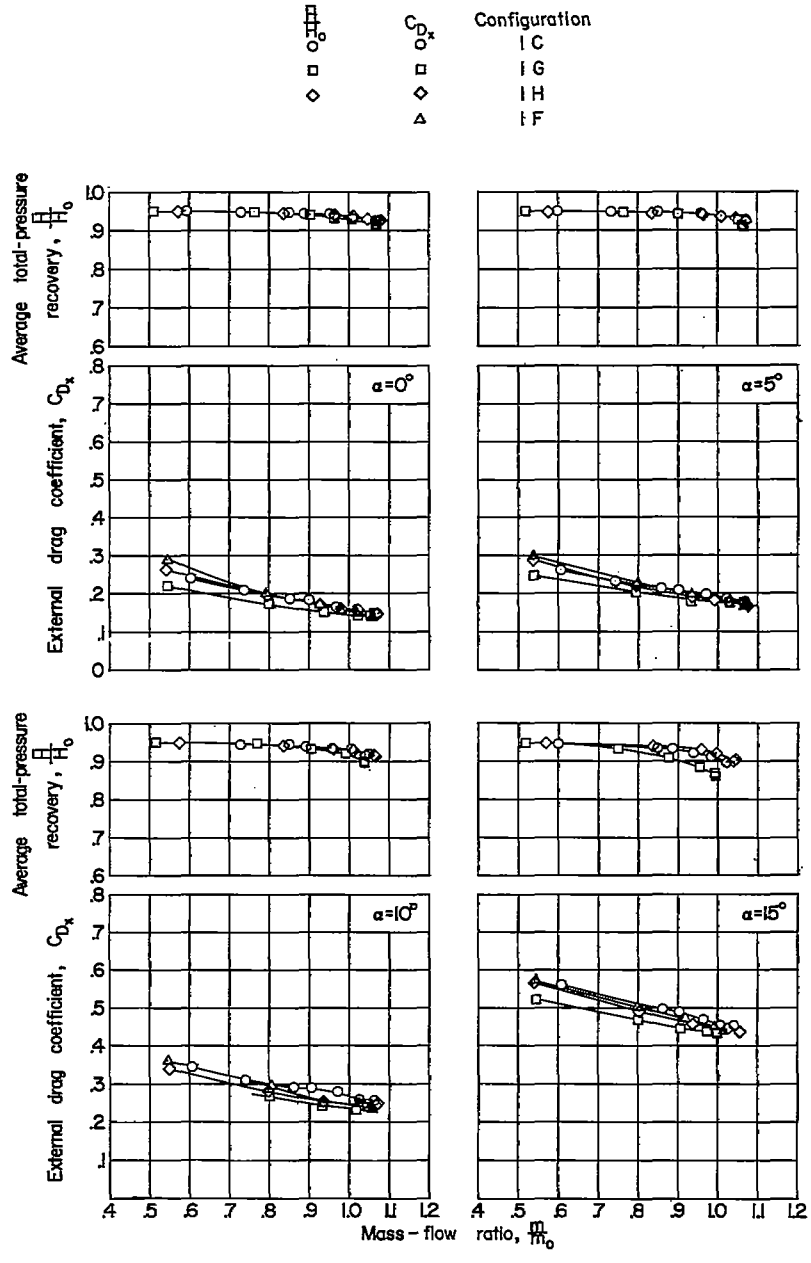

(a) $M_o = 1.41$.

Figure 14.- Average total-pressure recoveries and external drag coefficients for the inlets in the lip-camber series, and external drag coefficients for the inlet with lip or circular section.

[redacted]

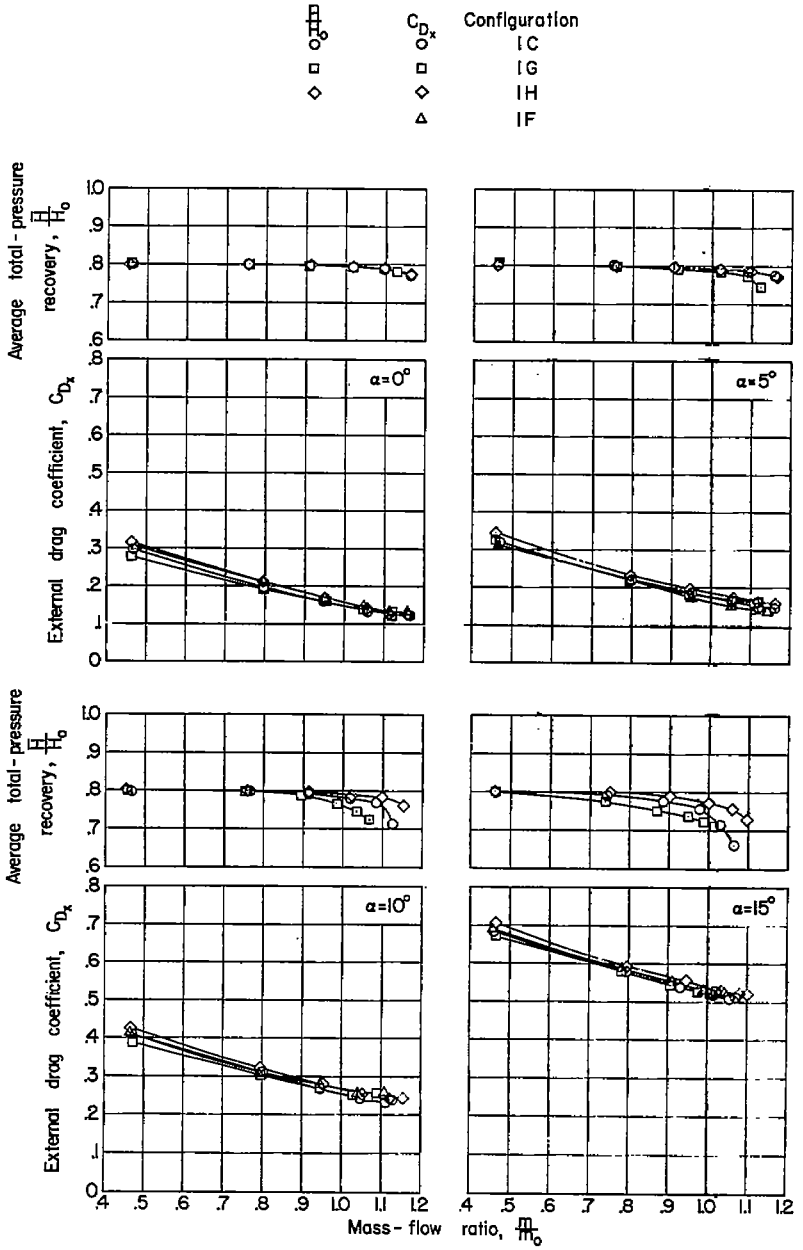

(b) $M_o = 1.81$.

Figure 14.- Concluded.

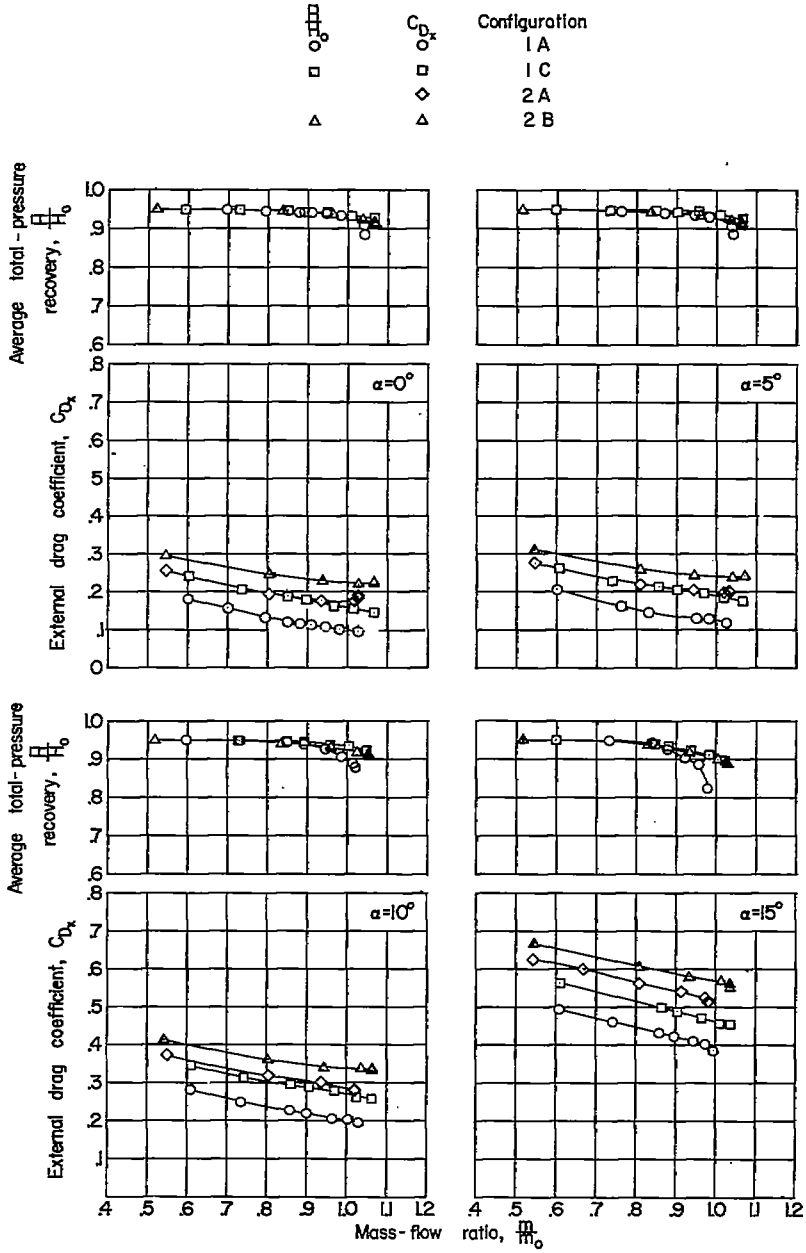

(a) $M_o = 1.41$.

Figure 15.- Average total-pressure recoveries and external drag coefficients for configurations having 5° and 10° forebody half-angles with comparable degrees of lip bluntness.

[redacted]

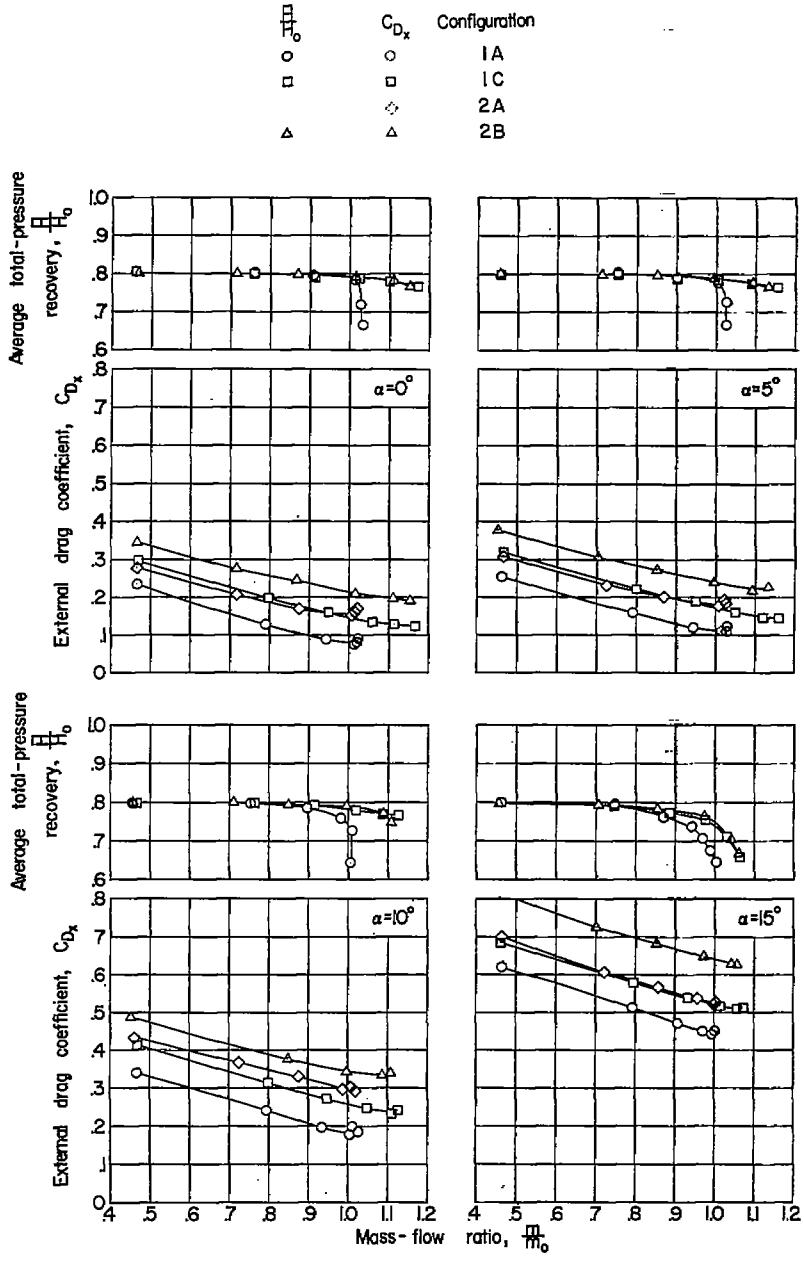

(b) $M_o = 1.81$.

Figure 15.- Concluded.

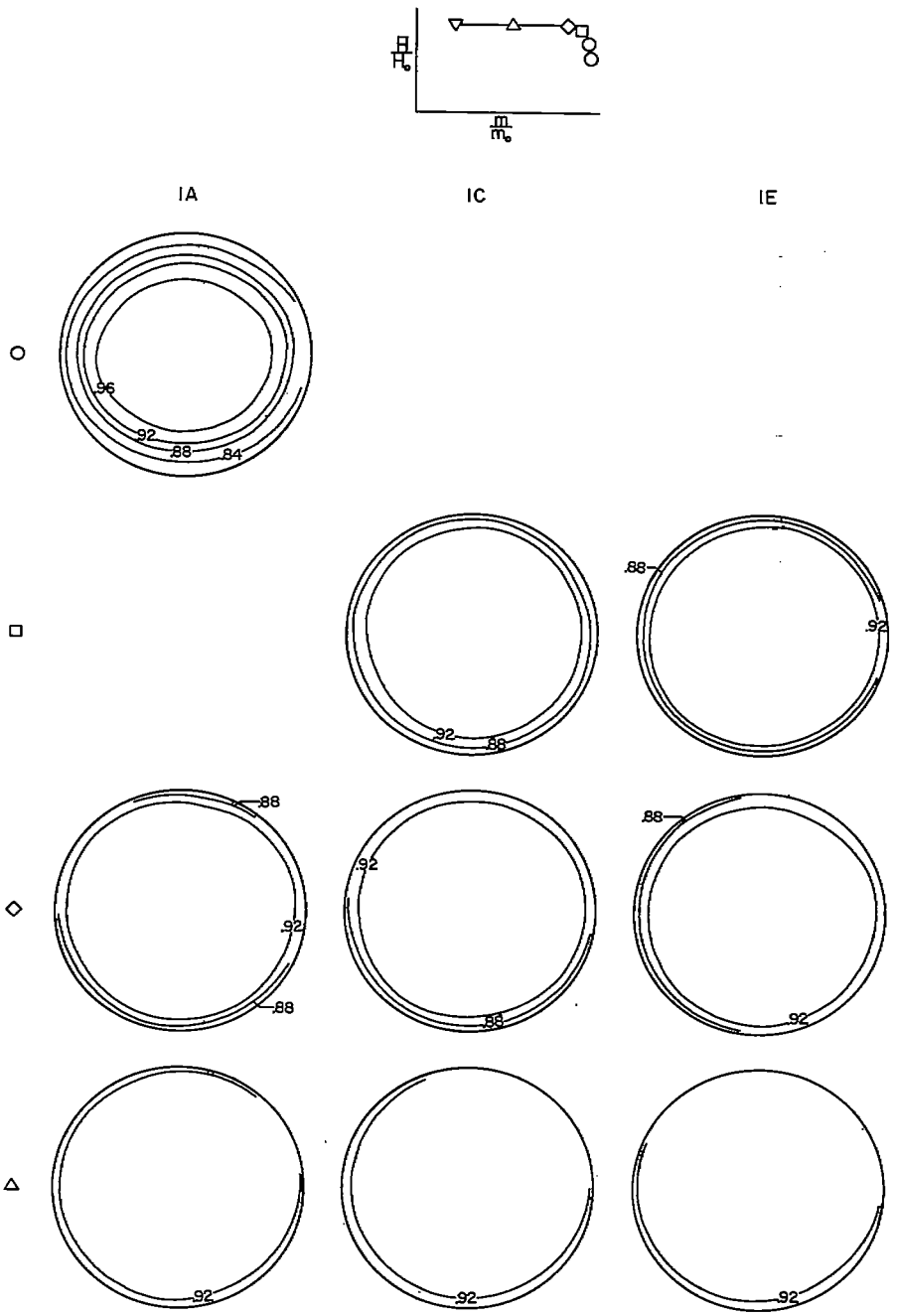

(a) $\alpha = 0^{\circ}$; $M_o = 1.41$.

Figure 16.- Duct total-pressure distributions for the inlet configurations in the lip-bluntness series.

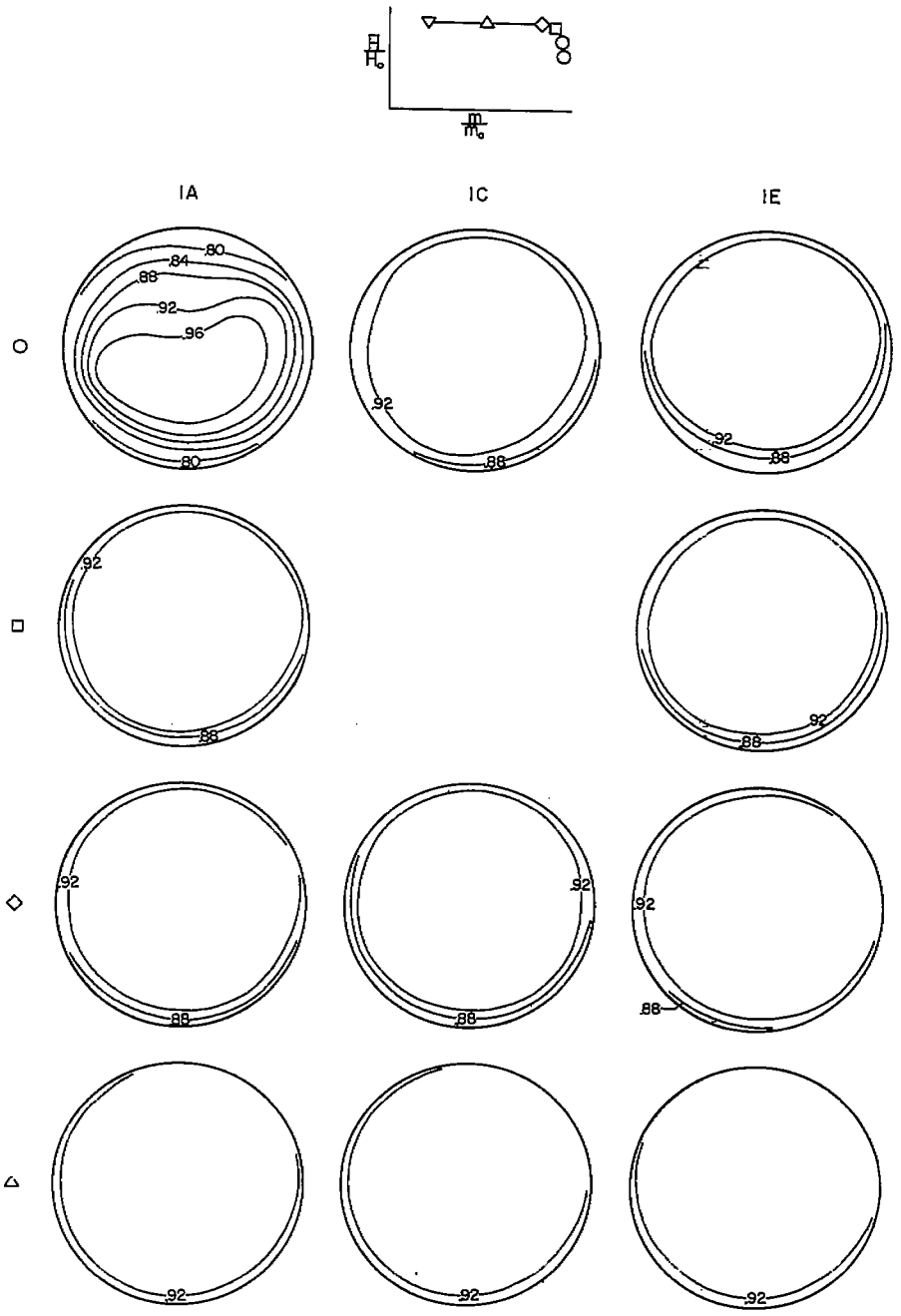

(b) $\alpha = 5^{\circ}$; $M_o = 1.41$.

Figure 16.- Continued.

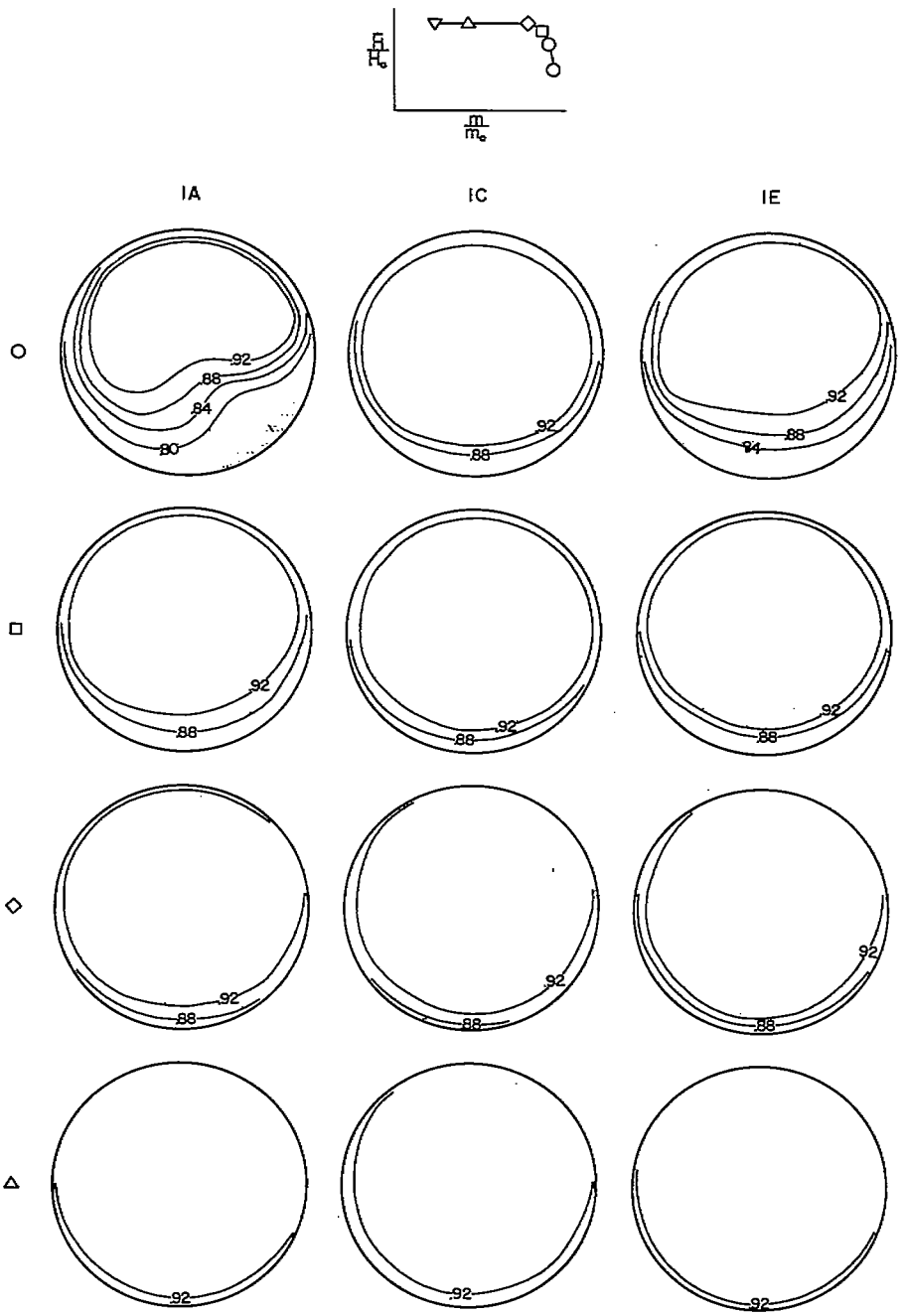

(c) $\alpha = 10^{\circ}$; $M_O = 1.41$.

Figure 16.- Continued.

[redacted]

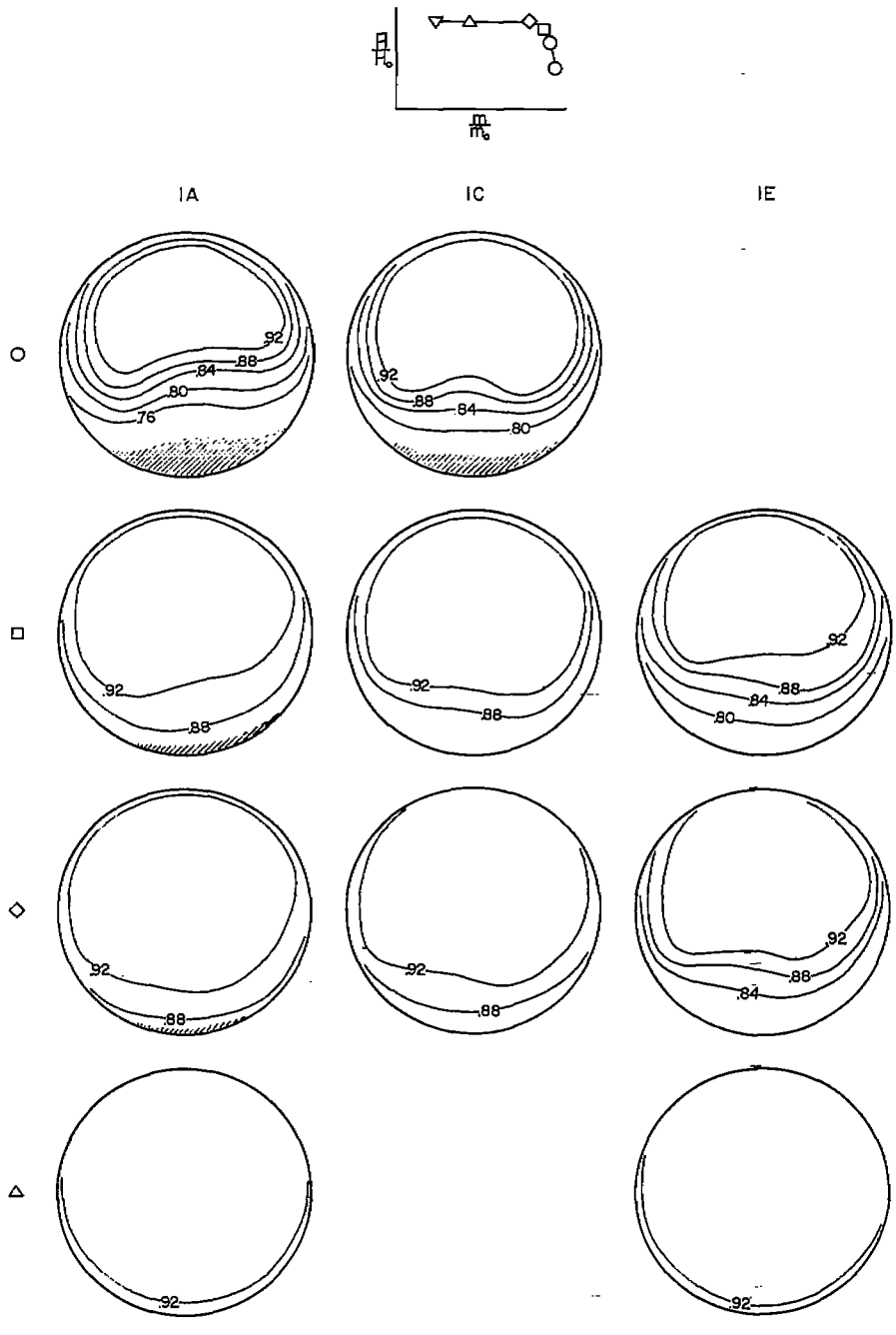

(d) $\alpha = 15^{\circ}$; $M_o = 1.41$.

Figure 16.- Continued. Shaded area indicates reverse flow.

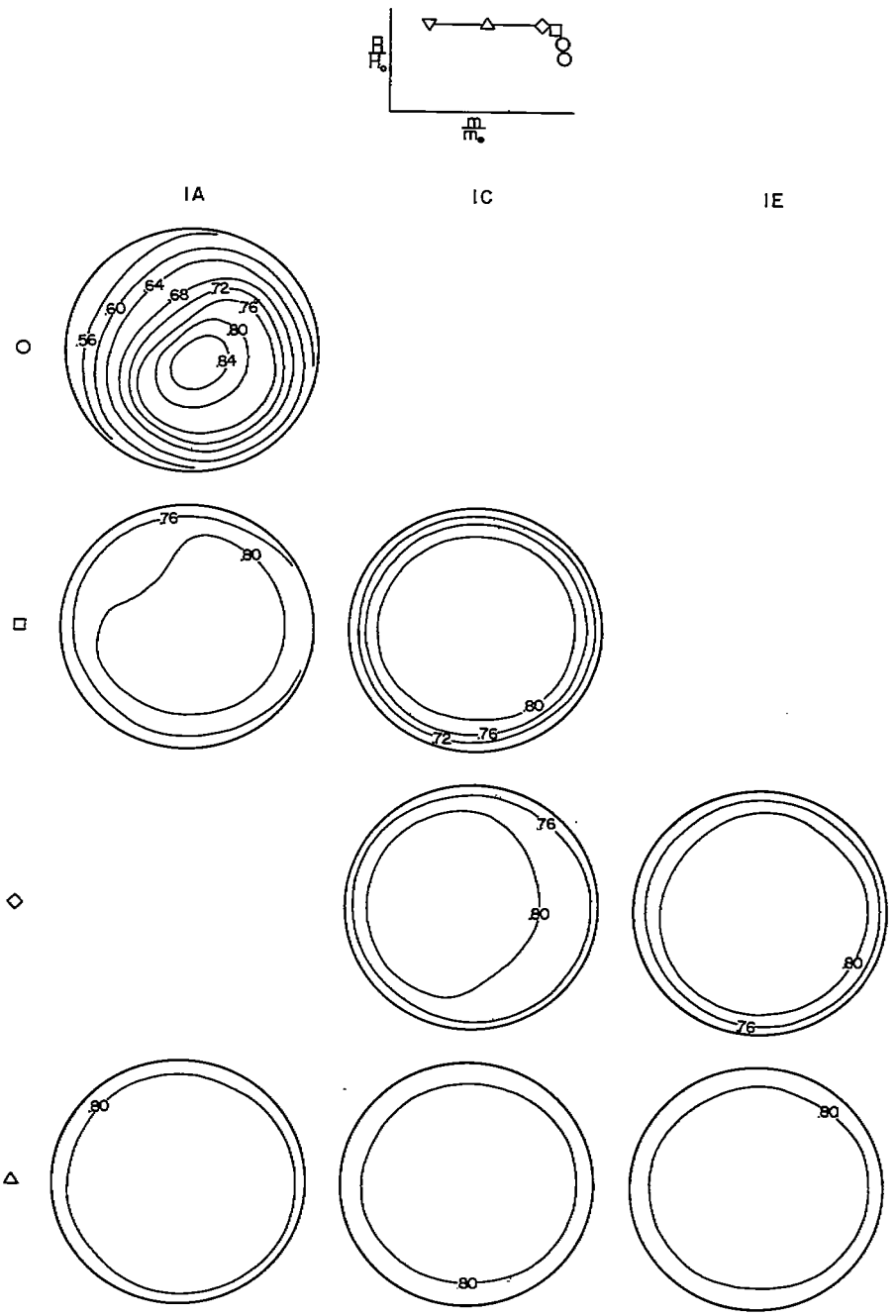

(e) $\alpha = 0^{\circ}$; $M_o = 1.81$.

Figure 16.- Continued.

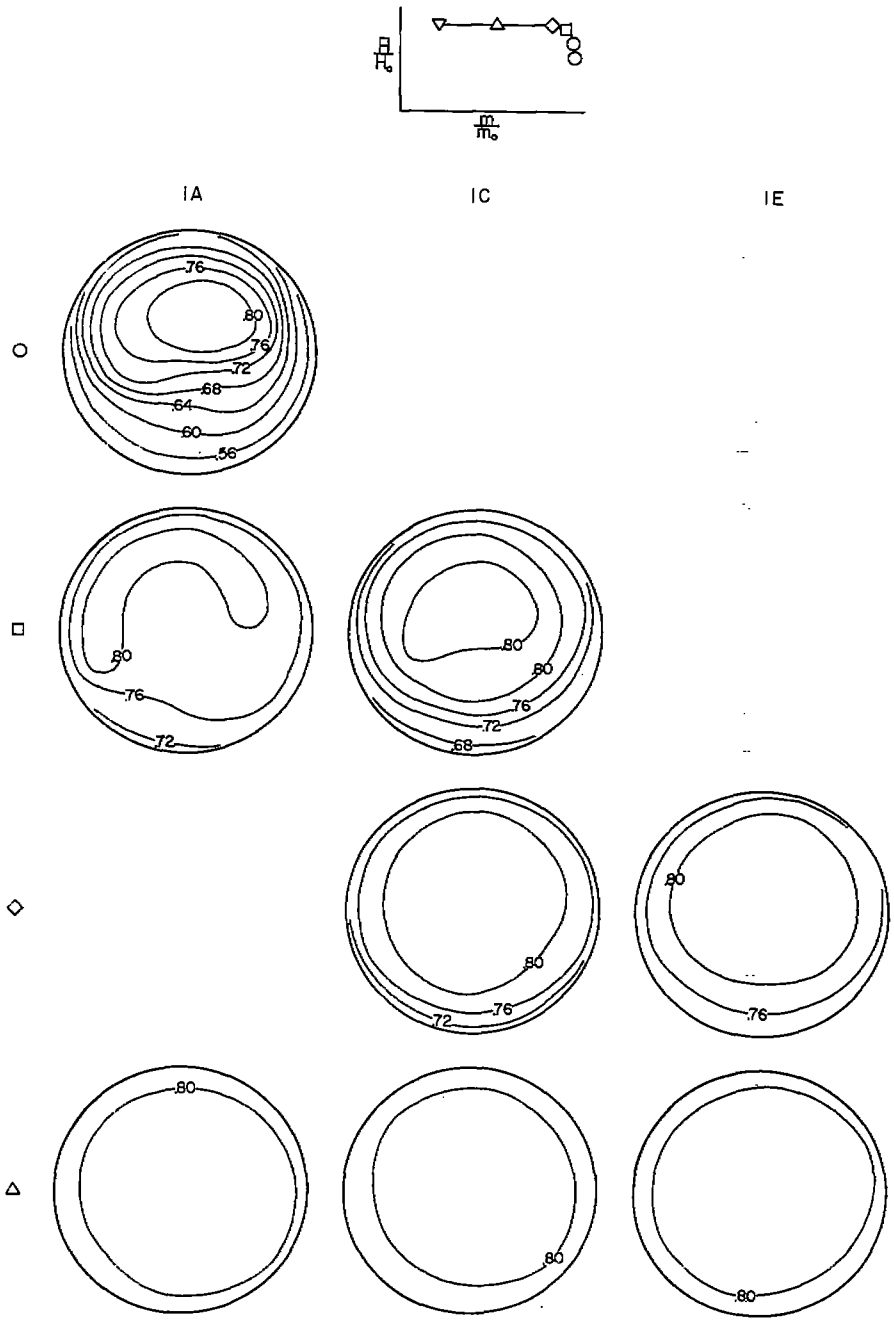

(f) $\alpha = 5^{\circ}$; $M_o = 1.81$.

Figure 16.- Continued.

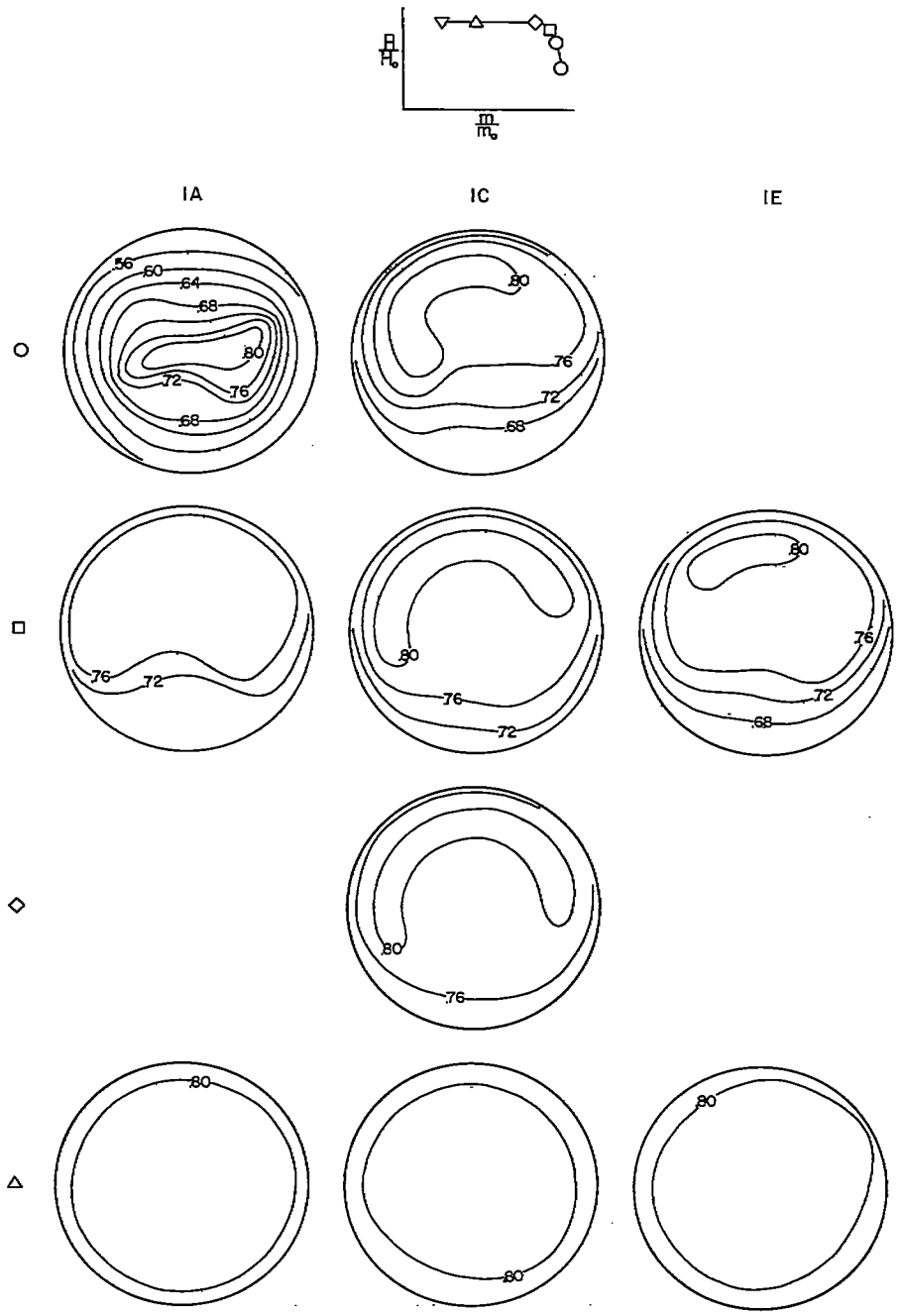

(g) $\alpha = 10^{\circ}$; $M_{O} = 1.81$.

Figure 16.- Continued.

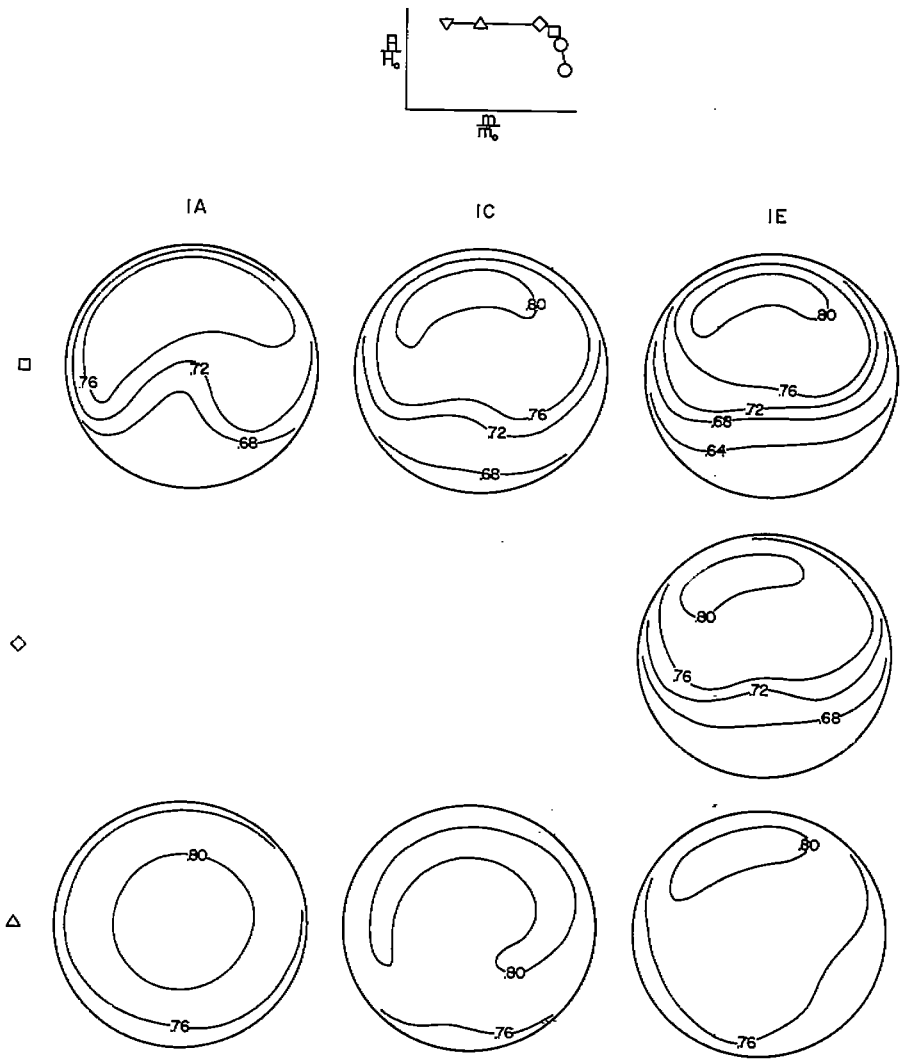

(h) $\alpha = 15^{\circ}$; $M_{\infty} = 1.81$.

Figure 16.- Concluded.

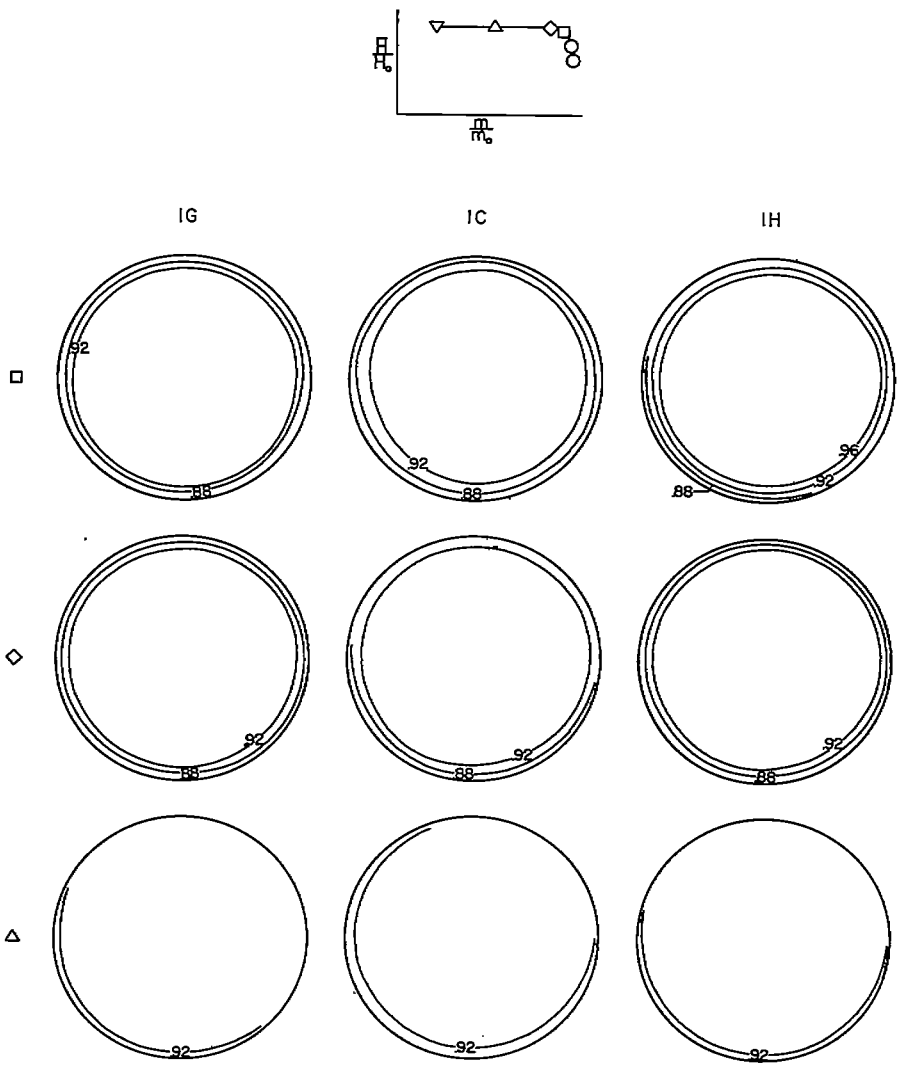

(a) $\alpha = 0^{\circ}$; $M_o = 1.41$.

Figure 17.- Duct total-pressure distributions for the inlet configurations in the lip-camber series. Shaded areas indicate reverse flow.

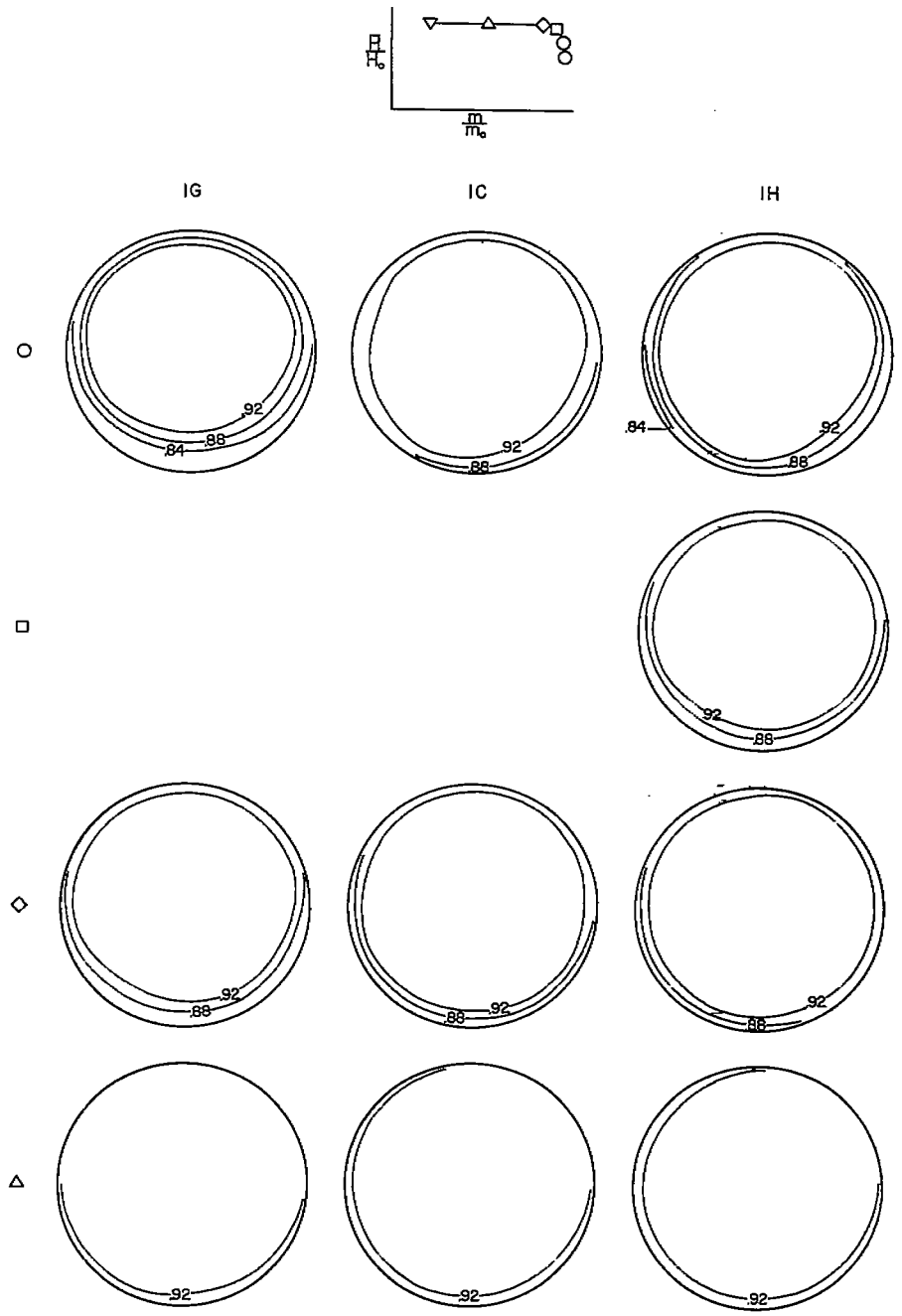

(b) $\alpha = 5^{\circ}$; $M_o = 1.41$.

Figure 17.- Continued.

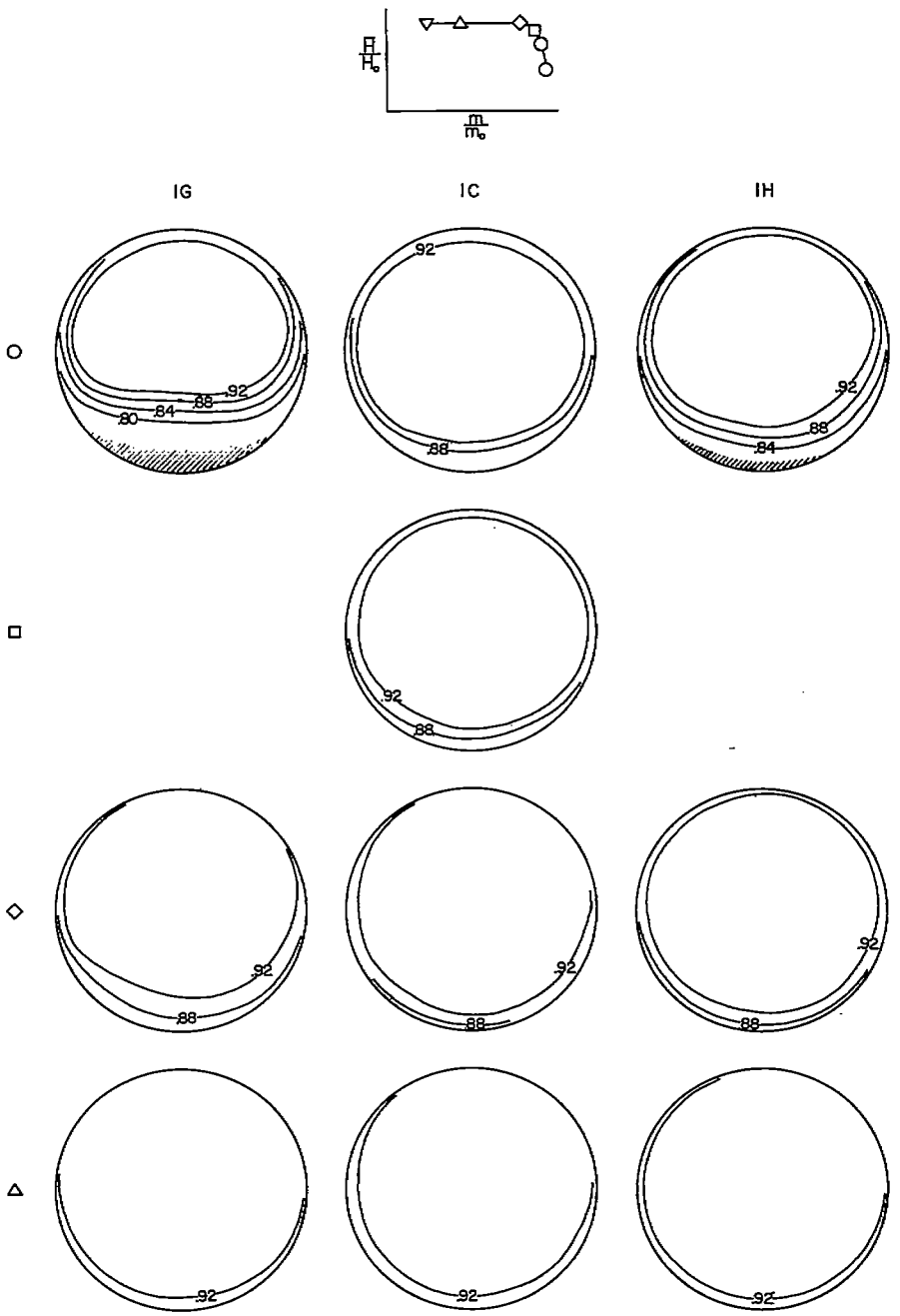

(c) $\alpha = 10^{\circ}$; $M_{O} = 1.41$.

Figure 17.- Continued.

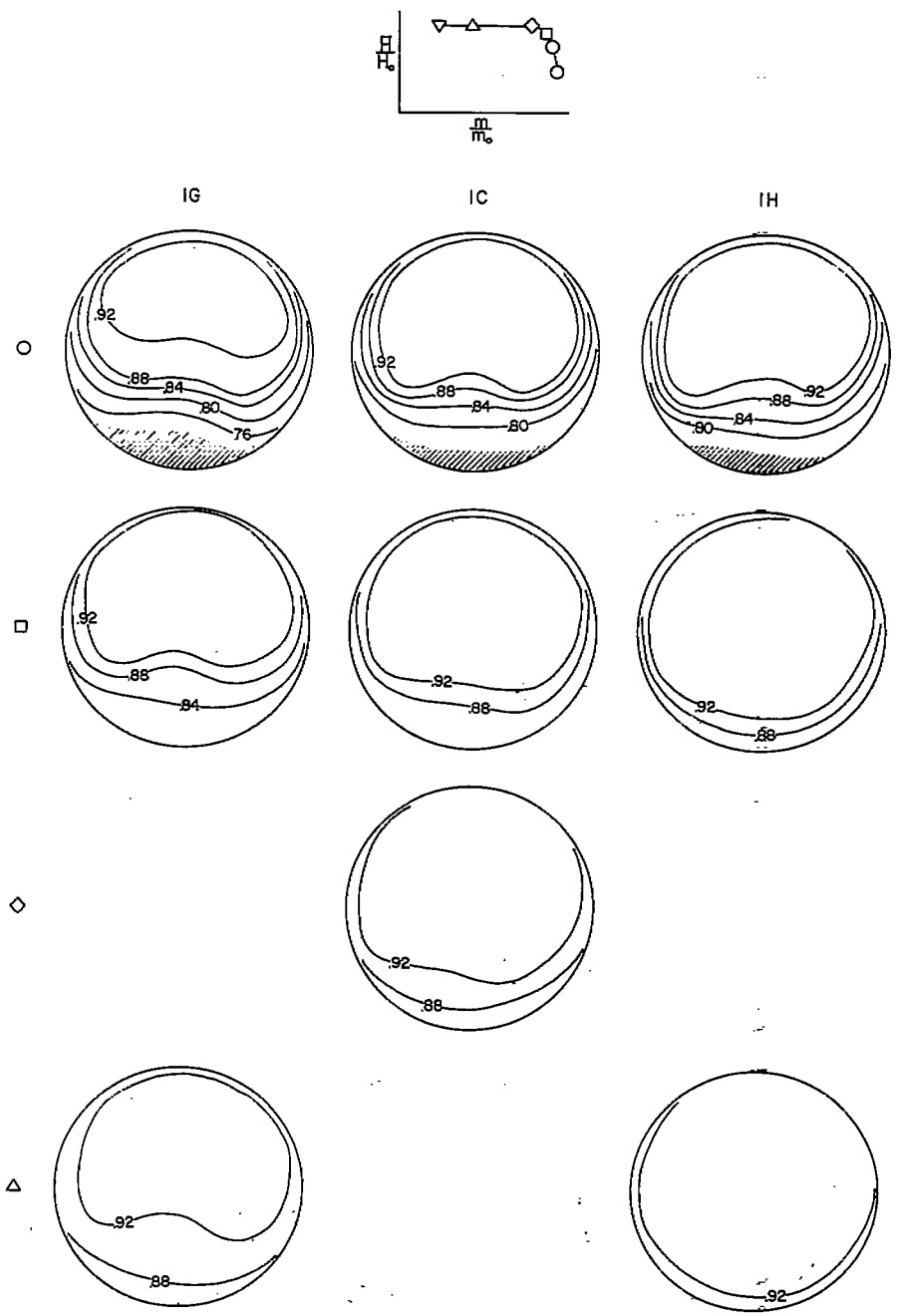

(d) $\alpha = 15^{\circ}$; $M_{O} = 1.41$.

Figure 17.- Continued.

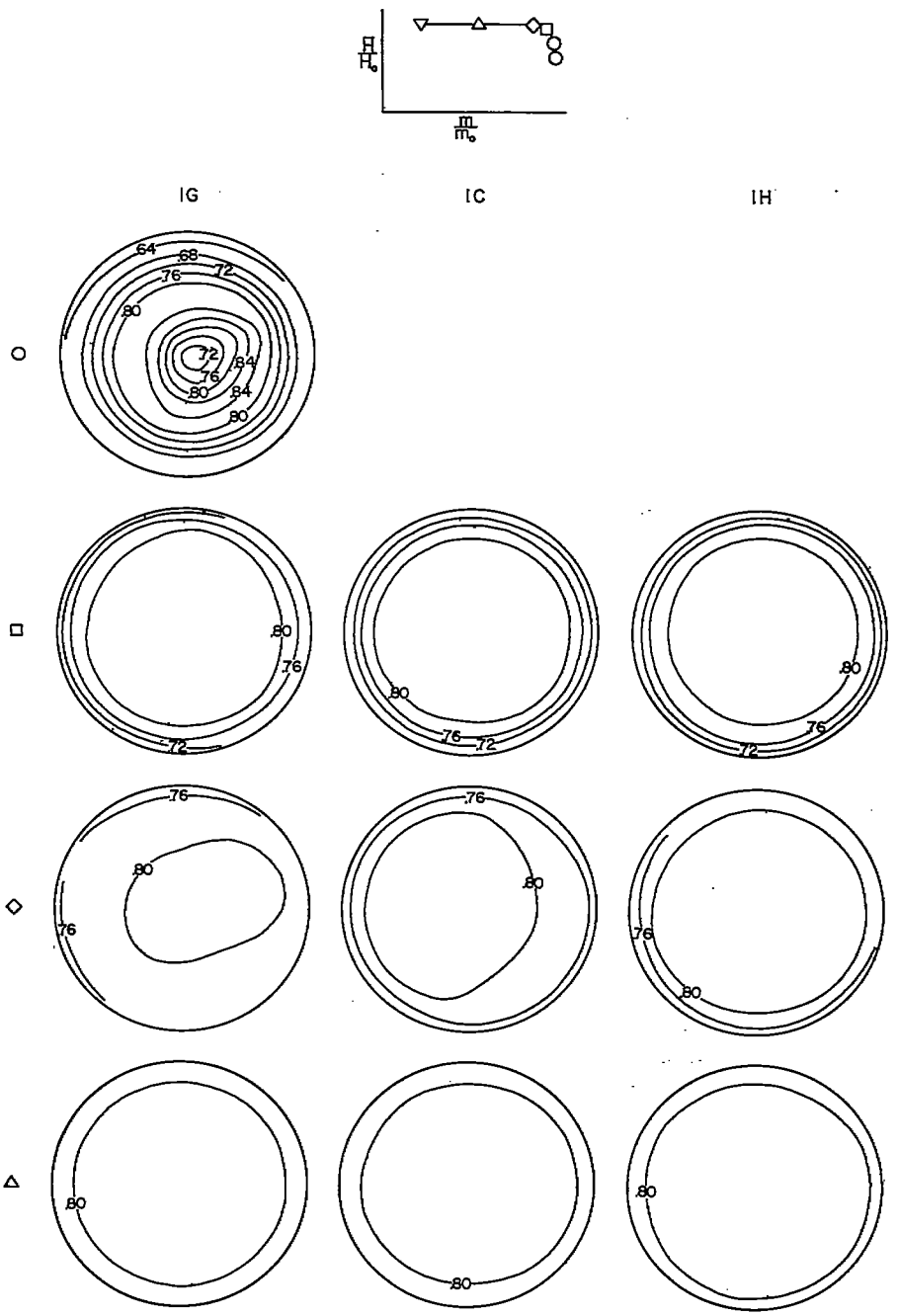

(e) $\alpha = 0^{\circ}$; $M_o = 1.81$.

Figure 17.- Continued.

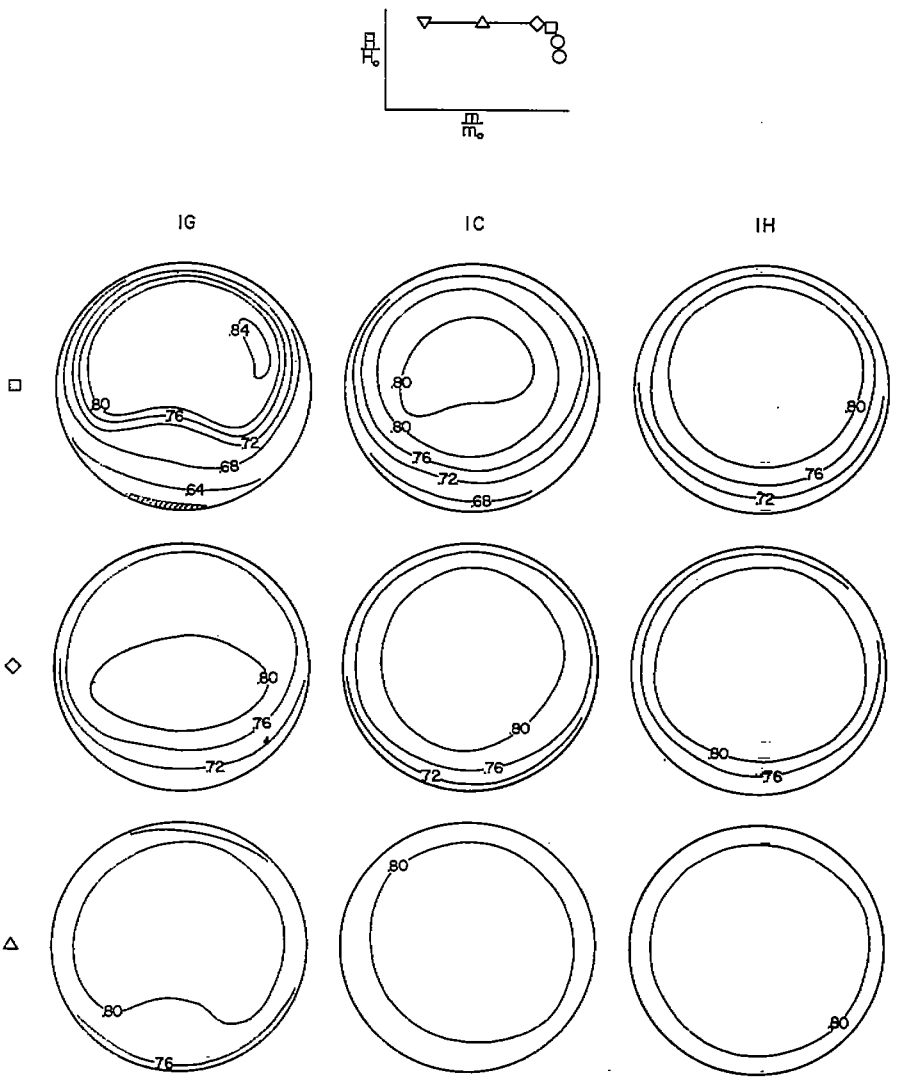

(f) $\alpha = 5^{\circ}$; $M_{o} = 1.81$.

Figure 17.- Continued.

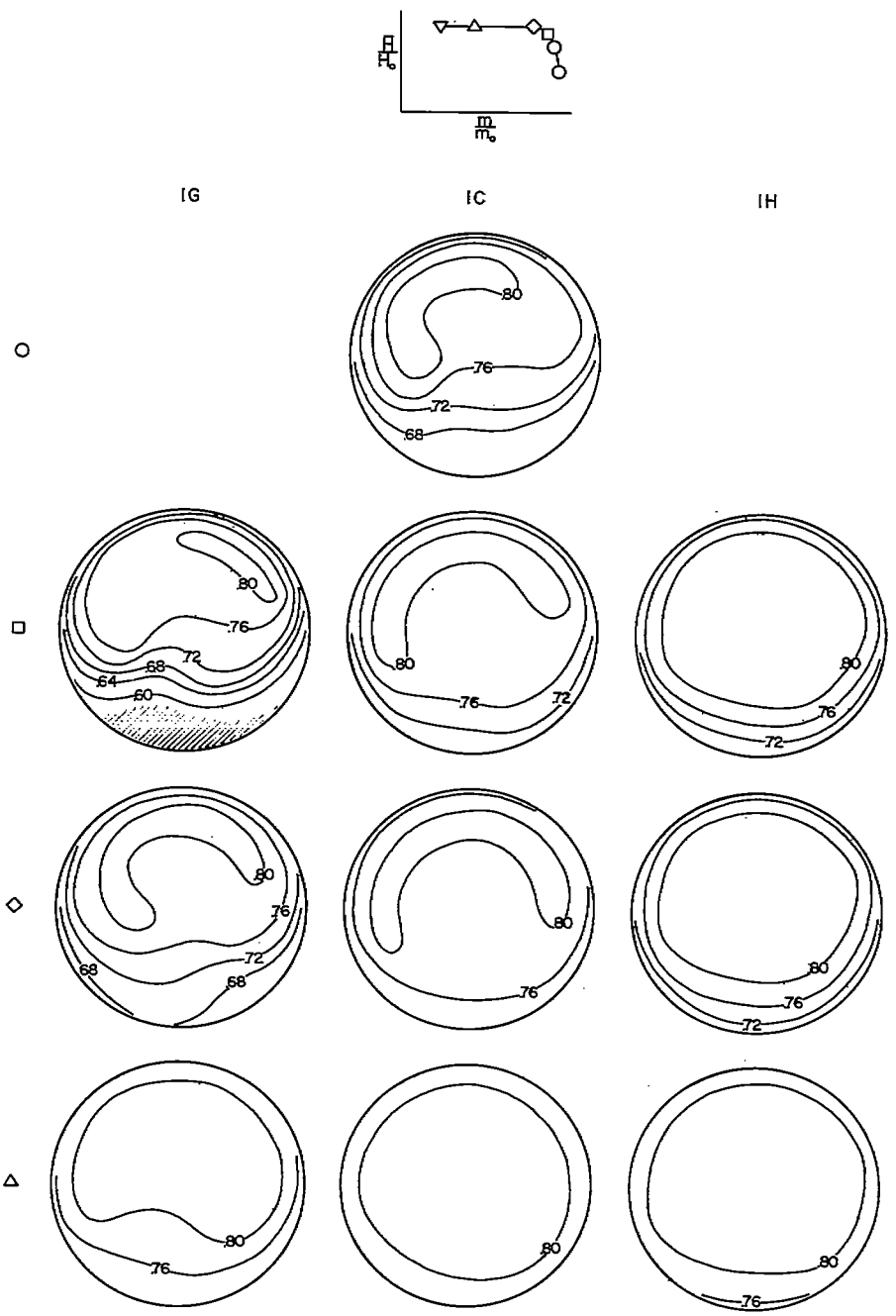

(g) $\alpha = 10^{\circ}$; $M_0 = 1.81$.

Figure 17.- Continued.

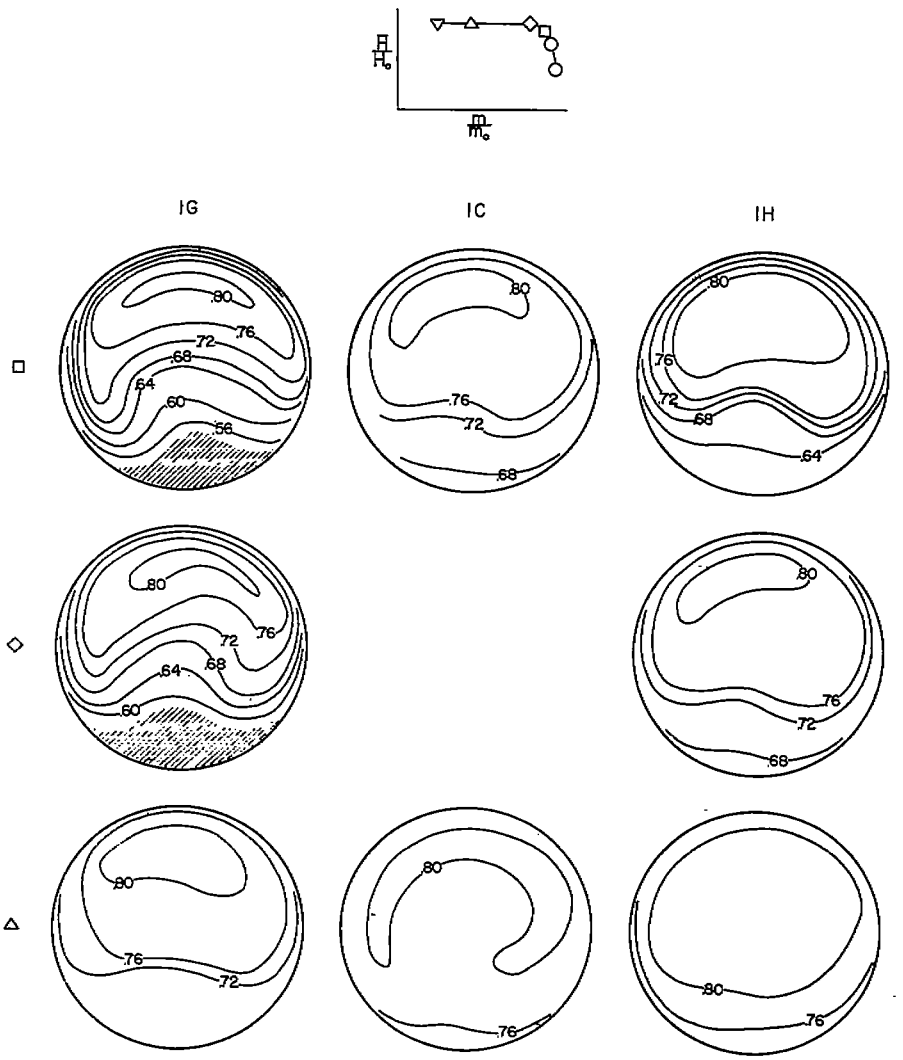

(h) $\alpha = 15^{\circ}$; $M_o = 1.81$.

Figure 17.- Concluded.

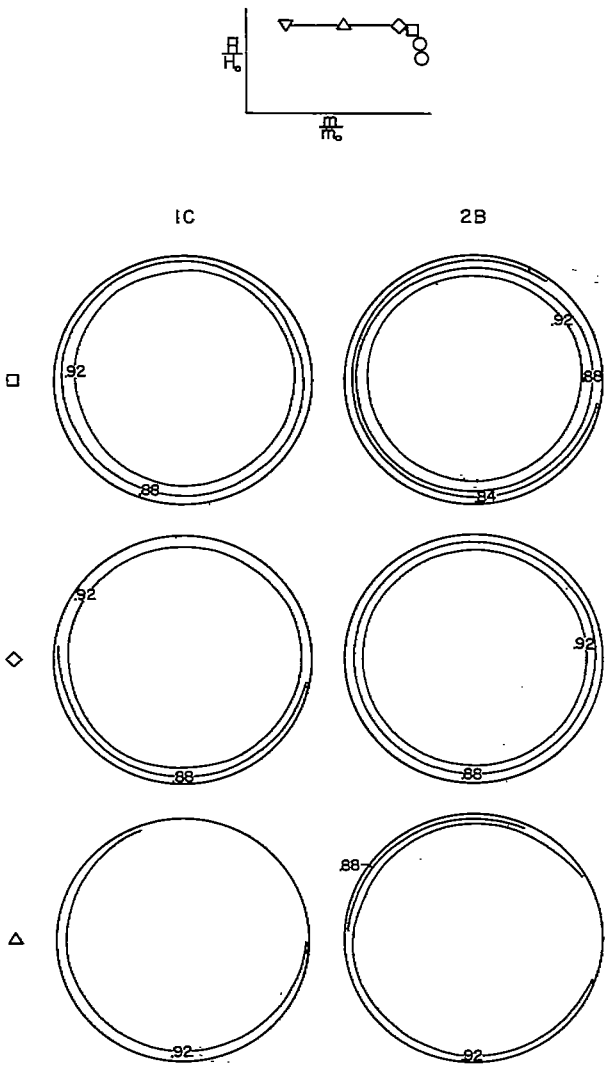

(a) $\alpha = 0^\circ$; $M_o = 1.41$.

Figure 18.- Duct total-pressure distributions of inlet configurations with the same degree of lip bluntness but having 5° and 10° forebody half-angles. Shaded areas indicate reverse flow.

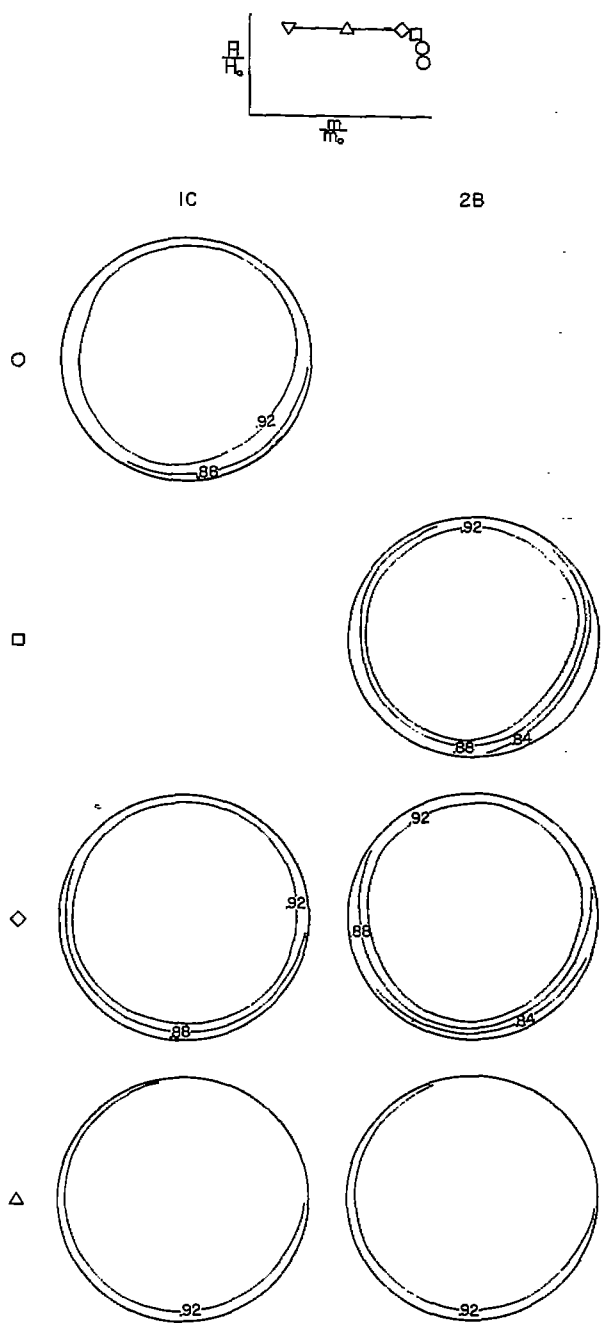

(b) $\alpha = 5^{\circ}$; $M_o = 1.41$.

Figure 18.- Continued.

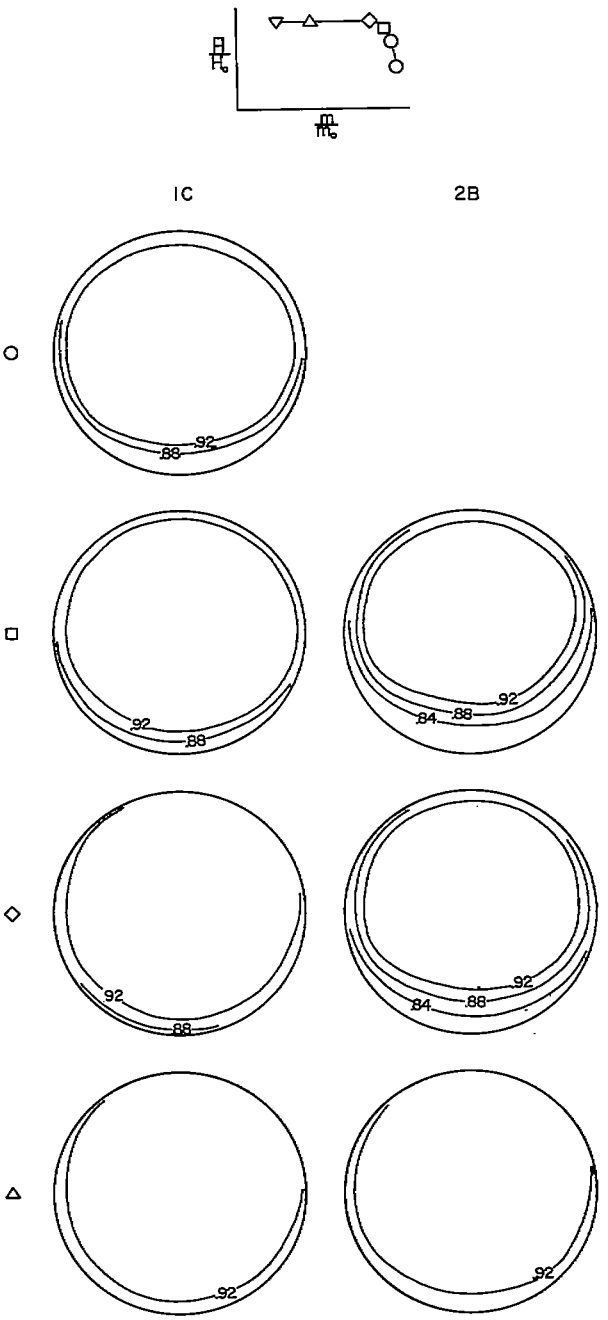

(c) $\alpha = 10^{\circ}$; $M_o = 1.41$.

Figure 18.- Continued.

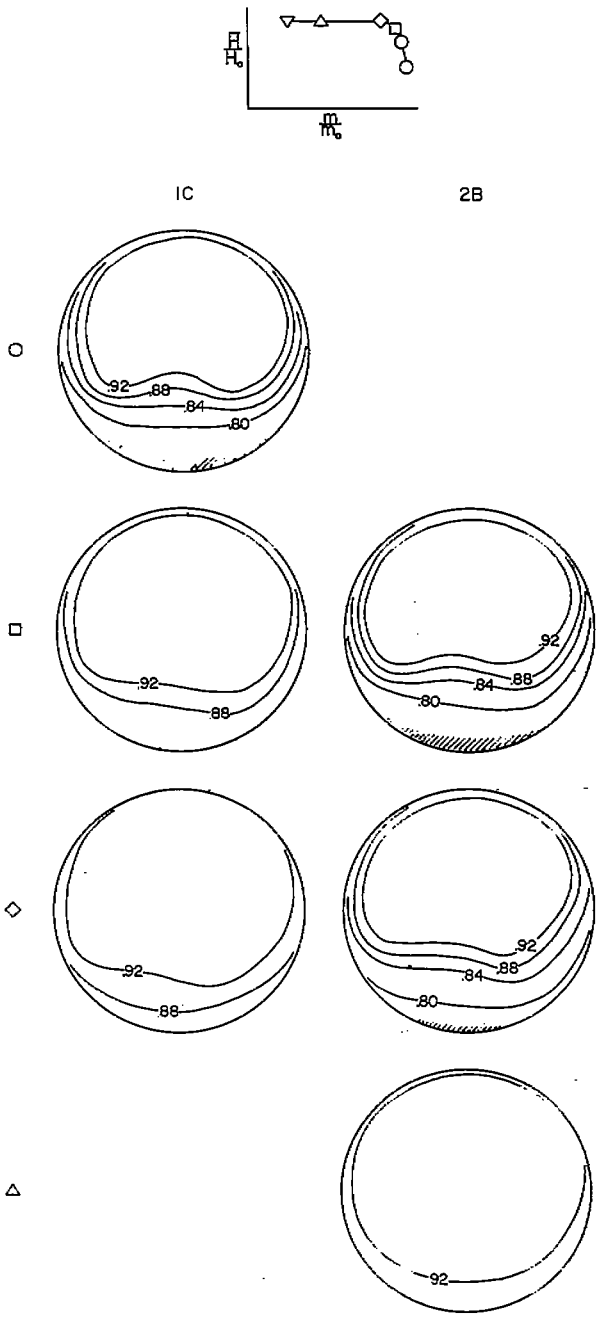

(d) $\alpha = 15^{\circ}$; $M_{\infty} = 1.41$.

Figure 18.- Continued.

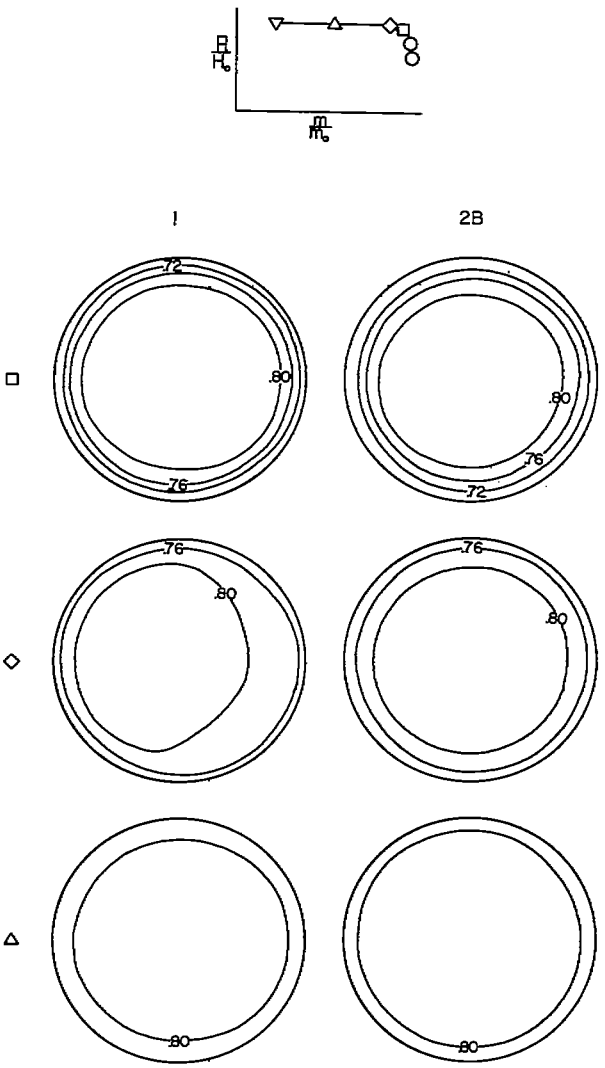

(e) $\alpha = 0^{\circ}$; $M_o = 1.81$.

Figure 18.- Continued.

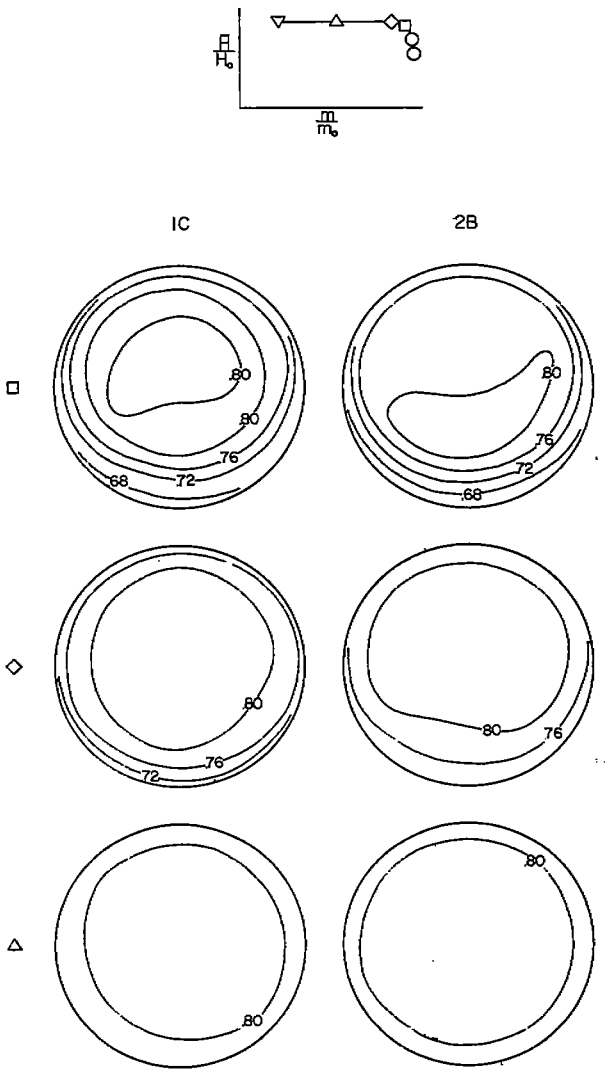

(f) $\alpha = 5^{\circ}$; $M_o = 1.81$.

Figure 18.- Continued.

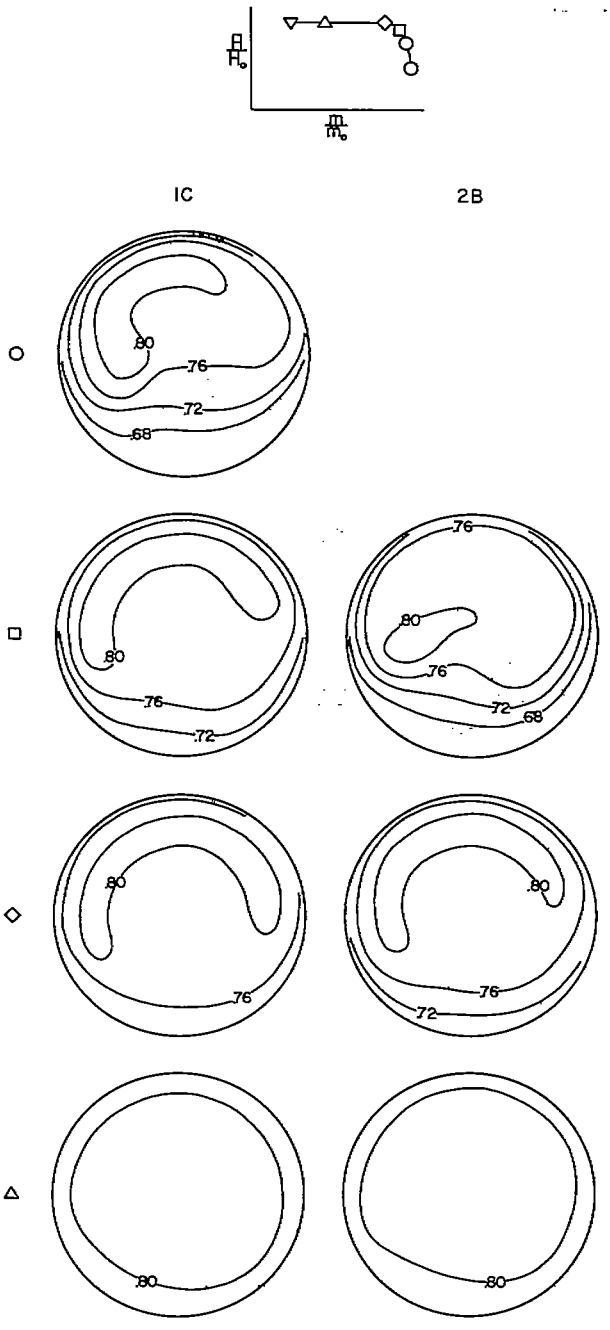

(g) $\alpha = 10^{\circ}$; $M_o = 1.81$.

Figure 18.- Continued.

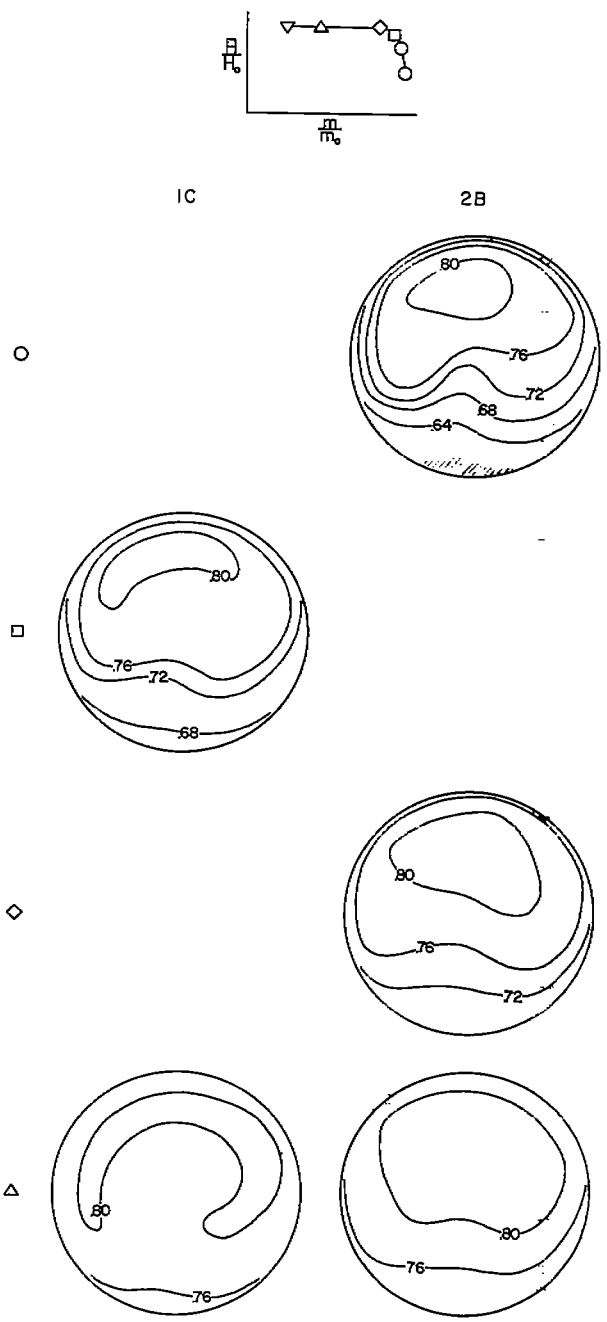

(h) $\alpha = 15^{\circ}$; $M_o = 1.81$.

Figure 18.- Concluded.

[redacted]

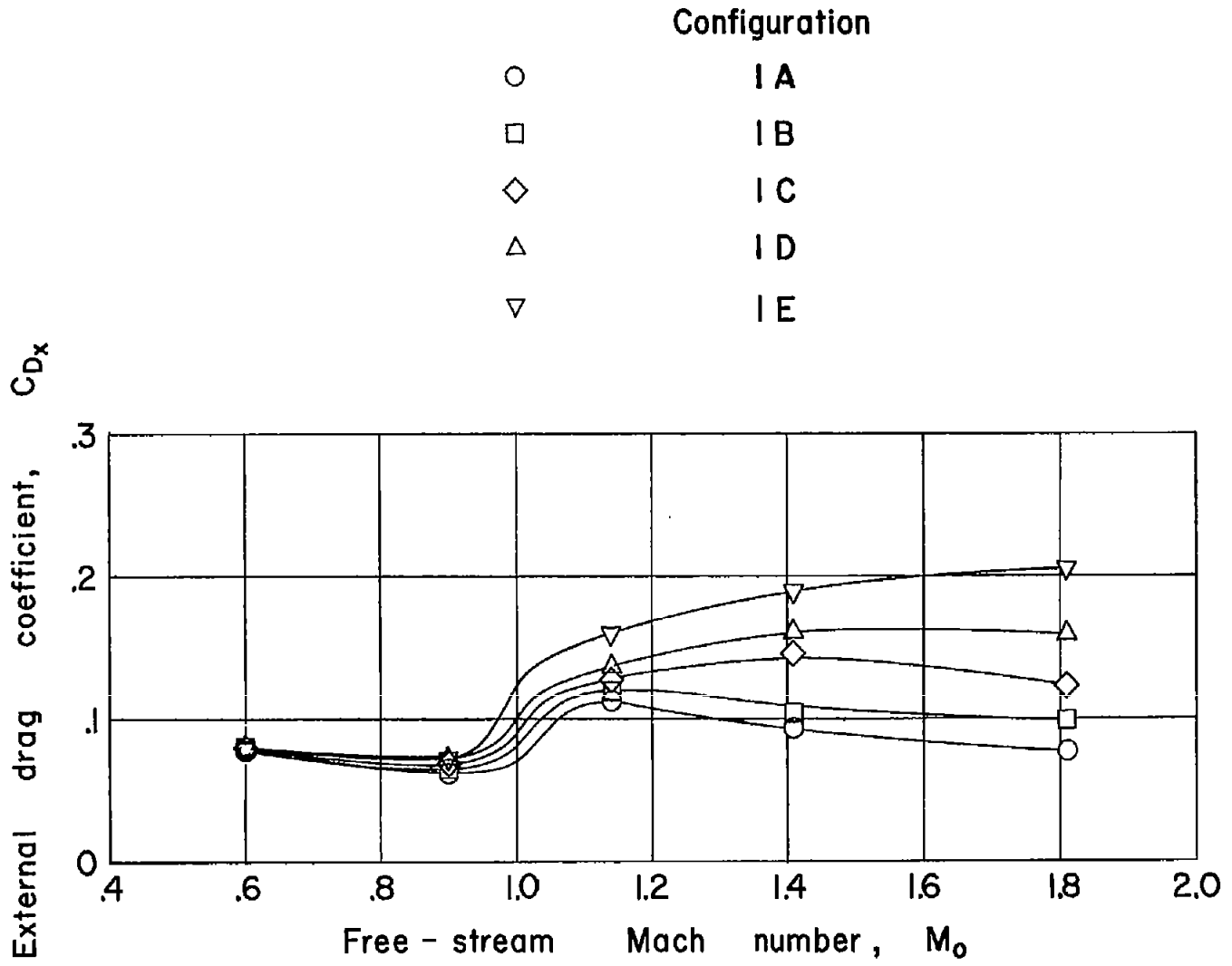

Figure 19.- Comparison of external drags of configurations varying in lip bluntness for conditions of near-sonic flow in the throats. $\alpha = 0^\circ$.

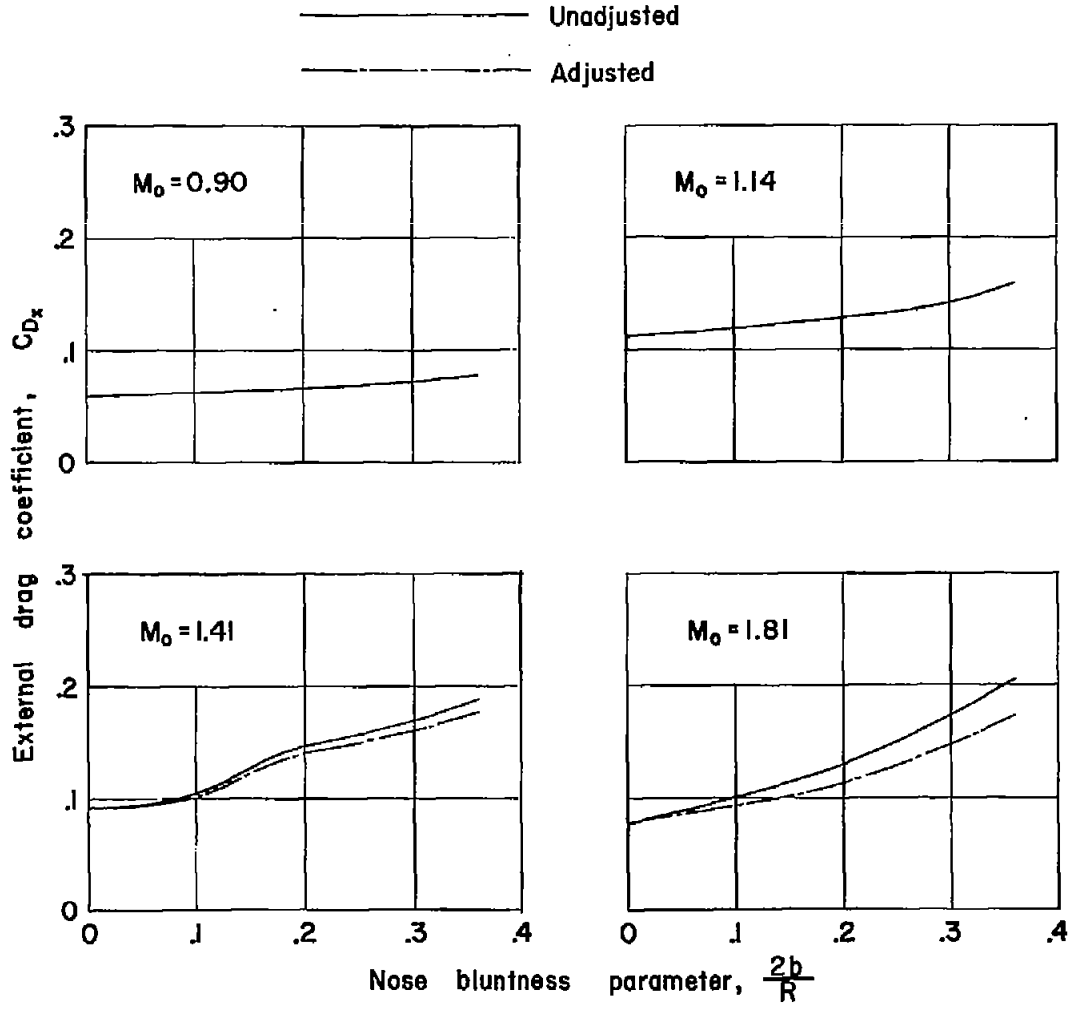

Figure 20.- Variation of external drag with lip bluntness for conditions of near-sonic flow in the inlet throats at $\alpha = 0^\circ$. Adjusted curves show drags for inlet configurations sized to have the same maximum mass flow.

NOTES: (1) Reynolds number is based on the diameter of a circle with the same area as that of the capture area of the inlet.

(2) The symbol * denotes the occurrence of buzz.

Report and facility	Description			Test parameters				Test data				Performance		Remarks
	Configuration	Number of oblique shocks	Type of boundary-layer control	Free-stream Mach number	Reynolds number $\times 10^{-6}$	Angle of attack, deg	Angle of yaw, deg	Drag	Inlet-flow profile	Discharge-flow profile	Flow picture	Maximum total-pressure recovery	Mass-flow ratio	
Confid. NM L57K08 Langley 4- by 4-foot tunnel	Normal-shock nose inlet	Normal	None	1.41 1.61	0.7 → 0.9 0.6 → 0.8	0 → 15 0 → 15	0 0	x x		x x	x x	0.95 0.80	0.6 → choke 0.5 → choke	Systematic variations of lip bluntness and lip camber were tested. Forebody half-angles of 5 and 10 degrees tested with sharp and moderately blunted lips.
Confid. NM L57K06 Langley 4- by 4-foot tunnel	Normal-shock nose inlet	Normal	None	1.41 1.61	0.7 → 0.9 0.6 → 0.8	0 → 15 0 → 15	0 0	x x		x x	x x	0.95 0.80	0.6 → choke 0.5 → choke	Systematic variations of lip bluntness and lip camber were tested. Forebody half-angles of 5 and 10 degrees tested with sharp and moderately blunted lips.
Confid. NM L57K06 Langley 4- by 4-foot tunnel	Normal-shock nose inlet	Normal	None	1.41 1.61	0.7 → 0.9 0.6 → 0.8	0 → 15 0 → 15	0 0	x x		x x	x x	0.95 0.80	0.6 → choke 0.5 → choke	Systematic variations of lip bluntness and lip camber were tested. Forebody half-angles of 5 and 10 degrees tested with sharp and moderately blunted lips.
Confid. NM L57K08 Langley 4- by 4-foot tunnel	Normal-shock nose inlet	Normal	None	1.41 1.61	0.7 → 0.9 0.6 → 0.8	0 → 15 0 → 15	0 0	x x		x x	x x	0.95 0.80	0.6 → choke 0.5 → choke	Systematic variations of lip bluntness and lip camber were tested. Forebody half-angles of 5 and 10 degrees tested with sharp and moderately blunted lips.

Bibliography

These strips are provided for the convenience of the reader and can be removed from this report to compile a bibliography of NACA inlet reports. This page is being added only to inlet reports and is on a trial basis.